UNIVERSITY OF CALGARY

Three-Dimensional Particle Diffusion in a Rotating Drum Reactor

by

Richard G. Sherritt

A THESIS

SUBMITTED TO THE FACULTY OF GRADUATE STUDIES

IN PARTIAL FULFILMENT OF THE REQUIREMENTS FOR THE

DEGREE OF DOCTOR OF PHILOSOPHY

DEPARTMENT OF CHEMICAL AND PETROLEUM ENGINEERING

CALGARY, ALBERTA

SEPTEMBER, 2001

Abstract

Mixing of non-cohesive granular solids in a partially-filled, horizontal, rotating drum occurs in the axial, radial and angular directions. Mixing in the axial direction is purely diffusive and can be represented accurately by a one-dimensional diffusion equation. From the abundance of experimental data in the literature, an empirical design correlation was derived to relate the particle dispersion coefficients in the axial direction to rotational speed, degree of fill, drum diameter and particle size. The axial-dispersion coefficient ranged from 1×10^{-7} to 1×10^{-4} m^2/s and in most cases increased with speed, drum diameter and particle diameter.

Unlike mixing in the axial direction, particle mixing in the radial and angular directions is a combination of convection and diffusion. Also, little published data exists to quantify the dispersion coefficients let alone the effects of rotational speed, degree of fill, drum diameter and particle size.

Dispersion in each direction is primarily due to the same phenomenon i.e random collisions in the active region. Relationships between the axial, radial and angular dispersion coefficients are proposed, allowing the radial and angular coefficients to be predicted from the more easily measured axial coefficient and an approximation of the relative thicknesses of the active and static regions. The proposed relationships are consistent with the radial and angular coefficients that can be determined from the limited experimental data available in the literature. The radial-dispersion coefficient is usually about 2 to 4 times larger than the axial-dispersion coefficient.

A granular solids mixing model for the transverse plane in a partially filled horizontal rotating drum is developed. The model includes convective mixing and particle diffusion perpendicular to the circulation streamlines. Using the proposed relationship between the axial- and radial-dispersion coefficients, the model simulates the effects of initial tracer orientation, fill level and scale-up on the mixing rate.

By adding heat conduction in the radial direction, the mixing model is extended to simulate wall-to-bed heat transfer. The model is used to predict the significance of mixing and scale-up on the wall-to-bed heat transfer.

Acknowledgements

Without the help and support of several people and organisations, I would not have been able to complete this thesis. Therefore it is with pleasure that I take this opportunity to express my thanks.

Financial support was provided by UMATAC Industrial Processes and the University of Calgary, and I thank Bill Taciuk and Professor Leo Behie for making this possible.

Daune Muir and Carol Dahl of UMATAC helped obtain referenced literature. Budd Perry of UMATAC arranged packing the drum used in the experiments and shipping it to Montreal. Navid Mostoufi of École Polytechnique de Montréal mounted the detectors and assisted in the execution of the RPT experiments. Professor Jamal Chaouki made the EPM's facilities available to me for the RPT experiments.

My supervisor, Dr. Leo Behie provided continuing encouragement and facilitated quick solutions when logistical problems arose. Dr. Anil Mehrotra offered welcomed and constructive technical comments.

Finally, I thank my wife, Carole, and children, Stephanie, Craig, and Andrea, for bringing balance to my world of work and school and my mom and dad for their unconditional love.

Table of Contents

List of Tables

List of Figures

Nomenclature

a	function of static and dynamic angle of repose, -
a, b, c, d	fitting parameters in Equation (51)
A	area between layers in static region, m
ATP	AOSTRA Taciuk Processor
B	zircon-to-coal mass feed ratio, -
c	tracer concentration, kg/m^3
$\mathbf{c}$	vector of tracer concentration, m^{-3}
c_o	maximum tracer concentration, kg/m^3
C	fraction of maximum tracer concentration, -
C_p	heat capacity, J/kg·K
CFD	computational fluid dynamics
d_p	particle diameter, m
D	diffusion coefficient, m^2/s
D_r	radial-dispersion coefficient, m^2/s
D_x	diffusion coefficient parallel to flow in active region, m^2/s
D_{yl}	diffusion coefficient perpendicular to flow in active region, m^2/s
D_z	axial-dispersion coefficient, m^2/s
D_{zl}	axial-diffusion coefficient in active region, m^2/s
D_θ	angular-dispersion coefficient, m^2/s
D^*	Savage's dimensionless diffusion coefficient, -
$\overline{D}$	Khakhar's dimensionless diffusion coefficient, -
DEM	discrete element modeling
e_p	particle coefficient of restitution, -
$f(h)$	bed depth function, -
F	feed rate, kg/s
$g_o(\nu)$	radial-distribution function, -
g	gravitational acceleration, 9.81 m/s^2
$g(h)$	bed depth function, -
h	bed depth, m
h	heat transfer coefficient, W/m^2·K
H	distance from middle of bed surface to drum centre, m
I	intensity of segregation, -
k	thermal conductivity, W/m·K
k	fitting parameter in Equation (51), m/s^2
K	constant corresponding to quantity of tracer, m
K	consistency index, kg/m· s^{2-m}
L	half surface chord length, m
m	flow behaviour index, -
m_{ij}	element of mixing matrix, -
$\mathbf{M}$	mixing matrix, -

n	rotational speed, rpm
n_c	critical rotational speed, rpm
N	number of stages or layers, -
p	probability, -
Pe	Peclet number, -
$\mathbf{P}$	matrix of transition probabilities, -
Q	heat transfer rate, W/m
r	static layer radius, m
R	drum radius, m
RTD	residence time distribution
t	time, s
$\langle t \rangle$	mean residence time, s
T	temperature, °C
$\mathbf{T}$	vector of temperatures, °C
u_z	mean axial velocity, m/s
u	stream velocity, m/s
v_x	velocity parallel to bed surface, m/s
V	volume, m^2
x	distance parallel to active region flow from middle of surface chord, m
X	volumetric fill fraction, -
y	perpendicular distance from bed surface, m
z	axial distance, m
Z	drum length, m

Greek letters

α	thermal diffusivity, m/s^2
$\overline{\alpha_s}$	fitting parameter that accounts for collision forces, -
β	contact angle, rad
γ	angle of drum incline to horizontal, deg
δ	thickness of active region, m
δ_0	thickness of active region at middle of surface chord, m
ε	maximum deviation from angle of steepest descent, deg
$\chi(\theta)$	concentration function, -
ϕ	dynamic angle of repose, rad
ϕ_s	static angle of repose, rad
η	apparent viscosity, kg/m·s
ν	solid fraction, -
θ	dimensionless time, -
θ	angle from axis perpendicular to bed surface, m
ρ	bulk density, kg/m^3

ρ_p	particle density, kg/m^3
Y	granular temperature, m^2/s^2
σ_t	residence time standard deviation, s
σ_θ	dimensionless residence time standard deviation, -
σ_z	standard deviation of displacement in axial direction, m
τ_1, τ_2	time in surface region and static region, s
ω	rotational velocity, s^{-1}
ζ	fraction of drum length, -

Subscripts

1	active region
2	static region
i	layer number
j	layer number or angular interval number
r	radial direction
y	perpendicular direction to bed surface
c	critical
p	particle
z	axial direction

CHAPTER 1
INTRODUCTION

Horizontal rotating drums, or rotary kilns, are commonly used for processing granular materials in the mineral, ceramic, cement, metallurgical, chemical, pharmaceutical, food, and waste industries. They are suited to processes that require high temperatures at near-atmospheric pressure. As chemical reactors, they are often designed using empirical procedures. There is significant economic incentive to develop a more fundamental understanding of a rotating drum for processing granular solids. For example, the AOSTRA Taciuk Processor (ATP) is a rotary kiln, developed by UMATAC Industrial Processes of Calgary Alberta, used to pyrolyse oil shale to produce oil vapours (Turner et al., 1989). The ATP consists of four zones for preheating, pyrolysing, combusting and cooling the shale. It was successfully piloted at a feed rate of 80 tonnes of oil shale per day. Heat transfer coefficients and residence times measured in the pilot kiln were used to scale-up to the 6000 t/d demonstration plant that is being commissioned presently in Queensland Australia. A kiln for a 25000-t/d commercial plant is being designed. Because the effects of scale-up on the complex hydrodynamic behaviour of the granular solids cannot be accurately predicted, generous safety factors are used to size the larger kilns. The estimated additional costs to build these safety factors into a single commercial ATP is in excess of $10 million.

1.1 Types of Bed Behaviour

Figure 1-1 shows a simple horizontal rotary kiln rotating about its z-axis. Most rotary kilns are inclined slightly, with the granular material entering at the upper end and flowing by gravity to the lower end. However, some kilns, like the ATP, are not inclined. Some rotary drums are simple cylinders without any internals. Others may contain flights on the inside surface of the wall. The flights lift and drop the particles into the gas stream. Lifting flights are common in rotary dryers where increasing the contact between

the particles and the gas stream is beneficial. In the ATP, the combustion and cooling zones contain lifting flights, while the preheat and pyrolysis zones do not.

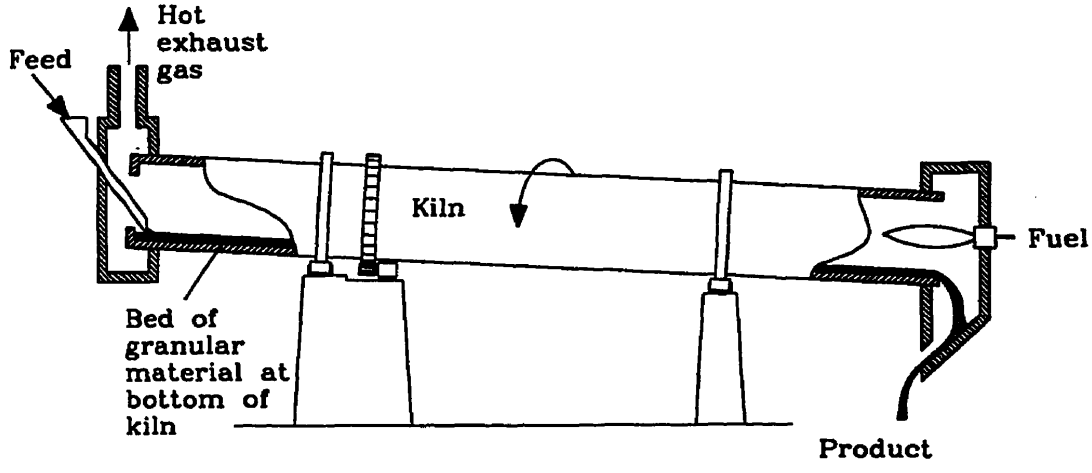

Figure 1-1 A simple, horizontal rotary kiln

In drums without lifting flights, the granular material forms a bed at the bottom of the kiln. The motion of the bed of particles in the transverse plane (perpendicular to the drum axis) as it moves from one end of the kiln to the other can be characterised as one of several possible behaviours. This behaviour depends on the operating conditions (rotational speed and degree of fill) and the friction of the particles with each other and with the surface of the drum wall (Henein et al., 1983a, 1983b). Figure 1-2 contains illustrations of the possible types of bed behaviour while Figure 1-3 shows a typical phase diagram for the possible types of bed behaviour. Mellmann (2001) gives criteria and equations to predict the transitions between the different types of behaviour.

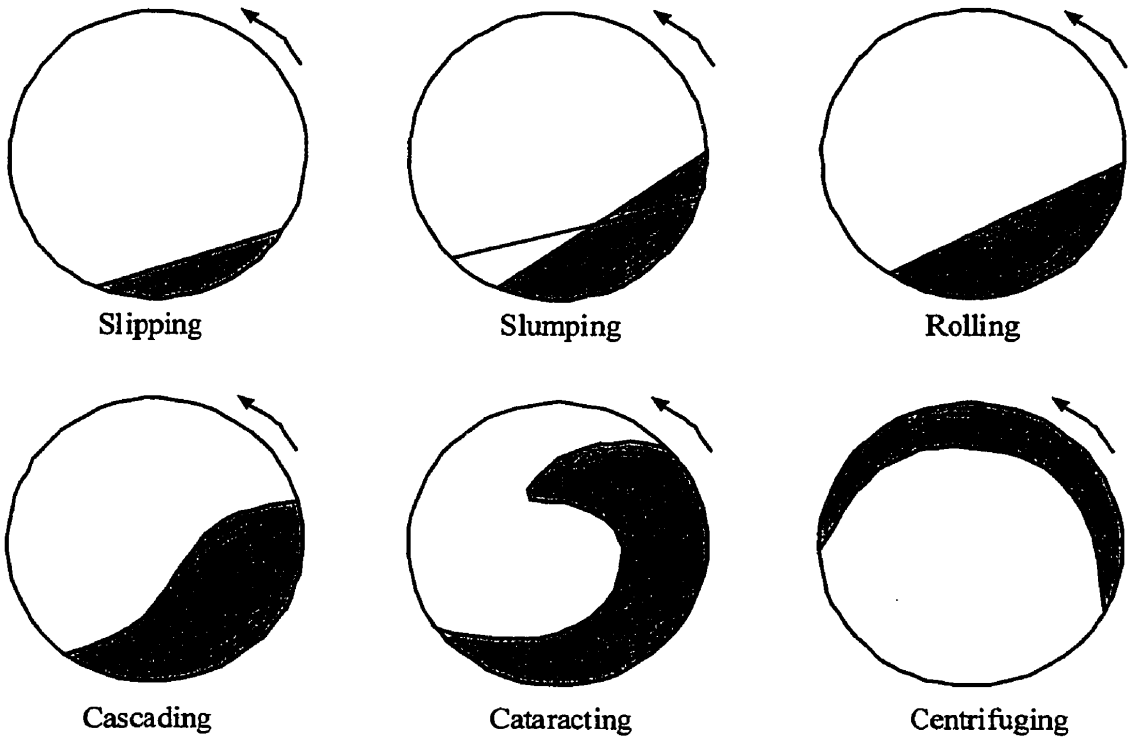

Figure 1-2 Possible modes of transverse bed behaviour in a partially-filled, horizontal, rotating drum

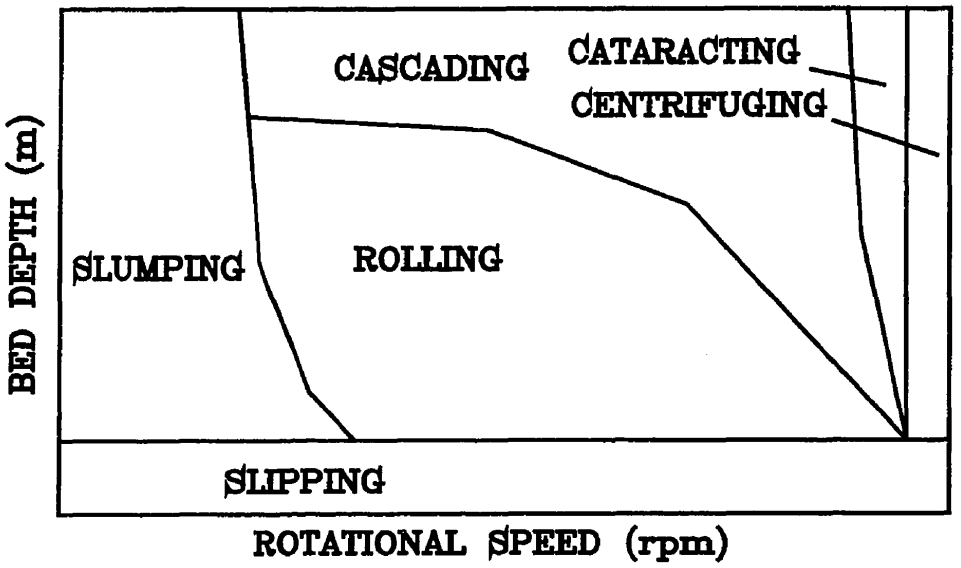

Figure 1-3 Phase diagram for possible modes of transverse bed behaviour in a partially-filled, horizontal, rotating drum

Slipping is an undesirable behaviour in which the bed of particles slips on the surface of the drum wall. Slipping usually occurs at low volumetric fill and can be prevented by roughening the surface of the wall. There are several types of slipping; but because sliding results in little or no mixing, there is little interest in slipping behaviour.

Centrifuging is the behaviour seen at high rotational speeds when the centrifugal force at the wall exceeds the gravitational force. The particles remain fixed to the wall. The speed at which centrifuging begins to occur is referred to as the *critical speed* and can be determined using the following equation.

$$n_c = \frac{60}{2\pi}\sqrt{\frac{g}{R}} \tag{1}$$

Centrifuging behaviour is also of little interest as rotary kilns operate well below critical speed. However the critical speed is used as a reference for other types of behaviour.

Slumping, rolling, cascading, and *cataracting* are non-slipping bed behaviours which occur between zero and critical speed. The particles in most rotary kiln reactors have slumping, rolling or cascading behaviour, while cataracting is common for grinding particles in ball mills. *Slumping* occurs at low rotational speeds (less than 3% of the critical speed). The particles that form a bed at the bottom of the drum will ride up one side of the wall due to the rotation. The particles on the sloped surface will periodically avalanche from the upper half of the surface to the lower half.

For both rolling and cascading behaviours, which occur between 3 and 30% of critical speed, the bed that forms at the bottom of the drum can be discerned as two regions. The lower region is the *static region*, in which the particles move upward with the rotation of the wall. Each particle is stationary relative to adjacent particles. Particles move with the static region until they reach the upper region that is called the *active region.* In the active region, the particles flow continuously and rapidly down the inclined surface of the bed. While in the active region, particles mix with adjacent particles due to random collisions. In the lower half of the active region, particles re-enter the static region to begin another cycle.

Rolling behaviour, which occurs at lower bed depth and fraction of the critical speed than cascading behaviour, is characterised by a flat upper surface as illustrated in Figure 1-4a. The active region has a parabolic shape and is about 15 to 20% of the total bed depth. The angle of the upper surface to the horizontal plane is known as the *dynamic angle of repose* of the granular material.

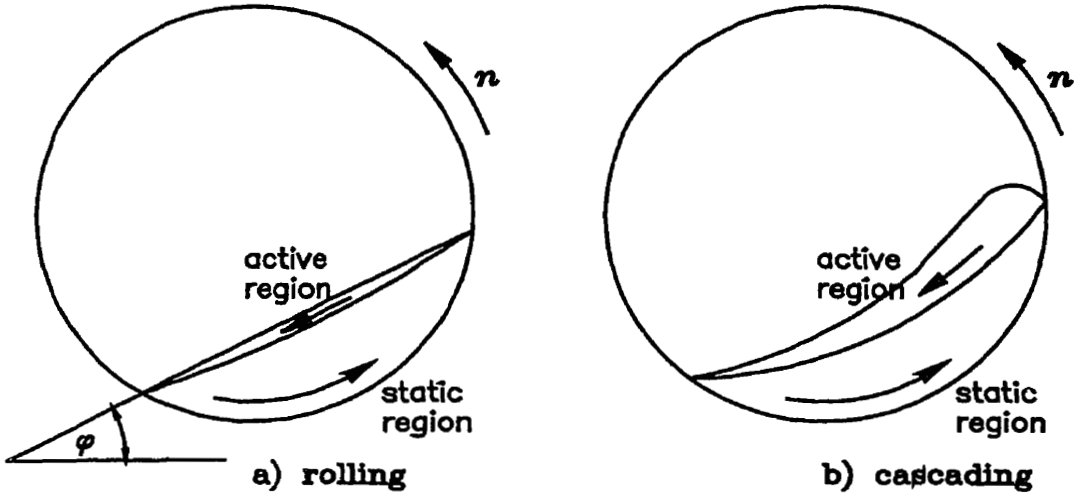

Figure 1-4 Transverse bed motion in a rotating drum with a) rolling behaviour and b) cascading behaviour

The rolling bed becomes a *cascading* bed at higher rotational speed and fill. The upper surface is deformed as shown in Figure 1-4b due to the increased centrifugal forces and increased particle acceleration and deceleration. Also the active region is thicker than that in a rolling bed due to the increased particle circulation rate in the cascading bed.

Figure 1-5 shows mean velocity profiles for the active and static regions of a rolling bed as measured by Boateng (1993). In the static region, particles move at the same angular velocity as the wall. In the active region, the mean particle velocity varies from the maximum at the bed surface (A), through a point of zero near the centre of the bed (B), to the same angular velocity as the wall at the interface with the static region (C). The velocity profile can be linear (as shown), concave or convex. A material balance must be satisfied for any cross-section perpendicular to the bed surface. For example, the net material crossing segment AC in the active region must equal the net material crossing segment CD in the static region.

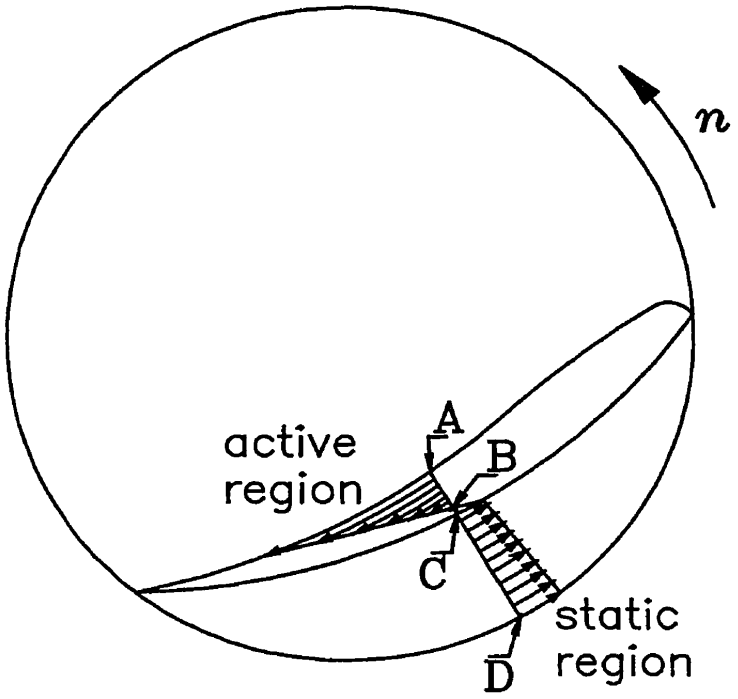

Figure 1-5 Typical particle velocity profile in a rotating drum with rolling/cascading behaviour

At still higher speeds, 30 to 100% of critical speed, particles reaching the upper surface of the bed are *cataracting* or airborne.

1.2 Particle Mixing in a Rotating Drum

In most rotary kilns, heat transfer from the wall or the gas space to the bed of granular material is a critical step in accomplishing their overall purpose. The mixing of the granular material in the *transverse plane* (perpendicular to the rotational axis) is important to understanding the mechanism for heat transfer from the periphery of the bed to the bulk of the bed. Two zones in the ATP rely on mixing in the transverse plane. In the preheat zone, heat is transferred from the wall to the bed. In the retort zone, hot ash is mixed with the preheated shale to heat the shale to the temperature that oil vapours are evolved.

For the design and scale-up of the ATP and most other rotary kilns, it is desirable to understand the effects that changes in kiln diameter, rotational speed and degree of fill have on heat transfer within the bed. But in order to accomplish this, a model of the motion and transverse mixing of the granular material is required. If heat transfer and chemical reactions could be incorporated into the model, then it would be possible to simulate various rotary kiln processes leading to more fundamental design procedures.

Rotating kilns are often treated as perfect plug flow reactors; that is, the granular bed is perfectly mixed in the transverse plane with negligible mixing in the axial direction. Assuming negligible mixing in the axial direction is a reasonable approximation for long rotary kilns. However, radial mixing in the transverse plane is not perfect and may actually be the controlling step in processes that involve heat transfer from the wall or a flame in the freeboard to the core of the bed. As shown in the literature review in the next chapter, much work has been done to measure mixing in the axial direction of a rotating drum. On the contrary, very little useful information is available for mixing in the radial direction.

A statistical variable can be used to describe the extent of mixing in a non-flowing bed of particles. Carley-Macauly and Donald (1962) use an index-of-mixing obtained from the variance (square of the standard deviation) of a number of small samples to which a correction is applied for the random variance owing to the sample size. Mixing is characterized as either convective mixing or diffusive mixing. Mixing in the axial direction in a horizontal rotating drum is slow and is characterized as purely diffusive mixing as the direction of mixing is perpendicular to the plane of particle circulation. Mixing in the transverse plane is much more rapid and is a combination of convective and diffusive mixing. For both types of mixing, the variance decays exponentially with time.

Although the index-of-mixing is shown to be useful in studying the effects of variables on the mixing rate, it is not easily adaptable to the prediction of heat transfer and reaction conversions in reactors.

Particles may be assumed to be perfectly mixed in the active region. The assumption implies that a particle leaving the static region mixes perfectly with other particles in the active region before re-entering the static region. The position of the particle as it leaves the static region has no influence on the position that the particle re-enters the static region. This mixing model is used by a number of authors (Wachters and Kramers, 1964; Wes et al., 1976; Lehmberg et al., 1977) to derive models for the heat transfer from the covered wall to the underside of the bed in a rotating drum. Wall-to-bed heat transfer coefficients predicted using the perfect mixing assumption are larger than experimental results (Wachters and Kramers, 1964). Although a gas film next to the wall (Lehmberg et al., 1977), changing wall temperature (Gorog et al., 1982), or heat losses to the gas space (Ferron and Singh, 1991) may contribute to the discrepancy, imperfect radial mixing is likely the major contributor (Wes et al., 1976).

1.3 Objectives of this Study

The objective of this study is to develop a transverse mixing model for the granular material in a horizontal, rotating drum. The model should be able to predict the effects of rotational speed, degree of fill, particle properties and especially drum diameter. The model should have the ability to be easily extended to include heat transfer and chemical reactions in the bed of granular material.

In order to accomplish this objective, the techniques that have been used to measure and model the mixing of cohesionless granular solids in a horizontal rotating drum in the axial direction and the transverse plane are reviewed. The information available for axial mixing is used to assist in developing a strategy to measure and model transverse mixing. Experimental data by others are examined to determine the effects of rotational speed, degree of fill, kiln diameter, and particle size on mixing in both the axial and radial directions. Relationships between the axial and transverse mixing are proposed allowing the transverse mixing to be estimated from the more easily measured axial mixing.

The proposed relationships are tested with published data. Particle tracking experiments are performed to provide data for axial and transverse mixing using the same granular material under the same conditions simultaneously. Finally, a predictive model for scale-up of rotary kiln reactors such as the ATP is developed. The model predicts the mixing in the transverse plane and is extended to predict wall-to-bed heat transfer.

1.4 Scope of this Study

In a rotating drum, the properties of the bed of particles and the drum itself can vary widely. To keep this study to a reasonable size, the scope is limited in a number of areas. The study is confined to cohesionless particles of uniform size in drums without lifting flights.

Segregation of particles in rotating drums due to differences in particle size, shape, surface roughness or density has been given considerable attention in the recently published literature (Nityanand et al., 1986; Pollard and Henein, 1989; Pershin, 1990; Alonso et al., 1991; Boateng, 1993; Ristow, 1994; Zik et al., 1994; Clément et al., 1995; Cantelaube et al., 1997; Van Puyvelde et al., 2000b). It has been shown that a binary mixture with a large difference in the particle physical properties will readily separate with particles of the same properties concentrating in the centre and the periphery of the bed. Because radial segregation occurs simultaneously with the opposing mixing phenomena, a model for segregation also requires an understanding of mixing. By limiting the discussion to a granular material with uniform particles, this work only considers mixing and does not consider this related phenomenon of segregation. While segregation is not included in the current study, the mixing model developed here can be readily extended to include segregation.

While this study is primarily concerned with drums with no internals or flights, some comparison of results to drums with flights is made.

CHAPTER 2
LITERATURE REVIEW

This chapter reviews previous studies to measure and model the behaviour of the bed of particles in a horizontal, rotating drum without lifting flights. Mixing in the axial direction as well as the plane perpendicular to the rotating axis is examined. Mixing in granular flows in general and the implications it has for the rotating drum are discussed. Finally, the role that mixing plays in the rate of heat transfer in the bed of particles is reviewed.

2.1 Bed Motion Models

In the study of rotating drum processes, several models to describe the bed motion have been used. The models may be categorised into several groups according to the method used to represent the flow behaviour in the active region. The groups are:

i) negligible active region,

ii) fluid flow analogies,

iii) dense-gas kinetic theory analogies, and

iv) discrete element modelling.

2.1.1 Negligible Active Region

Often the thickness of the active region and the time the particles are in the active region are assumed to be negligible. In some cases this is a reasonable assumption. Assuming a negligible active region, Saeman (1951), Vahl and Kingma (1952), and Kramers and Croockewit (1952) derive equations that have been shown to satisfactorily predict the average residence time of granular material in a rotary kiln with a rolling bed. However, because the active region in a cascading bed is larger than in a rolling bed, the assumption may not be as well suited to cascading beds and may give misleading results for higher rotational speeds and degrees of fill. Hogg et al (1974) apply a correction factor that doubles the slope of the bed in drums at higher speed and level of fill.

Experiments by Tscheng (1978) indicated that particles are in the active region 20-40% of the total time and experiments by Boateng (1993) indicated that the depth of the active region is 15 to 35% of the total bed depth. Nakagawa et al. (1993) measured an active layer thickness (including transition) from zero to 50 per cent of the bed depth. The thickness increased with rotational speed but at a decreasing rate. Woodle and Monro (1993) found that particle type had a large effect on the size of the active region. Van Puyvelde et al. (2000a) found that the active region occupied 20-40% of the total bed volume. The volume fraction occupied by the active region increases with increasing rotational speed and decreases with increasing fill. Three different drum diameters varying from 200 to 570 mm had no effect on the volume fraction. Likewise, the particle diameter was found to have no effect. Experimental results were fitted to the operating conditions by the following equation:

$$\frac{V_1}{V_T} = 0.0981\ln(n) + 0.00438\exp(8.744[0.5 - X]) \qquad (2)$$

2.1.2 Fluid Flow Analogies

If the particle size is small relative to the bed depth, then it is reasonable to treat a flowing granular material as a continuous fluid. Fluid flow analogies have been used to investigate fully developed gravity flow of granular materials in simple cases such as inclined chutes and vertical channels (Goodman and Cowin, 1971; Augenstein and Hogg, 1978; Savage, 1979). The governing equations are the same as those describing conventional fluids (i.e. Navier Stokes equations.) The viscosity of the granular material, which can only be determined experimentally, is in some respects similar to that of a Bingham fluid. The material will not flow until a critical shear stress or yield stress is applied. After yielding, the shear rate increases linearly with increased shear stress. However, for granular materials the yield stress is not constant and is linearly related to the normal stress. Also granular materials exhibit a phenomenon called dilatancy, where the bulk density or particle concentration must decrease before the material will shear. If

the particle concentration is reduced further, then the viscosity of the material decreases. Models of varying complexity have been proposed to account for the unique properties of flowing granular materials (Goodman and Cowin, 1971; Savage, 1979).

Perron and Bui (1992) show that assuming the granular material behaves as a pseudo-plastic fluid can approximate the motion of the bed of granular material in a rotating drum. They assume a flat upper surface for the bed and no slip at the wall. Mass and momentum conservation equations (Navier-Stokes equations) are solved using Computational Fluid Dynamic (CFD) code. Of the various models for the apparent viscosity examined, the velocity profile and thickness of the active and static regions are best predicted using the following relationship for the apparent viscosity and the shear rate.

$$\eta = K\left(\frac{du}{dy}\right)^{m-1} \tag{3}$$

Values for parameters K and m were found by fitting experimental data for alumina pellets in a rotating drum given by Tscheng (1978). However, because only one experiment was fitted, it was not shown that the parameters were properties of the granular material alone and independent of drum diameter, rotational speed and fill.

Khakhar et al. (1997) apply mass and momentum balances to predict the thickness profile and velocity of the active region. Assuming constant density and a flat upper surface, a mass balance gives the following relationship for the thickness of the active region:

$$\delta = \delta_0\left(1-\frac{x^2}{L^2}\right) \tag{4}$$

If the velocity in the active region is assumed to increase linearly with the distance from the interface between the static and active regions to the surface, then a momentum balance which includes gravity, frictional and collision forces yields the following relationship for the maximum thickness of the active region:

$$\delta_0 = L\left(\frac{\bar{\alpha}_s \omega^2 L}{a}\right)^{1/4} \tag{5}$$

where $\bar{\alpha}_s$ is an experimentally-derived dimensionless parameter that accounts for the collision forces and a, which is determined from the static and dynamic angles of repose, accounts for the frictional forces.

2.1.3 Dense-gas Kinetic Theory Analogies

Granular flows have been modelled using concepts from dense-gas kinetic theories (Lun et al., 1984). The methods are based on the similarities between the motion of particles in granular flow to the theory of molecular motion in a dense gas (Chapman and Cowling, 1970). The transfer of momentum and kinetic energy is assumed to be primarily by particle-to-particle collisions. For granular materials, the effect of the interstitial fluid is neglected.

To apply kinetic theories to granular flows, a property referred to as *granular temperature* Υ is given to the granular material. Granular temperature, analogous to the thermodynamic temperature of gases, represents the particle kinetic energy due to the difference between the velocity of the individual particles and the average velocity of the ensemble of the particles. Unlike the thermodynamic temperature of a gas, the granular temperature is not self-sustaining due to inelastic particle collisions.

As in the fluid flow analogies, the granular material is considered to be a continuum. The constitutive equations for granular flow using kinetic theory consider the conservation of kinetic energy in addition to momentum and mass. The equation for the conservation of kinetic energy includes an energy dissipation term that accounts for inelastic particle collisions. Energy dissipation introduces the coefficient of restitution for inelastic particle collisions as an important property affecting the material's flow behaviour. Kinetic theories also account for the dilation phenomena using the solids fraction ν, which is the ratio of the bulk density and the particle density, $\nu=\rho/\rho_p$.

The application of kinetic theory to granular flows has mostly been limited to simple flows such as inclined chutes and vertical channels. A few attempts to apply these concepts to granular material in a horizontal rotating drum have been made. Boateng (1993) divides the bed into active and static regions. The bed is assumed to have a flat upper surface. The governing equations for an element of the active region are derived from the conservation of mass, momentum and kinetic energy. The boundary conditions for the upper surface and the interface between the active and static regions are stated. Boateng recognises the similarities between the development of the active region and the development of a boundary layer for fluid flow at the leading edge of a flat plate. He adapts the classical approach from boundary-layer theory to define the active region. Experimental data are used to characterise the velocity profile of the active region and an iterative method is used to determine the thickness and granular temperature of the active region that satisfies the mass balance. The result agreed with experiments using spherical, near-elastic polystyrene beads. The model was less successful in predicting the more complex behaviour observed for irregularly shaped, inelastic rice and limestone.

Yank and Farouk (1997) apply the governing equations to the entire bed. They assume the upper bed surface is flat and there is no slip at the wall. The predicted velocity profiles are compared to data for spherical beads from Boateng and Barr (1996). The velocities agree at the bed surface and at the wall, but differ near the core. The prediction suggests a more gradual transition between the active and static regions.

2.1.4 Discrete Element Modelling

Discrete element modelling (DEM) is a simulation technique in which the particles are considered individually rather than as a continuum. The total force and moment on a particle are the sum of the contact forces and gravitational force. The subsequent motion of the particle is governed by Newton's second law, which leads to a group of second-order differential equations for each particle. The effect of the interstitial fluid id neglected. The motion of the entire granular mass is determined by

simultaneous numerical integration of all the differential equations for all the particles. An averaging procedure can be used to generate bulk properties and overall behaviours.

Until recently, most studies using DEM have been restricted to a few hundred particles and two dimensions due to excessive computational demands (Zhang and Campbell, 1992; Savage and Dai, 1993; Buchholtz et al., 1995). While the number of particles has currently been extended to several thousand (Baumann et al., 1995; Kohring 1995), an actual granular flow may consist of millions or trillions of particles. As computers continue to become more powerful and more efficient algorithms are developed, the number of particles in a simulation will increase and the computing time will decrease in the future. The current focus appears to be the development of efficient algorithms for irregularly shaped, in-elastic particles and parallel computing.

Even with its limitations, DEM has been a useful tool for studying granular materials by simulating a relatively small number of particles. DEM is used to simulate particle behaviour in a 2-dimensional rotating drum by Buchholtz et al. (1995). The model includes 500 square, inelastic particles and is capable of reproducing the transition from a slumping bed at low rotational speeds to a rolling bed at higher rotational speed. Baumann et al. (1995) use this technique to simulate a 2-dimensional drum with about 3000 circular particles. The model is used to study the mechanism of segregation at low rotational speed (slumping bed behaviour). No comparison to a real system is given. Kohring (1995) simulates a 3-dimensional drum with 1000 spherical, in-elastic particles. A rolling behaviour is observed but again no comparison to a real system is given. McCarthy and Ottino (1998) are able to simulate a drum with over 10 000 particles by using DEM for the active region only. Results are compared to real experiments with good qualitative agreement. Yamane et al. (1998) fit simulations of a 3-dimensional drum with 12 000 particles to real experiments by adjusting a parameter that accounted for the non-sphericity of the particles. Good agreement was obtained for the angle of repose, velocity profiles and the thickness of the active layer.

2.2 Mixing in the Axial Direction

The methods used by previous authors to model mixing of particles in the axial direction in horizontal rotating drums can be divided into the following groups:

1) finite stage transport,

2) Monte Carlo simulation,

3) discrete element modelling, and

4) dispersion model.

2.2.1 Finite Stage Transport

A common method used to represent a continuous reactor with some internal mixing is to connect a number of perfectly mixed reactors in series. The number of mixers is set to give the same response measured at the outlet of the reactor when a change in concentration is made at the inlet. If axial mixing is small, as in rotary kilns, then the number of mixers in series can be approximated from the mean and standard deviation of the residence time by the following equation:

$$N = \frac{\langle t \rangle^2}{\sigma_t^2} \tag{6}$$

From experiments by Wes et al. (1976) with a small drum, the axial length of one mixing unit is about 10% of the drum diameter. Similarly, Sai et al. (1990) found the length to be from 2 to 10 % of the drum diameter. Therefore, 100 or more perfect mixers in series could approximate a typical kiln with a length-to-diameter ratio of 10. One limitation of the mixers-in-series model is that it cannot predict the axial mixing in a non-flowing or batch reactor.

Mu and Perlmutter (1980) propose a scheme for the axial mixing in a rotary kiln similar to mixers-in-series. Except rather than a single mixer, each stage consists of a plug flow section followed by a mixed section. Each stage also includes a by-pass and a recycle stream. A stage is characterised by four parameters; the first two parameters are determined from the rotational speed and the volumetric fill. The other two parameters

and the number of stages are adjusted to match the response from a tracer experiment. For the one experiment reported, the length of one stage is about 12% of the drum diameter.

Kelbert and Royere (1991) propose another finite stage model. Each stage consists of a plug flow section and a mixed section in parallel, which correspond to the active region and the static region in a rolling bed, respectively. Only one parameter, the fraction of flow to the mixed section, is required in addition to the number of stages in order to fit the model to the rotary kiln. No mixing data is used to determine the parameter or the number of stages. Instead, the model is extended to include heat transfer, and experimental temperature data is used to determine values for the mixing parameter and the number of stages.

Another finite stage model is proposed by McTait et al. (1998). Each stage consists of 2 mixed sections and a plug flow section. One mixed section and the plug flow section, connected in series, represent the active and static regions, respectively. The second mixed section represents a stagnant core and exchanges mass with the first mixed section. The volume fractions of each section are approximated from observations for a typical drum. The exchange rate between the two mixed sections and the number of stages are adjusted to fit the residence time distribution of a tracer experiment. The model is able to fit the long response tail seen in the experiment.

2.2.2 Monte Carlo Simulation

A number of authors use Monte Carlo simulations to model mixing in the axial direction in a rotating drum. A Monte Carlo simulation is a mathematical experiment by which the expected outcome of a stochastic process is estimated by random sampling from the probability distributions that govern the events making up the process. The various attempts to predict the axial mixing in rotary drums using a Monte Carlo simulation differ in the events making up the motion of the particles and the probability distribution assigned to the magnitude or direction of each event. These attempts also differ greatly in their success to predict actual mixing behaviour.

Cahn and Fuerstenau (1967) consider a bed of particles that circulates in a plane perpendicular to the drum axis. The bed has a rotational speed that is greater than the drum speed. The drum is divided into sections of equal width perpendicular to the axis. A Monte Carlo simulation models the axial movement between the sections. The three probability distributions are

1) the number of particles that leave a section per bed revolution,

2) the direction the particles move, and

3) the axial distance the particles move.

Observations for an individual particle in a non-flowing or batch drum give the average bed rotational speed and the 3 probability distributions for various speeds and fill combinations used in the simulations. Axial mixing observed in non-flowing experiments is reported to agree with mixing predicted in the simulations. Unfortunately, Cahn and Fuerstenau (1967) do not publish the measured bed speeds or probability distributions. Some discussion is given about the effect of speed and fill on the probability distributions. More particles appear to leave a section and move a greater distance as speed and fill are increased.

Rogers and Gardner (1979) discern the following behaviour for a particle in a rolling bed: The particle moves on a fixed radius until it reaches the bed surface. On the bed surface, the particle is free to roll or tumble until it re-enters the bed at a new radius. While on the surface, the particle collides with other particles. Due to the collisions, the angle at which the particle descends deviates from the angle of maximum descent. The radial position determines the time for the particle to complete a cycle and the distance the particle rolls on the bed surface. The angle of descent determines the axial movement of the particle.

The two probability distributions used in the Monte Carlo simulation are:

1) the radius at which the particle re-enters the bed is a uniform distribution weighted for the number of particles at each radius, and

2) the angle of descent has a normal distribution about the angle of maximum descent. The standard deviation for the angle is determined at various fill levels from non-flowing experiments by Shoji et al. (1973).

Because the simulation of experiments with continuous flow by Shoji et al. (1973) showed good agreement, Rogers and Gardner (1979) conclude that axial mixing in flowing and non-flowing rotating drums with a rolling bed is primarily due to the same mechanism (i.e. collisions between particles in the surface region of the bed). They also conclude that the deviations in the angle of descent, and not the randomness in the radial position, control the dispersion mechanism. The value of the standard deviation of the angle of descent and its relationship to the volumetric fill are not reported. The effect of speed, drum diameter and particle properties are not investigated.

Black (1988) proposes a physical model similar to Rogers and Gardner (1974) except there is no deviation from the angle of steepest descent as the particle rolls down the bed surface. The probability distribution for movement in the radial direction is found by tracking a single particle in non-flowing experiments. Monte Carlo simulations predict axial mixing for hypothetical, flowing drums.

Kohav et al. (1995) give six variations of a model that, like Black's model, have no deviation in the axial direction from the path of steepest descent as particles roll down the bed surface. The models vary in the way the randomness of the radial position is treated. The simulations predict much less axial mixing than measured by experimenters. It is concluded that radial segregation must be the reason for the larger axial mixing observed in experiments. However, both Black (1988) and Kohav et al. (1995) overlook the contribution of particle collisions in the surface region. It is clear from their models that the predicted mixing is not sufficient when one considers the limiting case of no net flow as both would predict no mixing in the axial direction in a non-flowing drum.

A Monte Carlo simulation can give good predictions of axial mixing if the significant events are included. One disadvantage of a Monte Carlo simulation is the large amount of computing time required. Also no attempts have been made to relate the

probability distribution of the events with parameters such as rotational speed, volumetric fill, drum diameter and particle properties.

2.2.3 Discrete Element Modelling

Discrete element modelling (DEM) not only simulates granular flow (See §2.1.4), but also simulates the mixing of particles in the granular flow. The only attempt to use DEM to predict self-diffusion of particles in the axial direction in a rotating drum is by Kohring (1995). While results for a non-flowing drum are consistent with diffusive behaviour, no comparison is made to real experiments. The diffusion rate is about an order of magnitude larger than that measured by others in real experiments and increases more with rotational speed. The differences may be due to the material properties specified for the simulation not being typical of most materials.

2.2.4 Dispersion Model

The most common method of modelling axial mixing in both flowing and non-flowing, horizontal, rotating drum is the axial-dispersion model. Mixing in the axial direction is represented by the following one-dimensional diffusion equation.

$$\frac{\partial c}{\partial t} = D_z \frac{\partial^2 c}{\partial z^2} - u_z \frac{\partial c}{\partial z} \tag{7}$$

where D_z is the axial-dispersion coefficient. The advantage of the axial-dispersion model is that a single parameter is used to quantify the amount of mixing in the axial direction. The same model can be applied to both flowing and non-flowing drums. Also, the method can be easily adapted for determining heat transfer and reaction conversions. The model predicts a normal distribution that accurately describes mixing in a non-flowing batch drum. However, the tracer residence time in a continuous flowing drum is usually slightly skewed giving a slight deviation from the dispersion model. The particle dispersion coefficient has been determined from numerous experiments. Methods of determining the axial-dispersion coefficient from experimental data are reviewed in the next chapter.

2.2.4.1 Empirical Correlations

From their experimental results several researchers have made observations of the effect of various system parameters on the axial-dispersion coefficient in rotating drums. The effects of rotational speed, volumetric fill, feed rate, drum incline, and particle properties have been studied. Except for one experiment by Rutgers (1965), the effect of drum diameter on the axial dispersion has not been reported.

With all other variables held constant, increasing the rotational speed causes the axial dispersion to increase. Some experimenters such as Rutgers (1965) found that the axial-dispersion coefficient is proportional to the square root of the speed, whiles others such as Rao et al. (1991) found the coefficient to be directly proportional to speed.

Generally, the dispersion coefficient decreases as the volumetric fill is increased. Rutgers (1965) found the coefficient is inversely proportional to the square root of the volumetric fill fraction.

Some experimenters [Abouzeid et al. (1974), Hehl et al. (1978)] have studied the effects of rotational speed, feed rate, and drum incline in continuous flow drums. Because changing any one of these variables in a flowing drum will also change the drum fill, the effects observed by these experimenters are a combination of the effect of changing the fill in addition to the manipulated variable.

A number of experimenters have investigated the effects of particle properties on the dispersion coefficient. Abouzeid et al. (1974) reported that doubling the particle diameter has no effect on the axial diffusion, while Rao et al. (1991) found that increasing the particle diameter decreases the dispersion coefficient and Singh (1979) found increasing particle diameter increases the coefficient. Rutgers (1965) found that long particles give lower coefficients than spherical particles and that sticky particles give larger coefficients than non-cohesive particles. Rao et al. (1991) found that increasing the particle roughness increases the dispersion coefficient.

A couple of authors have attempted to correlate their experimental coefficients with the operating parameters and the properties of the granular material. Moriyama and

Suga (1974) give the following equation based on results from continuous flow experiments.

$$\frac{D_z}{u_z Z} = 9.46\times10^{-5}\left(\frac{F}{(2R)^3\rho n}\right)^{-0.516}\left(\frac{Z}{2R}\right)^{-0.524}\left(\frac{d_p}{2R}\right)^{0.604}(\tan\phi)^{-5.55} \tag{8}$$

Sai et al. (1990) give another equation also based on continuous flow experiments in which the two tracer materials were substantially different than the bulk material.

$$\frac{D_z}{u_z Z} = 0.000562\frac{\phi^{0.79}}{\gamma^{0.67} n^{1.06} \rho^{0.25}} \tag{9}$$

where the angle of repose ϕ and bulk density ρ are properties of the tracer material.

Sze et al. (1995) give the following equation for the axial dispersion of coal in a kiln fed a coal and zircon mixture.

$$\left(\frac{D_z}{u_z Z}\right)_c = \frac{0.0034}{\gamma^{0.11} n^{0.29} B^{0.94}}\left(\frac{d_{pz}}{d_{pc}}\right)^{0.28} \tag{10}$$

where B is the zircon-to-coal mass feed ratio.

Equations (8), (9) and (10) predict axial-dispersion coefficients of zero or no axial mixing in batch drums. This does not agree with experiments that indicate that dispersion coefficient to be about the same in batch and continuous flow drums.

2.2.4.2 Fundamental Correlations

Only a few researchers have attempted to relate the axial-dispersion coefficient to more fundamental parameters. Das Gupta et al. (1991) considered the motion of a particle in a rolling bed and derived the following equation for the axial-dispersion coefficient.

$$D_z = \frac{n\pi Z^3}{Rf(h)}\left[\cot^2\phi\left(\frac{dh}{dz}\right)^2 + \frac{1}{3}\varepsilon^2\right] \tag{11}$$

where $f(h)$ is a function of the bed depth h,

$$f(h) = 1 - \frac{(R-h)^2}{RL} \ln\left(\frac{R+L}{R-h}\right) \tag{12}$$

and L is half the length of the bed surface chord,

$$L = R\sqrt{1-\left(\frac{R-h}{R}\right)^2} \tag{13}$$

The empirical parameter ε is a measure of the particle's maximum deviation from the angle of steepest descent on the bed surface due to random collisions with other particles. Ideally, the parameter should only depend on the nature and size of the particles and the geometry of the surface region. The equation was compared to one set of experimental data and the maximum deviation angle needed to vary between 1° and 1.5° in order to obtain a fit.

The term containing *dh/dz* in Equation (11) represents the mixing due to the change in fill along a drum with continuous flow. The term is small in most continuous flow drums and equals zero for non-flowing drums. Therefore, Equation (11) indicates the mixing in both flowing and non-flowing drums is primarily due to the collision of particles in the active region as found in experiments. Equation (11) can be reduced to the following by setting *dh/dz* to zero and incorporating Equation (1):

$$D_z = \frac{\sqrt{2g}\,\varepsilon^2}{24}(n/n_c)^{1.0}(2R)^{1.5}\,g(h) \tag{14}$$

where $g(h)$ is the following function of bed depth:

$$g(h) = \left(1-\left(\frac{R-h}{R}\right)^2\right)^{3/2}\left(1-\frac{(R-h)^2}{RL}\ln\left(\frac{R+L}{R-h}\right)\right)^{-1} \tag{15}$$

The volumetric fill fraction is also a function of the bed depth.

$$X = \cos^{-1}\left(\frac{R-h}{R}\right) - \frac{L(R-h)}{R^2} \tag{16}$$

Function $g(h)$ is plotted against X in Figure 2-1. For fill fraction between 0.2 and 0.5, the value of $g(h)$ is near unity.

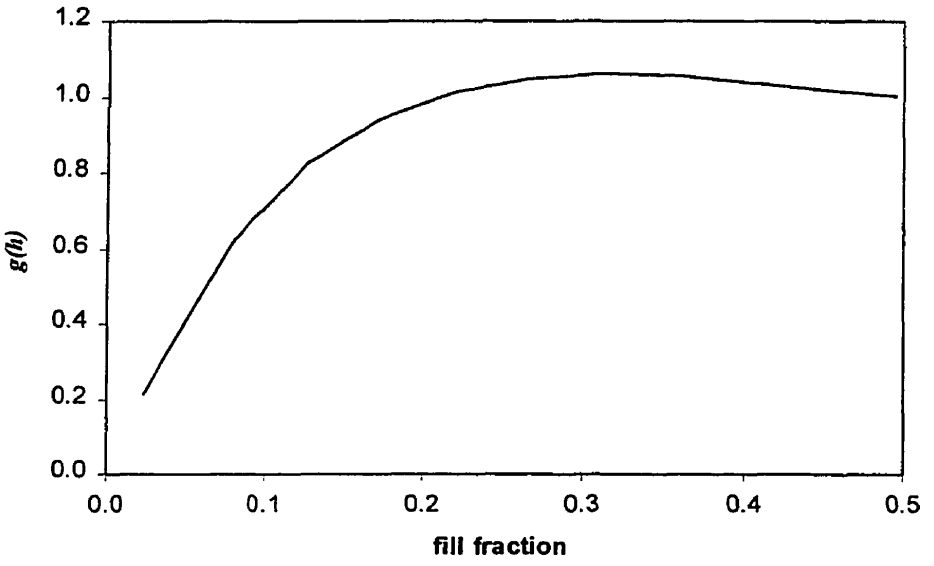

Figure 2-1 Relationship between bed depth function $g(h)$ to the volumetric fill fraction

Assuming that the deviation from the angle of steepest descent is not a function of speed, fill, or drum diameter, Equation (14) indicates that the axial-dispersion coefficient is proportional to the drum diameter raised to the 1.5 power, directly proportional to the relative rotational speed, and independent of the volumetric fill.

Rao et al. (1991) complement the model of Das Gupta et al. (1991) by considering axial diffusion in the active region. The overall axial-dispersion coefficient is related to the axial-diffusion coefficient in the active region by the following equation:

$$D_{z1} = D_z \frac{\langle \tau_1 \rangle + \langle \tau_2 \rangle}{\langle \tau_1 \rangle} \tag{17}$$

where $\langle \tau_1 \rangle$ is the mean time the particles spend in the active region and $\langle \tau_2 \rangle$ is the mean time particles spend in the static region. A method of approximating the times is given.

Rao et al. (1991) also proposed that both deviation from the angle of steepest descent and the axial-dispersion coefficient should correlate with the kinetic energy of the particles in the active region that depends on the dynamic angle of repose. Although no attempt is made to do so, it is suggested that the active region diffusion coefficient may be determined from collision theories for diffusion in granular flows.

2.3 Mixing in the Transverse Plane

The mixing of the granular material in the transverse plane is a result of both convection and diffusion (Hogg and Fuerstenau, 1972). Figure 2-2 shows the fixed paths or streamlines on which the particles tend to circulate. In the static region, the particles follow paths that are a constant distance from the wall. Particles leaving the static region at point A tend to return to the static region at point B, which is at the same radius r as point A. Particles in different streamlines circulate at different rates. The time for a particle to complete a cycle near the periphery of the bed is longer than the time near the core of the bed. Different circulation rates for the streamlines gives rise to convective mixing. Assuming a negligible active region thickness, Figure 2-3 illustrates convective mixing using a bed that is initially half black particles and half white particles. As the drum rotates, striations are formed increasing the length of the interface that divides the white and black particles. After only 0.6 of a drum revolution several striations have formed. The pattern illustrated in Figure 2-3 has been observed in experiments by Carley-Macauly and Donald (1962, 1964), Hogg and Fuerstenau (1972), and Lehmberg et al. (1977).

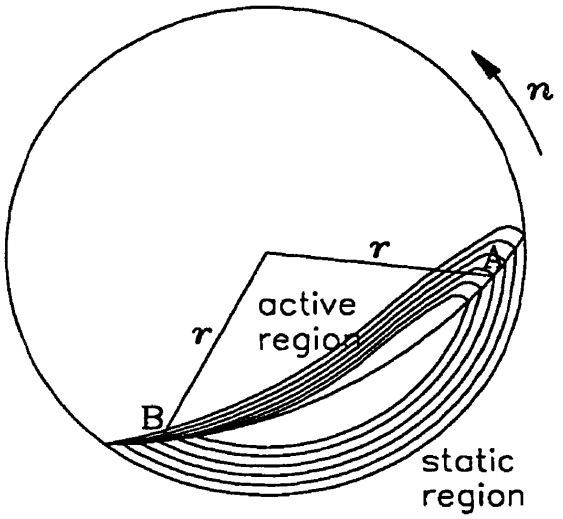

Figure 2-2 Streamlines in the transverse plane on which particles tend to circulate

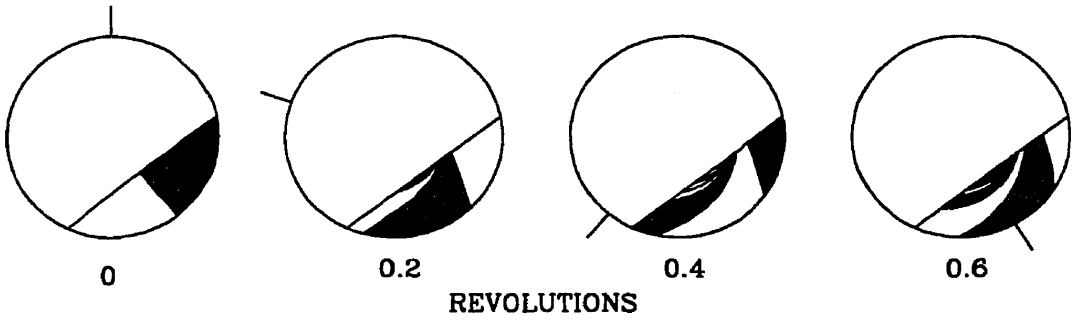

Figure 2-3 Striations produced by convective mixing in the transverse plane of a rotating drum

Convective mixing in a rotary drum is a function of the rotational speed and the degree of fill. If the thickness of the active region is constant then the mixing rate will be roughly proportional to the rotational speed. Convective mixing decreases as the drum fill increases. A drum with 50% fill has very little convective mixing as all streamlines have a similar circulation time.

While in the static region, particles stay on a streamline and have the same angular velocity as the wall. In the active region, however, particles may interchange between streamlines due to collisions with other particles. This random interchange of particles gives rise to dispersion in the radial direction. The collisions in the active region also affect the speed of a particle on a streamline, which gives rise to dispersion in the angular direction. Figure 2-4 from Inoue et al. (1970) illustrates the effects of convective mixing and diffusive mixing in the radial and angular directions in a rotating drum. The extent of the diffusive mixing is a function of the particle properties as well as the drum speed and degree of fill.

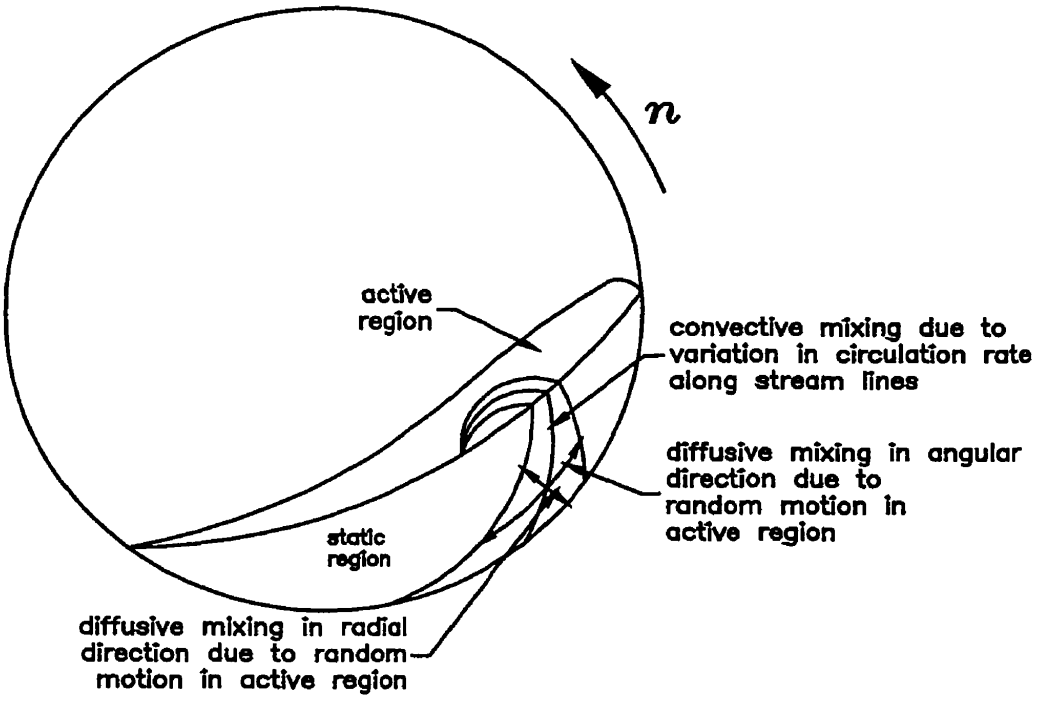

Figure 2-4 Effects of convective and diffusive mixing in the radial and angular directions in a rotating drum

Convective mixing may not be considered true mixing, as the black and white particles in Figure 2-3 are not truly mixed. However, by increasing the interfacial area between black and white sections, only a small amount of diffusive mixing is needed to obtain true mixing.

Methods that have been used to model mixing in the transverse plane of a rotating drum can be categorised as either transition probabilities or diffusion between streamlines. While Monte Carlo simulations could also be used to simulate transverse mixing, this has not been attempted. Oddly, while DEM has been used to study segregation in the radial direction in a rotating drum, it has not been used to study

transverse mixing except to observe the mixing phenomena such as by McCarthy and Ottino (1998).

2.3.1 Streamlines with Transition Probabilities

Pershin (1987) describes a model for both convective mixing and radial mixing that makes use of the concept of transition probabilities. The bed is divided into four concentric layers that correspond to the streamlines. In the active region, particles are assumed to stay in the current layer or migrate to the layer immediately above or below. The probability for each of the three possible paths is the same. Predictions are reported to agree with experimental results but few details are given about the experiments such as initial conditions, operating conditions and material properties.

A couple of authors have used a transition probability matrix to describe the migration of particles between the streamlines as they flow through the active region. The probability that a particle leaving the static region at radius r_i will re-enter the static region at radius r_j is given by p_{ij}, where $0 \leq p_{ij} \leq 1$, $1 \leq i \leq N$ and, $1 \leq j \leq N$. The sum of the probabilities for any streamline is equal to 1. Thus, the interchange of particles is described by an $N \times N$ matrix of probabilities where N is the number of streamlines.

A model by Inoue et al. (1970) simulates both convective and diffusive mixing using streamlines. A transition probability matrix is used to model the radial dispersion. The probability matrix is determined experimentally for several rotational speeds. The transition probability matrix is reduced and reported as a vector of standard deviations for each streamline. As the rotational speed is increased, the tendency for particles to remain on the same streamline after one cycle increases. Inoue et al. also include diffusive mixing in the angular direction with a distribution for the cycle time on each streamline. The rotational speed appeared to have little effect on the distribution of the cycle time for each streamline. The effects of fill and drum diameter are not studied.

Black (1988) describes a model to predict mixing and heat transfer in the radial direction. The effects of varying the number of streamlines as well as the transition probability matrix are studied. Although transition probability matrices are determined

from tracer experiments for different speeds, fill levels and drum diameters, the results are not used directly in the model.

2.3.2 Streamlines with Diffusion

Boateng and Barr (1996) simulate particle mixing and segregation in the transverse plane. Using rectangular co-ordinates in the active region and polar co-ordinates in the static region, the streamlines flow horizontally (parallel to the bed surface) in the active region and angularly (parallel to the wall) in the static region. The governing equations for elements in the active and static regions are derived for the steady-state case. No mixing or segregation occurs in the static region. Mixing in the radial direction is a result of diffusion in the vertical (perpendicular to the bed surface) direction in the active region.

$$D_{yl}\frac{\partial^2 c}{\partial y^2} - u_x(y)\frac{\partial c}{\partial x} = 0 \qquad (18)$$

Diffusion in the horizontal (parallel to the bed surface) direction is not included.

A finite difference model is developed to predict steady-state particle concentrations in the bed. Using their model for bed motion in a rotating drum based on dense-gas kinetic theory, the granular temperature and diffusion coefficient D_{yl} are predicted in addition to the thickness and velocity profile of the active region. The diffusion coefficient is assumed to be constant in the vertical direction but varies in the horizontal direction.

For the case with uniform particles (no segregation), the trivial solution of a perfectly mixed bed at steady state is obtained. When both mixing and segregation exist, the model predicts the extent of mixing at steady state. Good agreement is seen when steady-state predictions are compared to experimental results given by Henien (1983b).

Khakhar et al. (1997) describe a similar model that simulates mixing of uniform particles (no segregation). The model includes convective mixing due to the variation of the circulation rate with respect to particle's radial location and diffusive mixing perpendicular to the flow path in the active region. The amount of diffusive mixing is

determined by numerical integration of a particle's path in the active region. The movement perpendicular to the flow path is a Gaussian random number with a variance determined from an effective dimensionless diffusion coefficient $\overline{D}_{yl}$ and the size of the time step. The dimensionless diffusion coefficient perpendicular to the flow path in the active region was defined using the surface half-length L and the velocity ωL.

$$\overline{D}_{yl} = \frac{D_{yl}}{L(\omega L)} \tag{19}$$

Experiments were performed in a short 6.9-cm diameter cylinder at various speed, fill and particle size and type. The dimensionless coefficient was adjusted until the mixing rate matched the experimental results. A dimensionless coefficient of about 10^{-4} for sugar crystals and 3×10^{-3} for sugar balls was found to give the best fit with experiments.

2.4 Diffusion in Granular Flow

Since it is generally agreed that dispersive mixing of particles in a rotating drum in the axial and radial directions is primarily due to diffusion in the granular flow in the active region, it is useful to review the study of diffusion in granular flow in general. Both dense-gas kinetic theory and DEM have been used to study self-diffusion of particles in granular flow.

The use of the dense-gas kinetic theory analogies for granular flows (§ 2.1.3) not only provides a method to relate momentum transfer and kinetic energy but also provides a theoretical method of predicting particle diffusion. The diffusion coefficient is proportional to the particle diameter and the square root of the granular temperature as shown by the following equation (Hsiau and Hunt, 1993b)

$$D_y = \frac{d_p\sqrt{\pi Y}}{8(e_p+1)\nu g_o(\nu)} \tag{20}$$

where $g_o(\nu)$ is referred to as the radial distribution function. The recommended form of the function may vary but it equals unity at low-density flows and approaches

infinity as the particles approach a packed, rigid state. If the coefficient of restitution e_p is equal to 1 (elastic particles), Equation (20) reduces to the classical Chapman-Enskog result (Chapman and Cowling, 1970) for dense gases.

Hsiau and Hunt (1993b) consider particle diffusion in granular flow in a vertical chute. They compare mixing in the plane perpendicular to the flow direction from experiments and predictions using kinetic theory. Kinetic theory either over-estimates or under-estimates the amount of mixing depending on the form of the radial distribution function $g_o(\nu)$. They conclude that although kinetic theory is able to describe fundamental dependencies, it cannot accurately predict experimental results.

Savage and Dai (1993) use DEM (§2.1.4) to investigate self-diffusion in each direction in a simple granular flow. They found DEM gives diffusion coefficients about 20 to 40% larger than diffusion coefficients from dense-gas kinetic theory. The largest discrepancies are at higher solids fractions and for in-elastic particles. Note that both of these conditions apply to rotary kiln applications.

Figure 2-5 illustrates the co-ordinates used to study the components of diffusion in each direction due to a velocity shear. Figure 2-6 illustrates the non-dimensional components of the diffusion coefficient D^* in the three co-ordinate directions calculated from the simulation results. The non-dimensional coefficient is given by the following equation:

$$D^* = \frac{D}{d_p^2 \, dv_x/dy} \tag{21}$$

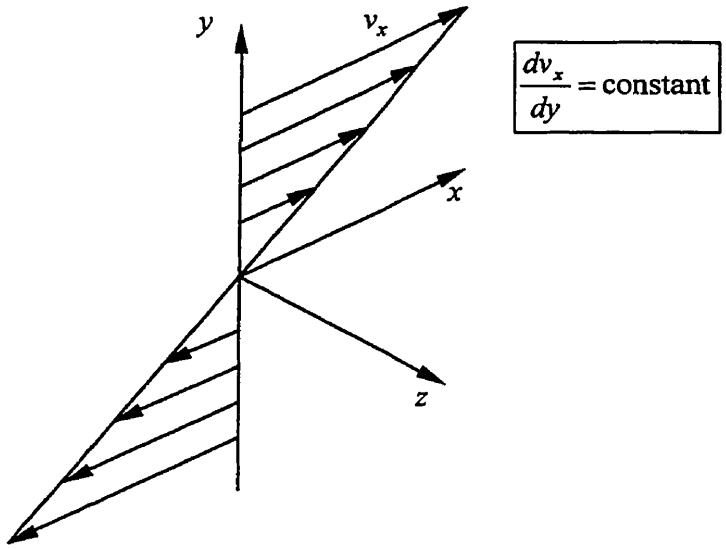

Figure 2-5 Co-ordinates for the DEM study of 3-D diffusion in simple granular shear by Savage and Dai (1993)

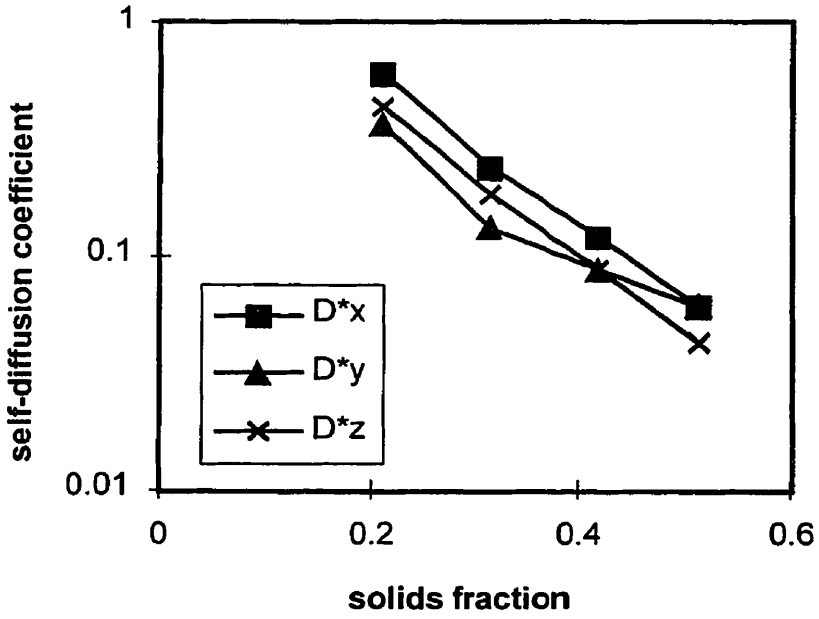

Figure 2-6 Non-dimensional diffusion coefficients in three co-ordinate directions for e = 0.9 (Savage and Dai, 1993) predicted by DEM

As expected, all components of the coefficient decrease as the solids fraction increases. The simulation predicts that the diffusion coefficient is not isotropic as the dense-gas kinetic theory assumes, with the coefficient in the stream-wise direction being larger by about 20%.

From DEM computer simulations, Campbell (1997) found that the diffusion in the x-direction (parallel to the flow direction) is always larger than that in the z-direction (perpendicular to the flow and the shear gradient) which is, in turn, larger than that in the y-direction (perpendicular to the flow and parallel to the shear gradient. The difference between the y- and z-direction diffusion became insignificant at higher densities and coefficients of restitution.

Hsiau and Jang (1998) and Hsiau and Shieh (1999 & 2000) confirmed with real experiments in a shear cell that the particle diffusion in the stream-wise direction was greater than that in the transverse direction. Applying this finding of anisotropic diffusion to the active region in a rotating drum, one would expect diffusion in the direction parallel to the bed surface and perpendicular to the rotation axis to be the largest. Diffusion in the axial direction would be slightly larger than diffusion in the vertical direction (perpendicular to the bed surface and perpendicular to the rotational axis). The significance of the relationship between diffusion in different directions in granular flow is discussed in the next chapter.

2.5 Heat Transfer

A few authors consider the effect that transverse mixing in a bed of granular solids has on heat transfer in rotary drums. Boateng (1998) highlights the contribution of radial-dispersion of particles on the gas-to-bed heat transfer in rotary kilns. Diffusion increases the effective thermal conductivity in the active region by as much as tenfold.

Leger et al. (1993) mixed cold solids into a preexisting bed of hot solids in a 0.61 m diameter drum. The temperature of the bed was measured at fixed locations. Oscillations in the temperature readings decayed with time until a uniform temperature

was reached. The rotational speed and the fill fraction affected the rate that the oscillations decayed. It was concluded that mixing in the bed greatly augmented the initial rate of heat transfer to the cold solids. It is interesting to note that, in the ATP retort zone, hot shale ash is mixed with cold oil shale. The rate of hydrocarbon evolution is related to the mixing of the hot and cold streams.

2.6 Summary

The thickness and the velocity profile in the active region of a bed of granular material in a rotating drum have been represented by a number of methods. Fluid flow analogy methods require experimentally obtained flow properties. Models employing dense-gas kinetic theory assume a flat upper surface and either an active region thickness or a velocity profile for the active region. Discrete element modelling gives the most realistic predictions with no assumptions but requires information about hard to measure particle properties and is currently limited to a system of a few thousand particles.

Mixing in the axial direction is primarily due to random particle collisions in the granular flow of the active region. The mixing can be represented by a number of models but the dispersion model is the most popular for several reasons. The model gives a good fit with experimental results. A single parameter, the dispersion coefficient, can quantify the mixing in both batch and continuous flow drums. There is no upper limit to the number of particles that can be modelled, and there is plenty of experimental data available in the literature from both batch and continuous flow experiments.

In the transverse plane, the particles tend to circulate on streamlines. Mixing is a result of both convection and diffusion. Convective mixing is due to the different circulation rates of the particles depending on the proximity of their streamline to the wall. Diffusive mixing is due to particle collisions in granular flow in the active region. Particles migrate to different streamlines and the particle speed deviates from the mean. The result is dispersion in the radial and angular directions. Only a few models have been proposed and only a small amount of experimental mixing data exists.

Diffusive mixing in a granular flow is anisotropic, but components of the diffusion coefficient differ only by about 20% in the three directions. The greatest diffusion coefficient is in the direction of flow.

CHAPTER 3
DISPERSION COEFFICIENTS FROM PUBLISHED DATA

Published results have shown that axial mixing in both batch and continuous flow rotating drums is primarily due to random particle collisions in the active region and can be represented by the diffusion equation. Mixing in the transverse plane is a combination of convective mixing and diffusion in the radial and angular directions. In this chapter, experimental data available in the literature are used to determine the particle dispersion coefficients in the axial, radial and angular directions of a granular bed in a rotating drum. The effects of rotational speed, drum diameter, fill level and particle size on the coefficients are determined.

Even though the actual particle diffusion occurs in the active region, the axial-dispersion coefficient determined here is the effective diffusion coefficient for the entire bed. If no diffusion occurs in the static region, then the product of the axial-diffusion coefficient and the time in the active layer equals the product of the axial-dispersion coefficient and the total cycle time. The axial-dispersion coefficient for the entire bed is related to the axial-diffusion coefficient in the active region by the following equation (Rao et al., 1991).

$$D_z = D_{z1} \frac{\langle \tau_1 \rangle}{\langle \tau_1 \rangle + \langle \tau_2 \rangle} \tag{22}$$

where $\langle \tau_1 \rangle$ and $\langle \tau_2 \rangle$ are the mean times the particle spends in the active region and the static region, respectively.

The radial-dispersion coefficient is determined for the radial distance in the static region of the bed even though the actual diffusion is due to the transition of particles among the streamlines in the active region. The radial-dispersion coefficient for the static region is related to the vertical-diffusion coefficient in the active region by the following equation.

$$D_r = D_{y1} \left(\frac{h - \delta_0}{\delta_0} \right)^2 \frac{\langle \tau_1 \rangle}{\langle \tau_1 \rangle + \langle \tau_2 \rangle} \tag{23}$$

where δ_0 and h-δ_0 are the thicknesses of the active region and the static region, respectively. The equation agrees with the observation that diffusion across a thin active region is magnified in a thicker static region.

Similarly, the angular-dispersion coefficient for the static region is related to the horizontal-diffusion coefficient in the active region by the following equation.

$$D_\theta = D_{x1}\left(\frac{2L+\beta R}{2L}\right)^2 \frac{\langle \tau_1 \rangle}{\langle \tau_1 \rangle + \langle \tau_2 \rangle} \tag{24}$$

where $(2L+\beta R)/2L$ is the ratio of the length of the total circulation path to the length of the active region.

If particle diffusion in the active region can be assumed to be isotropic (D_{z1} = D_{y1}= D_{x1}), then the radial- and angular-dispersion coefficients for the static region are related to the axial-dispersion coefficient for the entire bed by the following equations.

$$D_r = D_z\left(\frac{h-\delta_0}{\delta_0}\right)^2 \tag{25}$$

$$D_\theta = D_z\left(\frac{2L+\beta R}{2L}\right)^2 \tag{26}$$

With some knowledge of the dimensions of the active and static regions, these equations allow the radial- and angular-dispersion coefficients to be determined from data available for axial-dispersion. The validity of this hypothesis is examined in the results obtained in this chapter.

3.1 Axial-Dispersion Coefficient

Axial-dispersion coefficients in a rotating drum have been determined by a variety of methods by numerous authors. In some cases, experimenters report results of experiments but have not determined the coefficient. This section gathers all the available experimental results, determines the axial-dispersion coefficients and develops correlations for the effects of rotational speed, level of fill, drum diameter and particle diameter.

The axial-dispersion coefficient has been determined experimentally using tracers in both batch and continuous flow drums.

3.1.1 Continuous Flow Experiments

Axial dispersion in a flowing drum is described by the one-dimensional diffusion equation

$$\frac{\partial c}{\partial t} = D_z \frac{\partial^2 c}{\partial z^2} - u_z \frac{\partial c}{\partial z} \tag{27}$$

The axial-dispersion coefficient D_z from a flowing drum is almost always determined from the residence time distribution (RTD). The RTD is measured at the outlet end for a pulse of tracer injected at the feed end. An example of RTD data from Ray et al. (1994) is plotted in Figure 3-1. To derive the RTD equation, Equation (27) is first re-written with dimensionless variables. The dimensionless Peclet number is related to the dispersion coefficient by the following equation.

$$Pe = \frac{u_z Z}{D_z} \tag{28}$$

Dimensionless time, length and concentration variables are:

$$\theta = \frac{t}{\langle t \rangle}, \quad \zeta = \frac{z}{Z}, \text{ and } C(\theta, \zeta) = \frac{c(t,z)}{c_o} \tag{29}$$

The one-dimensional diffusion equation in dimensionless form is:

$$\frac{\partial C}{\partial \theta} + \frac{\partial C}{\partial \zeta} = \frac{1}{Pe} \frac{\partial^2 C}{\partial \zeta^2} \tag{30}$$

Prior to injecting the tracer at the inlet end, there is no tracer in the drum.

$$C(0, \zeta) = 0 \tag{31}$$

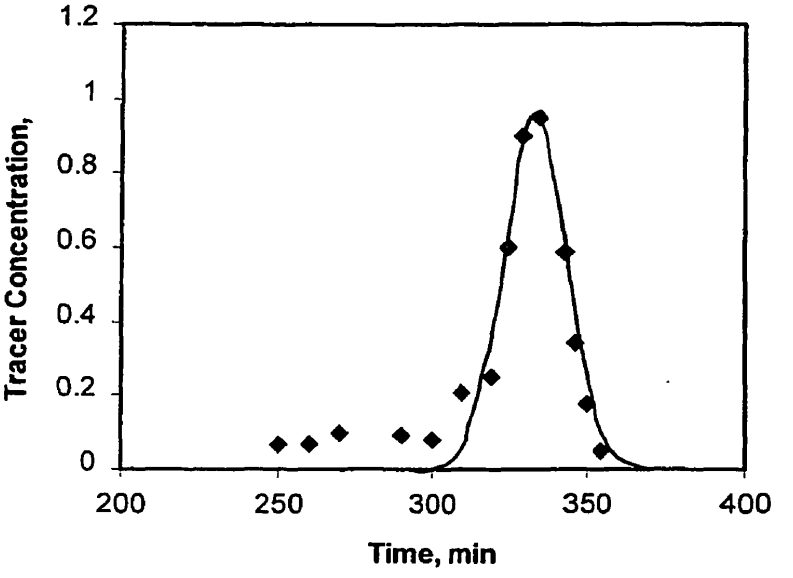

Figure 3-1 Example of residence time distribution in a continuous flow rotary kiln using a pulse of tracer injected at feed end from Ray et al. (1994)

The boundary conditions at any time are:

$$C(\theta,0) - \frac{1}{Pe}\frac{\partial C(\theta,0)}{\partial \zeta} = \chi(\theta)$$

$$\frac{\partial C(\theta,1)}{\partial \zeta} = 0 \qquad (32)$$

where $\chi(0) = 1$ and $\chi(\theta) = 0$.

Abouzeid et al. (1974) and Karra and Fuerstenau (1977) give the exact solution for the tracer residence time from Equation (30) with the conditions given by Equations (31) and (32). The dimensionless standard deviation from the mean residence time is related to the Peclet number by the following equation.

$$\sigma_\theta^2 = \frac{2}{Pe} - \frac{2}{Pe^2}\left[1 - \exp(-Pe)\right] \qquad (33)$$

where the dimensionless standard deviation of the residence time is the ratio of the standard deviation and the mean time.

For large Peclet numbers ($Pe > 50$), which is the case for low axial mixing in most rotating drums, Equation (33) can be simplified to the following equation that is used to approximate the axial-dispersion coefficient from the mean and standard deviation of the tracer residence time.

$$D_z = \frac{Z^2 \sigma_t^2}{2\langle t \rangle^3} \tag{34}$$

The mean residence time can also be calculated from the measured hold-up and feed rate. The result agrees with the mean time from the tracer response if there are no dead zones in the drum.

Sources of the results of RTD experiments of a continuously fed rotating drum are listed in Table 3-1. In cases when the axial-dispersion coefficient is not reported, it is determined by one of the following methods:

1. if the Peclet number is given, then the dispersion coefficient is determined using Equation (28),
2. if the mean and standard deviation of the residence time are given, then the dispersion coefficient is determined using Equation (34), and
3. if only the residence time distribution curve is given, then the mean and standard deviation of the residence time are calculated and the dispersion coefficient is determined using Equation (34).

A total of 124 coefficient values are obtained from 15 sources. The coefficients and most of the operating parameters such as drum diameter, rotational speed, fill and particle type and size are given in Table A-1 in Appendix A. Most of the experimenters vary the rotational speed and fill, but consider only one type of material and drum diameter. Drum diameters range from 0.080 m to 0.90 m. Coefficients are from all modes of bed behaviour and range from 1×10^{-7} to 1×10^{-4} m^2/s.

Table 3-1 Sources of experimental data from continuous-feed rotating drums from which particle dispersion coefficients in the axial direction are determined

Source	Drum diameter, m	Granular material	Particle diameter, mm
Karra and Fuerstenau (1977)	0.08	dolomite	0.357
Abouzeid et al. (1974)	0.08	dolomite	0.359
Rogers and Gardner (1979)	0.095	dry powder	0.335
McTait et al. (1998)	0.105	ballitini	0.2
Mu and Perlmutter (1980)	0.102	rice	2x5
Hatzilyberis and Androutsopoulos (1999)	0.12	lignite	9.6
Ang et al. (1998)	0.14	zircon +coal	1.7, 2.7
Sai et al. (1990)	0.147	ilmenite	0.2
Rutgers (1965)	0.16	rice, oats	2
Tscheng (1978)	0.1905	polystyrene	1.9x3.1x3.6
Hehl et al. (1978)	0.250	soda	0.137
Sugimoto (1968)	0.255	sand	1.5
Lebas et al. (1995)	0.6	coal	0.5-20
Wes et al. (1976)	0.6	potato starch	0.015-0.10
Rutgers (1965)	0.765	oat groats	2
Ray et al. (1994)	0.90	coal + ore	6-15

3.1.2 Batch Experiments

For batch or non-flowing experiments, the net axial velocity is zero, $u_z = 0$. From Equation (27), the one-dimensional diffusion equation reduces to:

$$\frac{\partial c}{\partial t} = D_z \frac{\partial^2 c}{\partial z^2} \tag{35}$$

Axial-dispersion coefficients for horizontal, rotating drums have been determined from batch experiments using several different initial conditions. Figure 3-2 illustrates the initial conditions used in batch experiments to measure axial mixing.

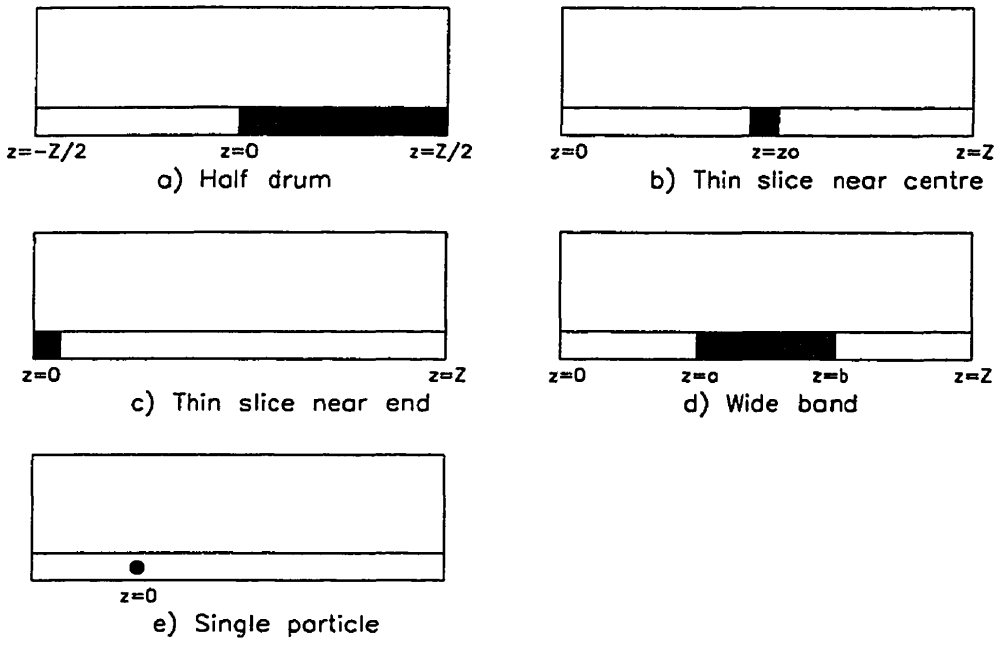

Figure 3-2 Initial tracer distributions used in a rotating drum to measure axial dispersion in batch experiments

Half drum

Hogg et al. (1966), Rao et al. (1991), Cahn and Fuerstenau (1967), Carley-Macauly and Donald (1962) and Wrightman and Muzzio (1998) begin their experiments with the drum divided at the centre of its length. Half the drum contains particles, which can be distinguished from the particles in the other half of the drum as shown in Figure 3-2a. Mathematically, the initial conditions are:

$$C(0,z) = 0 \quad (-Z/2 \le z < 0)$$
$$= 1 \quad (0 < z \le Z/2) \tag{36}$$

With no diffusion at either end of the drum, the boundary conditions are:

$$\left.\frac{\partial C(t,z)}{\partial z}\right|_{z=-Z/2} = 0$$

$$\left.\frac{\partial C(t,z)}{\partial z}\right|_{z=Z/2} = 0 \qquad (37)$$

The dispersion coefficient can be determined from the experimental results in a number of ways as shown by Hogg et al. (1966). If the mixing time is large, then the solution to Equation (35) with initial and boundary conditions given by Equations (36) and (37) is:

$$C(t,z) = \frac{1}{2} + \frac{2}{\pi}\exp\left(\frac{-\pi^2 D_z t}{Z^2}\right)\sin\frac{\pi z}{Z} \qquad (38)$$

The axial-dispersion coefficient at any time can be determined from the particle distribution by plotting C against $\sin(\pi z/Z)$. The result is a straight line with a slope equal to $(2/\pi)\exp(-\pi^2 D_z t/Z^2)$. The axial-dispersion coefficient is calculated from this slope.

The standard deviation of the reference material concentration at any long mixing time and the dispersion coefficient are related by the following equation:

$$\sigma_z^2(t) = \frac{2}{\pi^2}\exp\left(-\frac{2\pi^2 D_z t}{Z^2}\right) \qquad (39)$$

A plot of ln σ_z against t gives a straight line with slope $-\pi^2 D_z/Z^2$. The axial-dispersion coefficient can also be calculated from this slope.

If the mixing time is short, the drum can be treated as an infinite cylinder and Equation (35) can be solved to give:

$$C(t,z) = \frac{1}{2}\left(1 + \operatorname{erf}\frac{z}{2\sqrt{D_z t}}\right) \qquad (40)$$

A normal probability plot of $C(t,z)$ versus z yields a straight line of slope $1/\sqrt{(2D_z t)}$.

The standard deviation of the reference material concentration at short mixing time is related to the dispersion coefficient by the following equation:

$$\sigma_z^2(t) = \sigma_z^2(0)\left(1 - \frac{4}{Z}\sqrt{\frac{2D_z t}{\pi}}\right) \tag{41}$$

A plot of the variance σ_z^2 versus square root of time gives a straight line of slope $-4/Z\sqrt{2D_z/\pi}$.

If the data are from a DEM computer simulation, then the average location of the particles is more accurately determined than the particle concentration. Kohring (1995) gives the following solution for the average particle position:

$$\langle z \rangle = \frac{8Z}{\pi^3}\exp\left(-\frac{\pi^2 D_z t}{Z^2}\right) \tag{42}$$

A plot of ln $\langle z \rangle$ against t gives a straight line with slope $-\pi^2 D_z/Z^2$. The axial-dispersion coefficient from the DEM experiment can be calculated from this slope.

Thin slice near centre

Shoji et al. (1973) begin their batch experiments with a thin slice of tracer loaded perpendicular to the axis at distance ξ from the end of the drum as shown in Figure 3-2b. Mathematically, the initial condition is:

$$C(0,z) = 0 \quad (0 \le z \le Z)$$
$$C(0,z_o) = 1 \tag{43}$$

For short mixing times, the drum can be treated as if it has infinite length.

Solution of Equation (35) gives the following equation for the cumulative mass fraction of tracer:

$$\int_0^z C(t,z)dz = \frac{1}{2}\left(1 - \operatorname{erf}\frac{z_o - z}{2\sqrt{D_z t}}\right) \tag{44}$$

A plot of the cumulative mass fraction of tracer on a normal probability scale versus z gives a straight line from which the dispersion coefficient can be determined.

No method is given to solve for the dispersion coefficient from the concentration of tracer after long mixing times when the effect of the end walls can no longer be neglected.

Thin slice at end

Hogg et al. (1969) begin batch experiments with a thin slice of tracer loaded perpendicular to the axis at one end of the drum as shown in Figure 3-2c. Mathematically the initial conditions are:

$$C(0,z) = 0 \quad (0 \le z \le Z)$$
$$C(0,0) = 1 \tag{45}$$

For short mixing times, the drum can be treated as a semi-infinite cylinder and the solution of Equation (35) is given by the following equation:

$$C(t,z) = \frac{1}{2\sqrt{\pi D_z t}} \exp\left(-\frac{z^2}{4 D_z t}\right) \tag{46}$$

The axial-dispersion coefficient at any short time can be determined from the experimental results by plotting ln C against z^2. The result is a straight line with a slope equal to $-1/(4D_z t)$. The axial-dispersion coefficient is calculated from the slope.

No method is given to solve for the dispersion coefficient from the concentration of the tracer after long mixing times when the effect of the far wall can no longer be neglected.

Wide band

Singh (1979) begins his experiments with a wide band of tracer perpendicular to the axis near the centre of the drum as shown in Figure 3-2d. The initial conditions are:

$$C(0,z) = 0 \quad (0 \le z < z_1, \; z_2 < z \le Z)$$
$$= 1 \quad (z_1 \le z \le z_2) \tag{47}$$

The effects of the end wall are included in the boundary conditions:

$$\left.\frac{\partial C(t,z)}{\partial z}\right|_{z=0} = 0$$

$$\left.\frac{\partial C(t,z)}{\partial z}\right|_{z=Z} = 0 \qquad (48)$$

Equation (35) is solved with these initial and boundary conditions using a finite difference approximation and numerical integration. The dispersion coefficient is found by trial and error to get the best fit to the measured concentration profiles.

Single particle

Parker et al. (1997) determine the axial-dispersion coefficient by tracking the random movement of a single radioactively labelled tracer particle in a batch drum. The tracer particle has the same properties as the other particles in the drum and is located so the end walls do not affect its movement. At the start of each time increment ($t = 0$), the tracer is at the origin $z = 0$ as shown in Figure 3-2e. The displacement for numerous short time increments gives a distribution of displacements for the specified time increment. With no drum end effects on the axial movement of the tracer particle, the drum is treated as infinitely long in the axial direction. The distribution of the tracer displacement z is found by solving the diffusion equation with the same initial and boundary conditions as the drum with a thin slice of tracer:

$$C(t,z) = \frac{1}{\sqrt{4\pi t D_z}} \exp\left[-\frac{z^2}{4tD_z}\right] \qquad (49)$$

The axial-dispersion coefficient is related to the standard deviation of the tracer displacement in the axial direction after time interval t by the following equation.

$$D_z = \frac{\sigma_z^2}{2t} \qquad (50)$$

A plot of the variance of the tracer displacement and the time interval gives a straight line with a slope of $2D_z$.

Sources of experimental data from batch rotating drums from which particle dispersion coefficients in the axial direction are determined are listed in Table 3-2. The nine sources provide 55 coefficients. The coefficients and most of the operating parameters such as drum diameter, rotational speed, fill and particle type and size are given in Table A-2 in Appendix A. Most of the experimenters vary the rotational speed and fill, but consider only one type of material and drum diameter. The drum diameters range from 0.076 m to 0.144 m. Coefficients range from 1×10^{-7} to 1×10^{-4} m^2/s.

Table 3-2 Sources of experimental data from batch rotating drums from which particle dispersion coefficients in the axial direction are determined

Source	Drum diameter, m	Granular material	Particle diameter mm
Rao et al. (1991)	0.076	sodium (bi)carbonate	0.125, 0.214, 0.388
Singh (1979)	0.10	glass beads	0.68 - 0.78
Shoji et al. (1973)	0.095	silicon carbide	0.335
Hogg et al. (1969)	0.102	glass beads	0.100
	0.051	quartz	0.253
Hogg (1969)	0.10	glass beads	0.090
Cahn and Fuerstenau (1967)	0.102	lucite beads	6.35
Carley-Macauly and Donald (1962)	0.102	sand	0.6-0.85
Wrightman and Muzzio (1998)	0.0106		0.066
Parker et al. (1997)	0.136	glass beads	1.5
	0.144	glass beads	3
	0.100	glass beads	3

3.1.3 Empirical Correlations

Equations of the following form are derived using multiple regression to relate the 179 axial-dispersion coefficients listed in Tables A-1 and A-2 in Appendix A to the relative speed, diameter, particle size and volumetric fill.

$$D_z = k\,(n/n_c)^a\,(2R)^b\,d_p^c\,X^d \tag{51}$$

where D_z = axial-dispersion coefficient, m^2/s

n/n_c = relative speed, fraction of critical
R = drum radius, m
d_p = particle diameter, m, and
X = fill level, volume fraction.

Values for the fitting parameters k, a, b, c, and d are determined for all the data together and for individual types of bed behaviour. Because some experimenters do not report the type of bed behaviour, drums rotating at less than 3% of the critical speed are assumed to have slumping behaviour. Drums rotating between 3% and 30% of critical speed are assumed to have rolling or cascading behaviour. Drums rotating at more than 30% of critical speed are assumed to have cataracting behaviour. The effect of bed depth on the bed behaviour is neglected. However, only drums that are less than 50% full are used in the regressions. Results are summarised in Table 3-3.

Table 3-3 Parameters (regression coefficients) for axial-dispersion coefficients using Equation (51), $X < 0.5$

Bed behaviour	k	a	b	c	d
All modes $n/n_c<1$	1.10×10^{-3}	0.39	1.15	0.46	-0.43
Slumping $n/n_c<0.03$	4.27×10^{-6}	-0.35	0.85	0.21	-0.50
Rolling and cascading $0.03<n/n_c<0.3$	5.82×10^{-4}	0.44	1.29	0.35	-0.55
Cataracting $0.3<n/n_c<1.0$	4.30×10^{-2}	0.90	1.22	0.87	-0.02

The test for significance (F-test) of the regression model indicates that for all modes together and for individual bed behaviour modes there is good confidence of a relationship. Axial-dispersion coefficients predicted by Equation (51) with parameters from Table 3-3 for all bed behaviour modes are compared to the measured data in Figure 3-3. The standard error of the predicted coefficient is plus 100% and minus 50%. The standard errors of the predicted coefficient for individual bed behaviour modes are similar or less. The error between the predicted and experimental coefficients is due to the differences in the properties (stickiness, roughness, shape) of the variety of materials

used, sliding behavior and experimental error. In general, the coefficients from batch experiments are slightly lower than the coefficients from continuous flow experiments at the same speed, fill and diameters. This suggests that some axial mixing in continuous flow drums could be due to the non-uniform axial velocity from the core to the periphery of the bed.

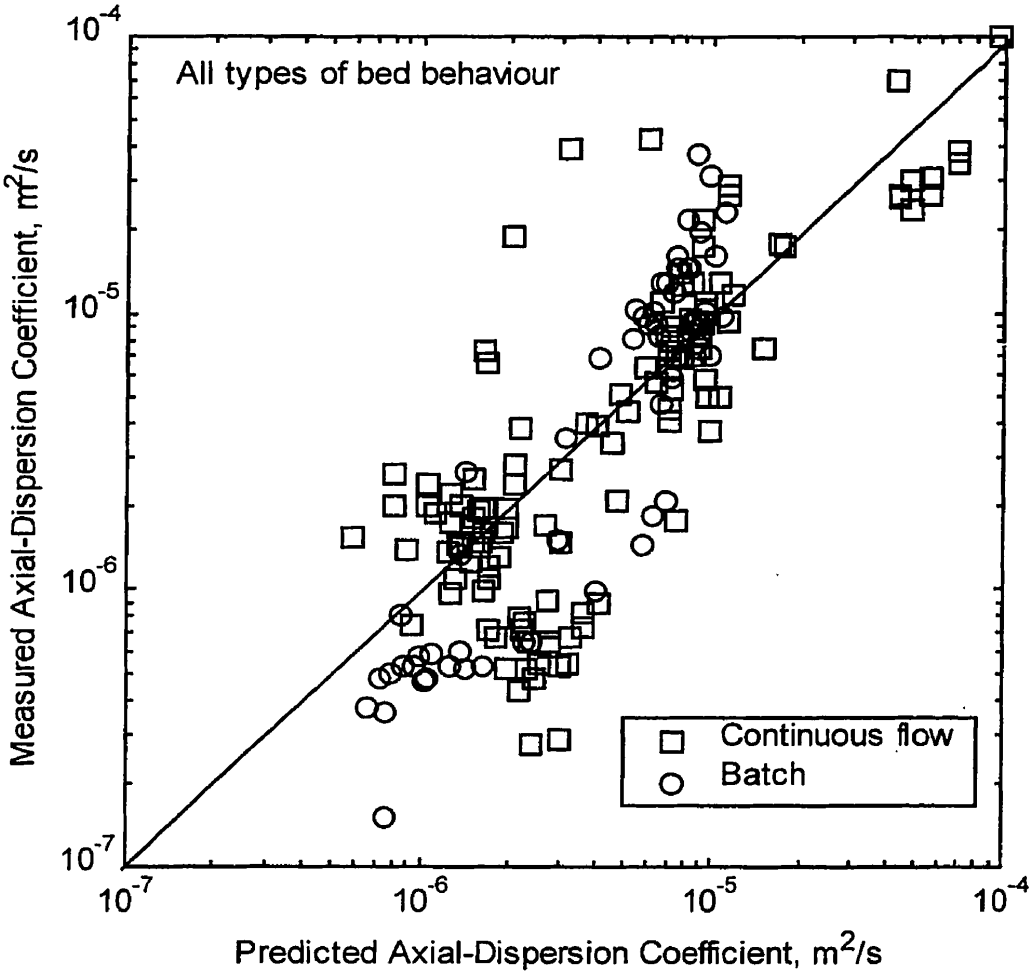

Figure 3-3 Comparison of axial-dispersion coefficients given by Equation (51) with fitting parameters for all modes of bed behaviour to experimental coefficients

Effect of Drum and Particle Diameter

Fitting parameters in Table 3-3 indicate that the axial-dispersion coefficient increases when the drum or the particle diameter is increased. The regression indicates that for all types of behaviour the coefficient is approximately proportional to the drum diameter ($D_z \propto R$). The majority of the tests used to derive the correlations use drums with diameters of about 0.1 m and the largest drum was 0.90 m. This is much smaller than the size of a typical industrial drum that is 3 to 5 m diameter. Therefore, considerable extrapolation is required to apply Equation (51) to industrial-sized drums.

For all types of behaviour, the axial-dispersion coefficient increases proportionally with the square root of the particle diameter ($D_z \propto d_p^{0.5}$). This is qualitatively consistent with both dense gas kinetic theory and DEM experiments.

Effect of Speed

For slumping behaviour, the axial-dispersion coefficient appears to decrease with an increase in the rotational speed. For rolling and cascading behaviour, the coefficient is approximately proportional to the square root of the speed ($D_z \propto n^{0.5}$). For cataracting behaviour, the coefficient is nearly directly proportional to the speed ($D_z \propto n$).

Effect of Fill

For slumping, rolling and cascading behaviour, the axial-dispersion coefficient decreases as the volumetric fill is increased. The coefficient is approximately inversely proportional to the square root of the fill fraction ($D_z \propto X^{-0.5}$). For cataracting behaviour, the fill has little effect on the coefficient ($D_z \propto X^0$). However, the test of significance on individual regression coefficients (t-test) indicated that there is a poor relationship between the coefficient and fill for cataracting behaviour. All other regression coefficients for both individual bed behaviour and all modes together are significant.

Comparison to Drums with Lifting Flights

Sherritt et al. (1996) report the axial-dispersion coefficients for experiments with rotating drums with flights attached to the wall to lift and spill the particles. The coefficients for drums with lifting flights are about two orders of magnitude larger ranging between 1×10^{-5} to 1×10^{-3} m^2/s. This can be expected considering the additional energy imparted on the particles.

With or without lifting flights, the effect of drum diameter on the coefficient is about the same ($D_z \propto R$). The effect of rotational speed is similar to that in a cataracting drum ($D_z \propto n$). This is likely due to the particles in both a cataracting drum and a drum with lifting flights bounce after made airborne. Unlike drums without flights, the dispersion coefficient appears to increase with hold-up in drums with flights ($D_z \propto X$).

3.2 Radial-Dispersion Coefficient

While experimental results for axial mixing in rotating drums are widely reported, only a few attempts have been made to measure diffusive mixing in the radial direction. Even fewer attempts have been made to determine the radial-dispersion coefficient.

Hogg and Fuerstenau (1972) provide data from experiments that begin with an initial condition that illustrates convective mixing (See Figure 2-3). The experimental data is used to determine the additional mixing due to diffusion in the radial and angular directions. The radial-dispersion coefficient D_r in the small experimental drum is reported to be about 0.5×10^{-7} m^2/s.

Using a model for bed motion in a rotating drum based on dense-gas kinetic theory, Boateng (1993) predicts that the vertical-diffusion coefficient in the active region D_{yl} in a typical industrial rotary kiln (larger than 1 m) is about 1×10^{-7} m^2/s. No experimental data are available for comparison. The radial-dispersion coefficient D_r would be larger.

Black (1988), Clément et al. (1995) and Inoue et al. (1970) report data from radial mixing experiments in rotating drums but do not determine the radial-dispersion

coefficient. In each set of experiments, data are collected by tracking the movement of a single tracer particle in the transverse plane. The tracer is viewed through a transparent end wall. Boateng (1993) reports that data collected in this manner may give slightly more mixing due to the end wall effects. The end walls cause the particles to remain in the static region longer, thus reaching a higher position before shearing into the active region. Due to the higher release position, the velocity of the particles in the active region is higher and the thickness of the active region is less than for the bed that is not influenced by the end wall. Due to the higher shear gradient in the active region, it is likely that the presence of the end wall has increased the diffusive mixing in most of the experimental observations.

All three experimenters describe the same behaviour for the tracer particle. While in the static region, the tracer particle follows a path at a fixed radius. Upon reaching the surface of the bed, the tracer tumbles down the surface and re-enters the static region. The radius that the tracer re-enters the static region can change due to mixing in the active region but the tracer tends to re-enter the static region near the same radius that it left.

Similar data were collected by each of the experimenters. The static region was divided into a number of concentric layers of equal thickness. A run consisted of several thousand cycles of the tracer particle passing from the active and to the static region and back. For each cycle, the layer in the static region occupied by the tracer was determined and recorded.

Using the data collected in these experiments, the radial-dispersion coefficients can be determined just as Parker et al. (1997) use axial distribution data for a single tracer particle to determine the axial-dispersion coefficient in a non-flow drum. However, a couple of factors complicate the determination of the radial-dispersion coefficient. The end walls in the axial mixing experiments are far enough from the tracer particle that their effect on the axial dispersion can be ignored, simplifying the analysis. For the radial mixing experiments, the boundaries in the radial direction (the outer periphery and the centre of the bed) are a short distance if not immediately next to the tracer particle and

cannot be ignored. Also, in the axial mixing experiments, because the cross-sectional area of the bed perpendicular to the drum axis is constant, the probability distribution is the same as the concentration distribution. In the radial mixing experiments, the area perpendicular to the dispersion direction increases as the radius increases. The probability distribution is not equal to concentration distribution.

Parker et al. (1997) showed that the probability distribution of a single particle for many short time intervals can be treated in the same manner as the results from an experiment that begins with a thin layer of tracer. In the axial mixing experiments, a thin layer of tracer at either one end or near the centre of the drum is used to determine the dispersion coefficient by Hogg et al. (1969) and Shoji et al (1973), respectively. In both cases, by using short mixing times, the effect of the end walls can be neglected. Because the transverse boundaries on the radial dispersion cannot be ignored, neither of the solution methods used in these axial mixing experiments can be used here. Instead, a method analogous to the method used by Singh (1979) to determine axial-dispersion coefficients for a non-flow experiment initiated with a wide band of tracer is used. The diffusion equation is solved with the appropriate initial and boundary conditions using a finite difference approximation and numerical integration. The dispersion coefficient is found by trial and error to get the best fit to the measured probability distribution after one cycle.

To derive the finite difference approximation, the static region is divided into N concentric layers as shown in Figure 3-4. Layer 1 is at the core and layer N is next to the wall. Each layer has thickness Δr. A mass balance for the jth concentric layer in the static region is:

$$\begin{bmatrix}\text{Diffusion rate}\\ \text{of tracer}\\ \text{into layer } j\end{bmatrix} = \begin{bmatrix}\text{Diffusion rate}\\ \text{of tracer out}\\ \text{of layer } j\end{bmatrix} + \begin{bmatrix}\text{Accumulation}\\ \text{rate of tracer}\\ \text{in layer } j\end{bmatrix} \tag{52}$$

The diffusion and accumulation rates are expressed in terms of tracer concentration.

$$-AD_r\left.\frac{\partial C}{\partial r}\right|_j = -AD_r\left.\frac{\partial C}{\partial r}\right|_{j+1} + A_j\Delta r\frac{\partial C_j}{\partial t} \tag{53}$$

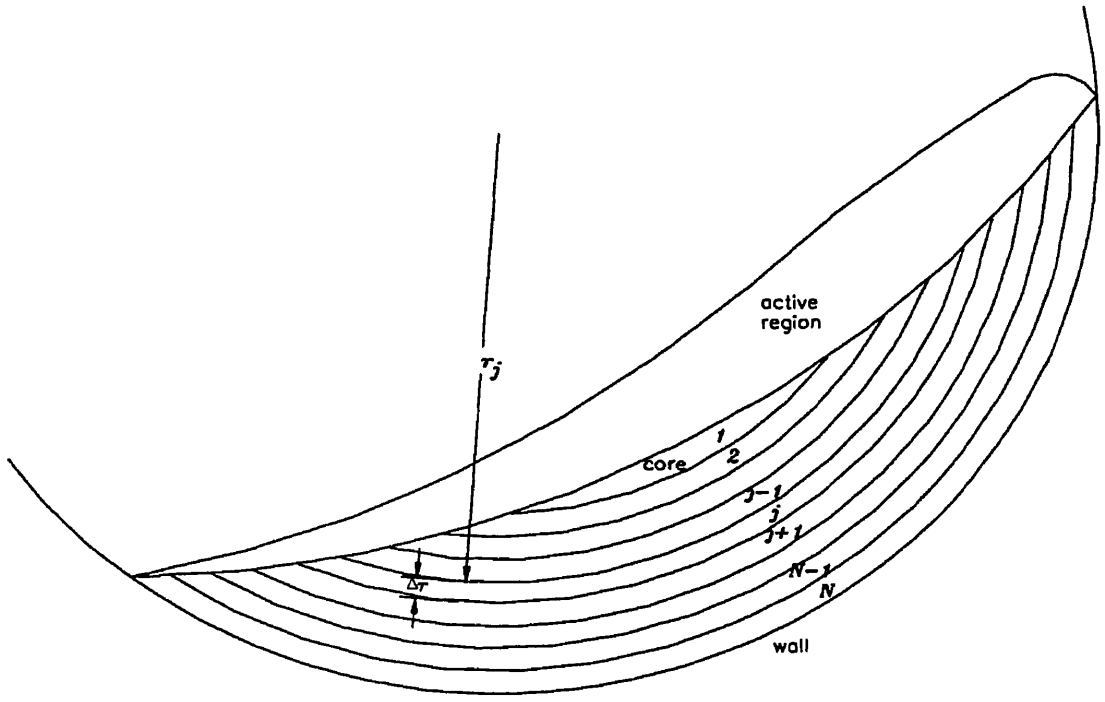

Figure 3-4 Discretization of static region into concentric layer for determination of radial-dispersion coefficient from particle tracking experiment

Particles cannot diffuse outside the boundaries giving the following boundary conditions:

$$\left.\frac{\partial C}{\partial r}\right|_{j=1} = 0 \quad \text{and} \quad \left.\frac{\partial C}{\partial r}\right|_{j=N+1} = 0 \tag{54}$$

The dispersion coefficient is assumed to be the same for all layers. For layers 2 through N-1, the partial derivatives are approximated by finite differences to obtain the following equation:

$$-A_j D_r\frac{(C_j - C_{j-1})}{\Delta r} = -A_{j+1} D_r\frac{(C_{j+1} - C_j)}{\Delta r} + A_j\Delta r\frac{(C_{j,t+\Delta t} - C_j)}{\Delta t} \tag{55}$$

Using the boundary conditions above, the finite difference equation for the core layer and the layer next to the wall are:

$$0 = -A_2 D_r \frac{(C_2 - C_1)}{\Delta r} + A_1 \Delta r \frac{(C_{1,t+\Delta t} - C_1)}{\Delta t} \tag{56}$$

$$-A_N D_r \frac{(C_N - C_{N-1})}{\Delta r} = A_N \Delta r \frac{(C_{N,t+\Delta t} - C_N)}{\Delta t} \tag{57}$$

From the particle tracking data from one experiment, the radial-dispersion coefficient is determined for each layer by considering all the cycles with the tracer particle entering the active region in layer *i*, where layer *i* is any one of the concentric layers. When the particle passes though the active region it is distributed among all the layers including the initial layer.

The initial condition is analogous to one of the concentric layers (layer *i*) containing the entire tracer at time zero. All other layers contain no tracer at time zero. The following states the initial condition:

$$p_{j \neq i, t=0} = 0$$

$$p_{j=i, t=0} = 1 \tag{58}$$

The concentration of tracer in the element is related to the probability distribution by the following equation:

$$C_j = \frac{p_{ij} A_i}{A_j} \tag{59}$$

Substituting into Equation (55) and solving for $p_{i,t+\Delta t}$ gives:

$$p_{j,t+\Delta t} = p_j + D_r \Delta t \left[\frac{p_{j+1} - 2p_j + p_{j-1}}{\Delta r^2} \right] \quad j = 2 \ldots N-1 \tag{60}$$

At the wall and the centre of the bed,

$$p_{N,t+\Delta t} = p_N + D_r \Delta t \left[\frac{p_{N-1} - p_N}{\Delta r^2} \right], \text{ and } p_{1,t+\Delta t} = p_1 + D_r \Delta t \left[\frac{p_2 - p_1}{\Delta r^2} \right] \tag{61}$$

For each layer, an initial guess for the dispersion coefficient is made. The set of N equations given by Equations (60) and (61) are integrated simultaneously by taking small

time steps until the time of one cycle is reached. Time steps that are 2% of the cycle time are sufficiently small to obtain a converged result. The predicted distribution of the tracer among the layers after one cycle is compared to the experimental distribution of the tracer particle. The sum of the square of the difference between the predicted and experimental probability for each layer is determined. A new approximation for the dispersion coefficient is made and the process is repeated until the sum of the squares is minimised and the 'best fit' dispersion coefficient is obtained for layer *i*.

3.2.1 Data from Clément et al. (1995)

Clément et al. (1995) give results for particle tracking experiments using a 0.16 m diameter drum about half full of steel beads. The drum was only 1 bead diameter (1.5 mm) thick and had one glass end for viewing the bed of beads. One layer of beads was glued to the cylindrical wall to prevent slipping. The drum was rotated slowly (0.33 rpm) causing the bed to have a slumping behaviour. The position of a single tracer particle differing only in colour from the rest of the particles in the bed was tracked by video. The tracer particle was tracked for 40 minutes or 13 revolutions of the drum.

Clément et al. (1995) divided the static region of the bed into 12 concentric layers of equal thickness of three particle diameters (4.5 mm). The transition probability distribution of the tracer p_{ij} is given for three different layers entering the active region, one near the wall, one near the centre of the bed, and one midway in between.

Since the cycle time was not reported, the active region is assumed to have negligible thickness and the time per cycle is approximated by the contact time of the particles next to the wall. Because the drum was close to half full, all the particles including those in the core had cycle times that were about the same as the particles next to the wall. The time for one cycle was:

$$t = \frac{60\,\beta}{2\pi n} = 0.5\,\frac{60\ \text{s/min}}{0.33\,\text{rpm}} = 90\,\text{s} \tag{62}$$

The radial-dispersion coefficient is determined for each of the three layers for which data is given. Results are given in Table 3-4. Figures 3-5 through 3-7 show 3

plots comparing the measured probability histogram to "best fit" prediction for each layer.

Table 3-4 Radial-dispersion coefficients determined from experimental data given by Clément et al. (1995)

Initial layer, *i*	Mean radius of initial layer (m)	Radial diffusion coefficient D_r (m^2/s)
2	0.0290	1.78×10^{-6}
7	0.0515	1.41×10^{-6}
13	0.0785	2.11×10^{-6}
Average		1.77×10^{-6}

R=0.08 m, X= 0.5, n= 0.33 rpm, n/n_c = 0.031, d_p= 1.5 mm, N=13, Δr=4.5 mm

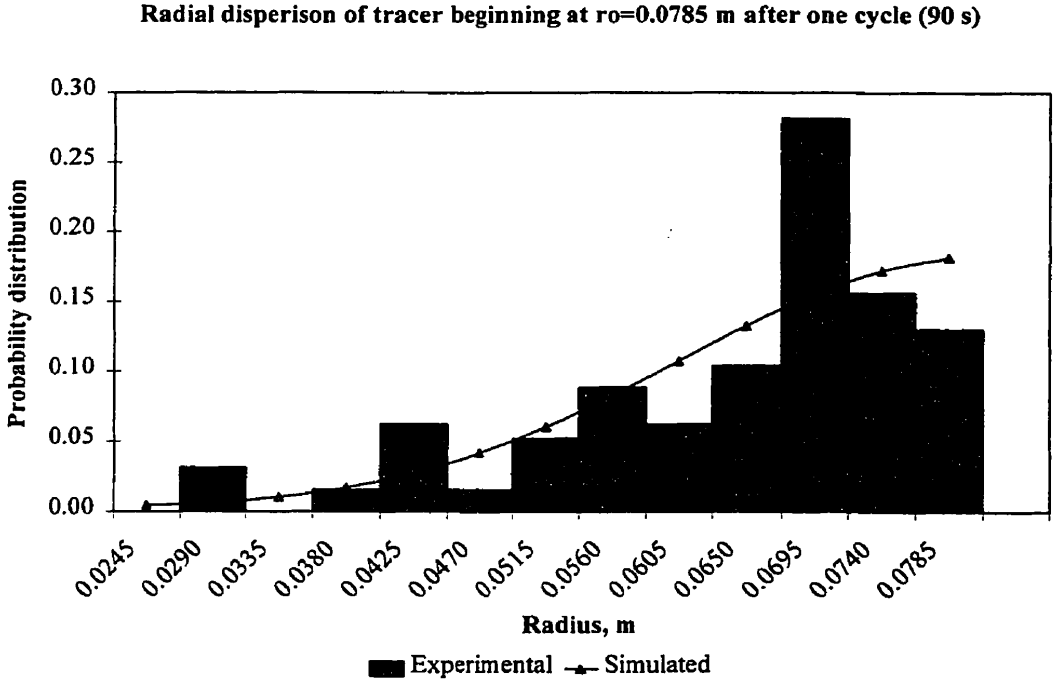

Figure 3-5 Comparison of predicted (using 'best fit' dispersion coefficient) and experimental (Clément et al, 1995) radial distribution of a particle initially in an outer layer

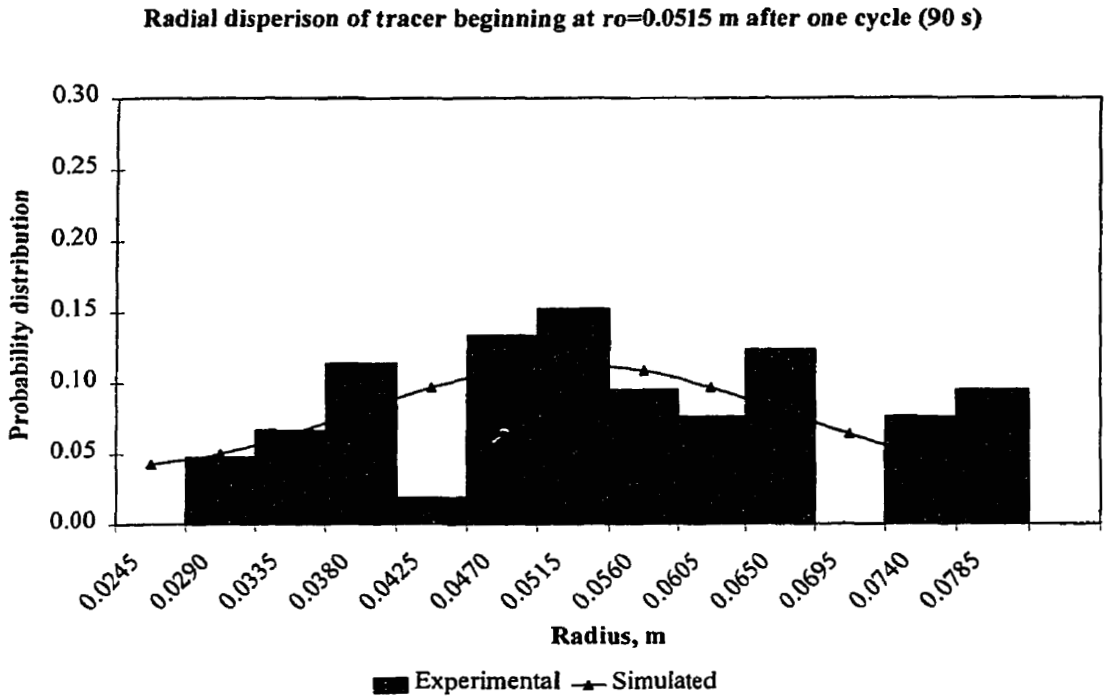

Figure 3-6 Comparison of predicted (using 'best fit' dispersion coefficient) and experimental (Clément et al, 1995) radial distribution of a particle initially in a layer between the wall and the core of the bed

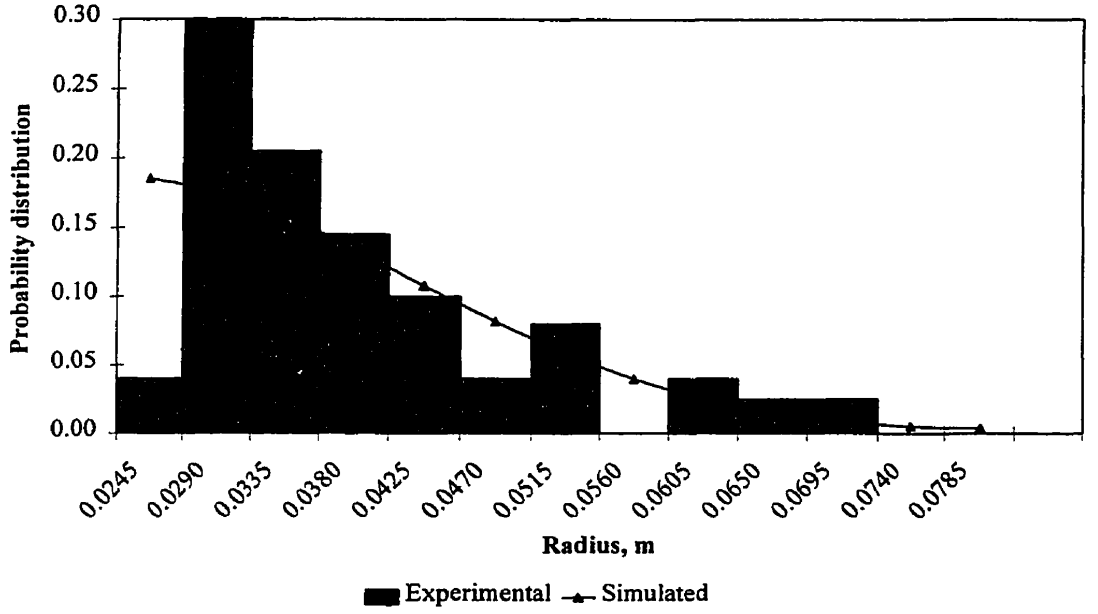

Figure 3-7 Comparison of predicted (using 'best fit' dispersion coefficient) and experimental (Clément et al, 1995) radial distribution of particles initially in a layer near the core of the bed

The average radial-dispersion coefficient for the three layers is D_r=1.77×10^{-6} m^2/s. The predicted axial-dispersion coefficient is calculated from Equation (51) using the parameters from Table 3-3 for slumping bed behaviour. According to the hypothesis at the beginning of this chapter, the square root of the ratio of the radial coefficient and the axial coefficient should approximate the ratio of the thickness of the static region to the active region. The square root of the ratio of the coefficients is 1.63. Clément et al. (1995) do not report the ratio of the thicknesses, but a figure near 4 is expected for a bed with slumping behaviour. Therefore, for this experiment, the radial-dispersion coefficient is lower than expected, but not unreasonable.

3.2.2 Data from Black (1988)

Black (1988) performed numerous experiments with two drums (0.30 m and 0.45 m diameter). Both drums were only a single particle thick with one transparent end wall to view the bed of particles. The single layer of particles consisted of ceramic spheres 6.5-7.5 mm diameter with 3 types of surface (uncoated, sand coated, and PTFE coated). The rotational speed was varied from 6 to 18 rpm giving rolling and cascading bed behaviour. The bed level was varied from 15 to 24 volume percent fill. A single particle differing only by colour from the other particles was tracked by video. The static region was divided into concentric layers that correspond to each row formed naturally by the uniform spherical particles. The thickness of a layer was not stated by Black but is assumed to be 7 sin (60°) or 6 mm. The number of layers varied from 6 to 12 depending on the diameter of the drum and volumetric fill fraction.

Results were given for 32 experimental runs. Each run included tracking the tracer particle for 3000 to 13000 cycles. A matrix **M** was given where element m_{ij} was the number of occurrences of the tracer particle leaving the static region in layer i, tumbling through the active region, and re-entering the static region in layer j. The transition matrix was represented by a three-dimensional histogram as shown in Figure 3-8 through 3-10. As pointed out by Black (1988), if there were no radial mixing then the histogram would appear as in Figure 3-8. Particles leaving the static region in layer i would re-enter the static region in layer i. If mixing in the radial direction were perfect, then the histogram would appear as in Figure 3-9. Particles leaving the static region in layer i would be equally distributed among all the layers when re-entering the static region. The histogram for a typical run is shown Figure 3-10. The particles were distributed across all the layers, but tended to return to the same layer or layers adjacent to the initial layer after tumbling through the active region. Any memory of the initial position appeared to be lost after about 3 cycles.

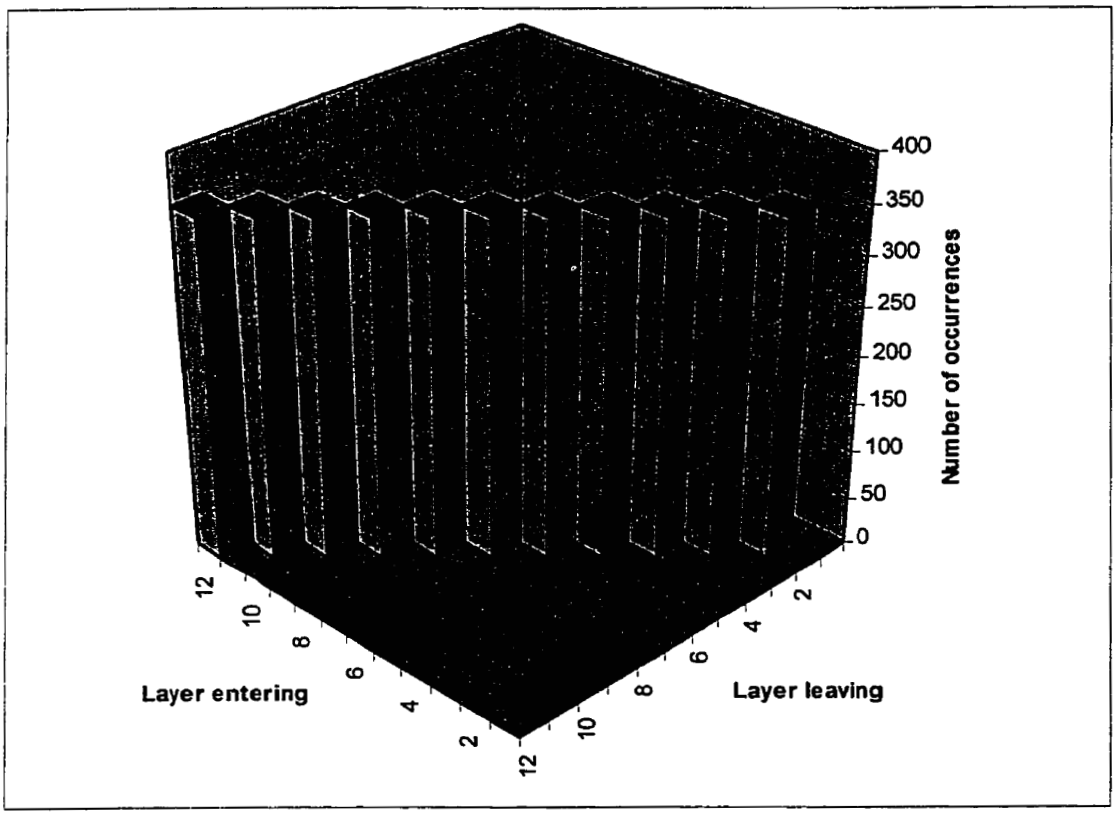

Figure 3-8 Mixing histogram for hypothetical drum with no radial mixing

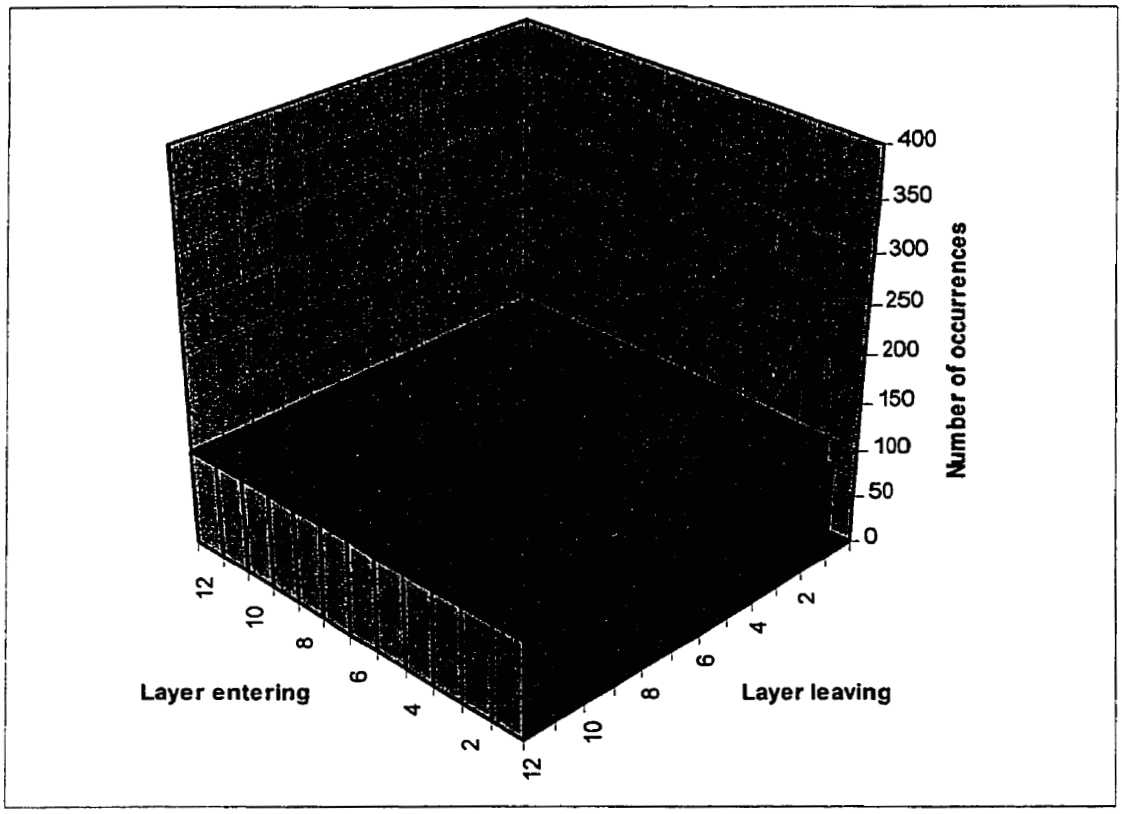

Figure 3-9 Mixing histogram for hypothetical drum with perfect radial mixing

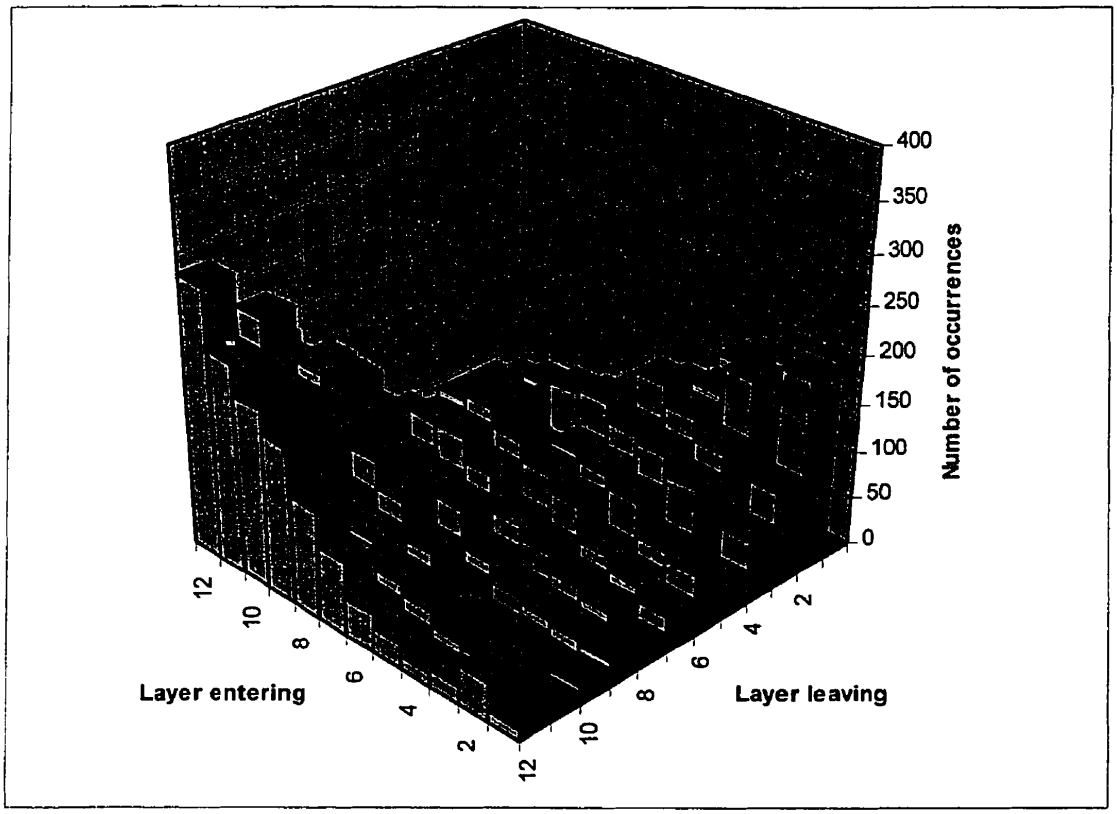

Figure 3-10 Radial mixing histogram for Run 33 from Black (1988)

To determine a radial-dispersion coefficient from the data given by Black (1988), first the probability matrix **P** is found by dividing each element of matrix **M** by the total number of cycles leaving the static region from the same layer.

$$p_{ij} = \frac{m_{ij}}{\sum_j m_{ij}} \tag{63}$$

Elements of the transition probability matrix **P** are all between 0 and 1 and the sum of each row is one. Figure 3-11 shows the histogram for matrix **P** for a typical experiment.

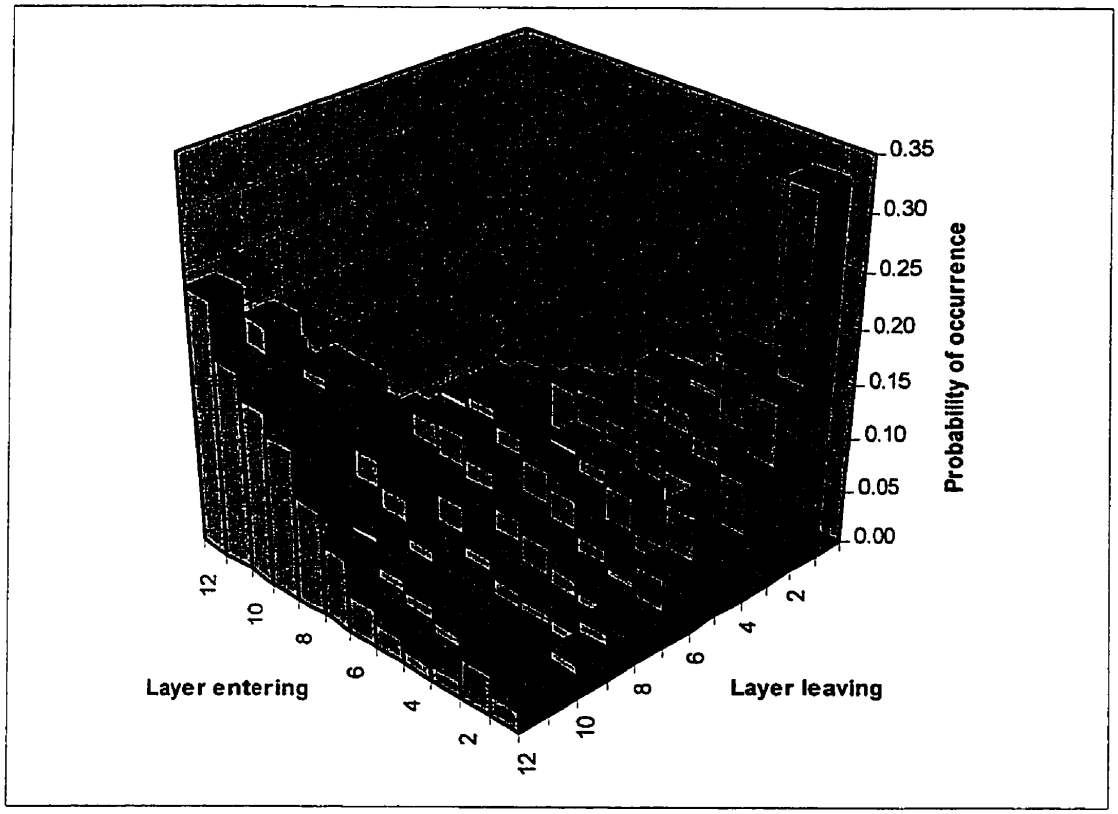

Figure 3-11 Probability distribution histogram obtained for Run 33 from Black (1988)

The method outlined at the beginning of §3.2 is used to determine a radial dispersion coefficient for each layer. The cycle time was not reported, so it is approximated by the contact time of the outside layer with the wall. All layers are assumed to have the same cycle time. The actual cycle time of an outside layer is likely larger and the inner layers are likely shorter than the approximated time. Therefore, the coefficient is likely overstated for the outer layers and understated for the inside layers.

The core layer is not included in determining the least squares fit because Black could not determine a cycle while the tracer remained in the core and could not report the number of occurrences that the tracer in the core would remain in the core. The probability of entering and leaving the core also depends on the size of the core. The size

of the core varied from test to test affecting the probability of the tracer entering and leaving the core. Therefore, the core layer is not included in the determination of the dispersion coefficient.

For each run, a radial-dispersion coefficient is determined for each layer. Table 3-5 shows the results from a typical run. The coefficient varies about 20%, but no correlation between the coefficient and the radius of the layer is apparent for any of the runs. This does not mean that the radial-dispersion coefficient does not change with radius, only that it could not be determined from this set of data.

Table 3-5 Radial-dispersion coefficients for Run 33 from Black (1988)

Initial layer, *i*	Radius of initial layer (m)	Radial-dispersion coefficient D_r (m^2/s)
1	0.159	5.83×10^{-5}
2	0.165	1.61×10^{-4}
3	0.171	1.24×10^{-4}
4	0.177	8.25×10^{-5}
5	0.183	9.38×10^{-5}
6	0.189	1.03×10^{-4}
7	0.195	9.52×10^{-5}
8	0.201	1.12×10^{-4}
9	0.207	1.40×10^{-4}
10	0.213	1.46×10^{-4}
11	0.219	1.18×10^{-4}
12	0.225	1.20×10^{-4}
Average		1.13×10^{-4}
Std. Dev.		2.86×10^{-5}

R=0.225 m, X= 0.24, n= 12.1 rpm, n/n_c = 0.19, d_p= 7 mm, N=12, Δr=6 mm

The mixing matrix predicted by the "best fit" dispersion coefficients is shown by the histogram in Figure 3-12. The coefficients for each layer are averaged to get a coefficient for the run. The mixing matrix is determined for the average coefficient and the result is shown by the histogram in Figure 3-13 for the same example run.

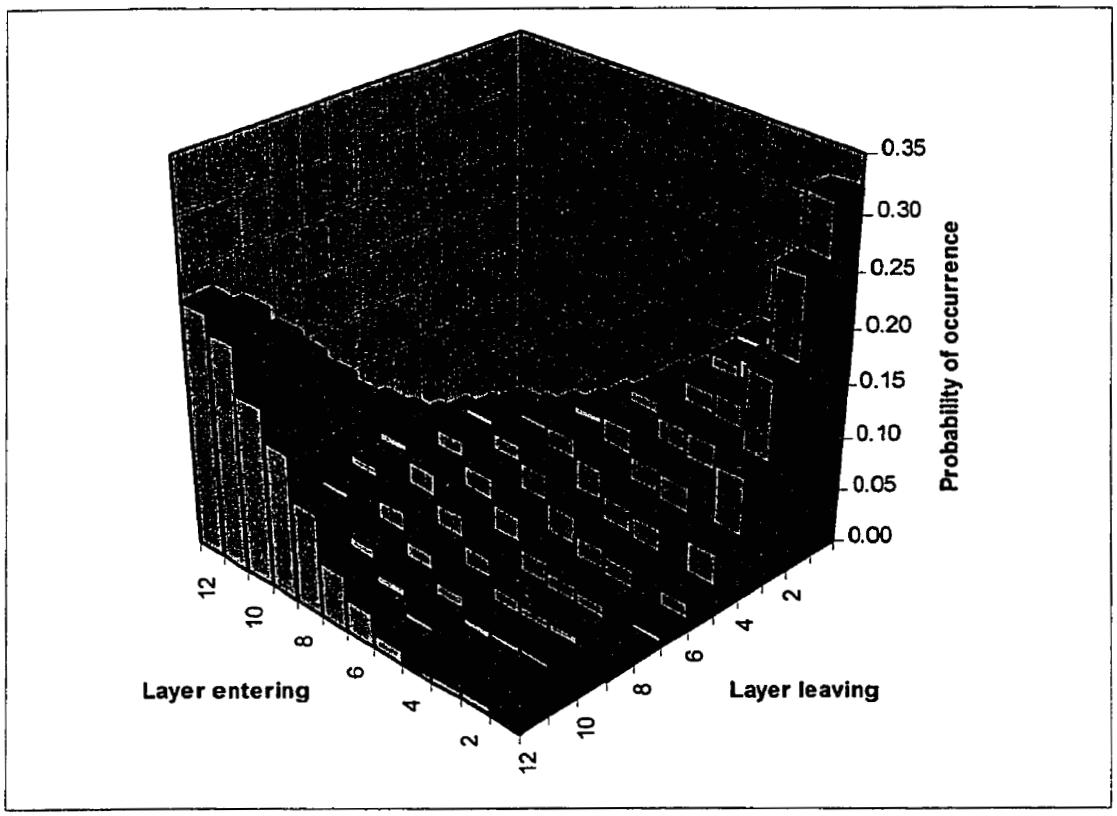

Figure 3-12 Probability distribution histogram using best fit radial-dispersion coefficient for each layer – Run 33 from Black (1988)

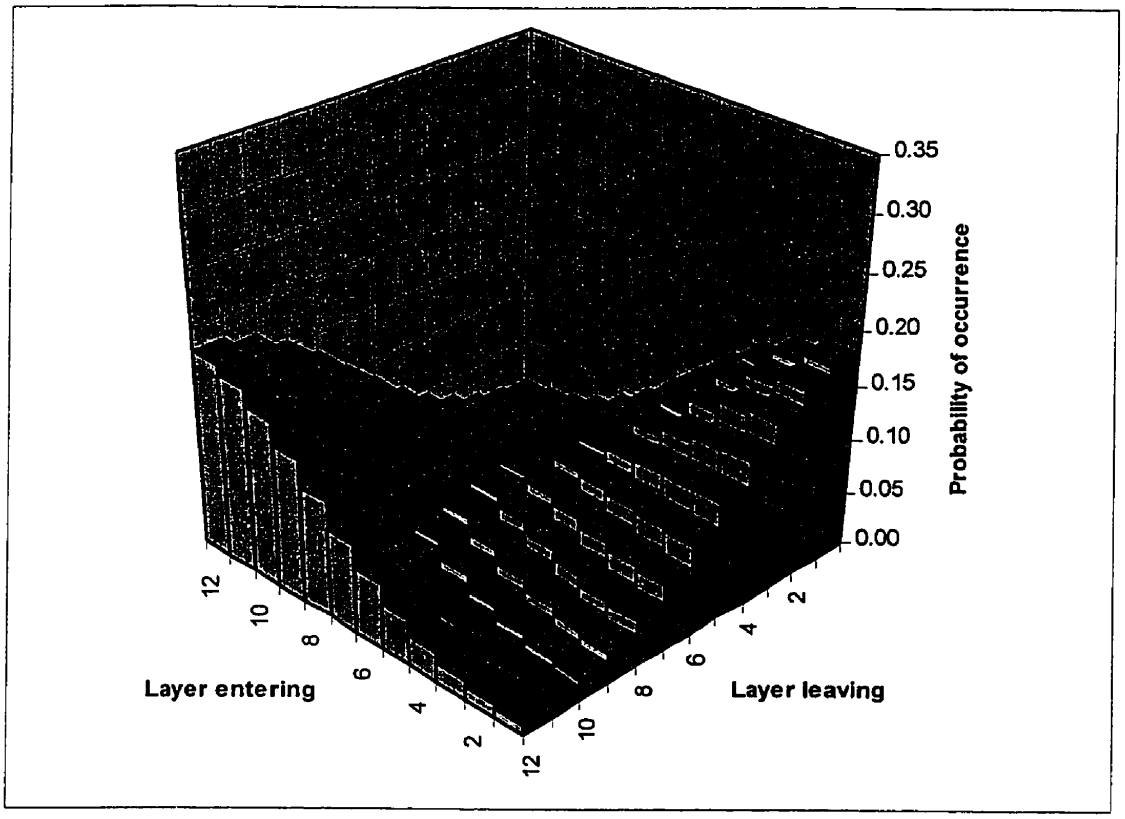

Figure 3-13 Probability distribution histogram predicted using average radial-dispersion coefficient for all layers – Run 33 from Black (1988)

Tables 3-6 through 3-8 give the average coefficients determined for each run for the 3 types of particle surfaces.

Table 3-6 Radial-dispersion coefficient for uncoated particles from experiments by Black (1988)

Run no.	Drum dia m	Fill fraction	Rotational speed, rpm	Relative speed, fraction of critical	Radial-dispersion coefficient, D_r (m^2/s)	Predicted axial-dispersion coefficient D_z (m^2/s)	$(D_r/D_z)^{0.5}$
6	0.300	0.20	18.2	0.236	8.72×10^{-5}	2.68×10^{-5}	1.81
7	0.300	0.20	6.75	0.087	1.01×10^{-4}	1.75×10^{-5}	2.40
9	0.300	0.20	9.37	0.121	8.00×10^{-5}	2.01×10^{-5}	1.99
11	0.300	0.20	14.8	0.192	8.08×10^{-5}	2.45×10^{-5}	1.82
12	0.300	0.24	14.8	0.192	1.02×10^{-4}	2.22×10^{-5}	2.14
13	0.300	0.24	6.78	0.088	7.24×10^{-5}	1.59×10^{-5}	2.14
14	0.300	0.24	9.30	0.120	9.35×10^{-5}	1.82×10^{-5}	2.27
15	0.300	0.16	14.9	0.193	7.99×10^{-5}	2.81×10^{-5}	1.69
16	0.300	0.16	10.0	0.129	8.74×10^{-5}	2.37×10^{-5}	1.92
23	0.300	0.16	18.0	0.233	1.01×10^{-4}	3.05×10^{-5}	1.82
25	0.450	0.20	5.66	0.090	1.08×10^{-4}	3.99×10^{-5}	1.90
26	0.450	0.20	7.65	0.121	8.96×10^{-5}	3.41×10^{-5}	1.62
27	0.450	0.20	12.1	0.192	1.23×10^{-4}	4.15×10^{-5}	1.72
28	0.450	0.15	5.66	0.090	6.03×10^{-5}	3.42×10^{-5}	1.33
29	0.450	0.16	7.65	0.121	8.84×10^{-5}	3.90×10^{-5}	1.51
30	0.450	0.16	12.1	0.192	6.00×10^{-5}	4.75×10^{-5}	1.12
31	0.450	0.24	5.66	0.090	1.32×10^{-4}	2.71×10^{-5}	2.21
32	0.450	0.24	7.56	0.121	1.10×10^{-4}	3.09×10^{-5}	1.89
33	0.450	0.24	12.1	0.192	1.13×10^{-4}	3.76×10^{-5}	1.73

$d_p = 7\ mm$

Table 3-7 Radial-dispersion coefficient for PTFE-coated particles from experiments by Black (1988)

Run no.	Drum dia m	Fill fraction	Rotational speed, rpm	Relative speed, fraction of critical	Radial-dispersion coefficient, D_r (m^2/s)	Predicted axial-dispersion coefficient, D_z (m^2/s)	$(D_r/D_z)^{0.5}$
17	0.300	0.20	9.37	0.121	1.01×10^{-4}	2.01×10^{-5}	2.24
18	0.300	0.20	14.70	0.190	8.65×10^{-5}	2.44×10^{-5}	1.88
19	0.300	0.20	6.98	0.090	6.22×10^{-5}	1.77×10^{-5}	1.87
20	0.300	0.24	6.98	0.090	8.91×10^{-5}	1.61×10^{-5}	2.36
21	0.300	0.24	9.40	0.122	1.22×10^{-4}	1.83×10^{-5}	2.58
22	0.300	0.24	14.70	0.190	1.14×10^{-4}	2.21×10^{-5}	2.27

d_p=7 mm

Table 3-8 Radial-dispersion coefficient for sand-coated particles from experiments by Black (1988)

Run no.	Drum dia m	Fill fraction	Rotational speed, rpm	Relative speed, fraction of critical	Radial-dispersion coefficient, D_r (m^2/s)	Predicted axial-dispersion coefficient D_z (m^2/s)	$(D_r/D_z)^{0.5}$
34	0.300	0.20	6.75	0.087	9.75×10^{-5}	1.75×10^{-5}	2.36
35	0.300	0.20	9.37	0.121	1.09×10^{-4}	2.01×10^{-5}	2.32
36	0.300	0.20	14.70	0.190	1.30×10^{-4}	2.44×10^{-5}	2.31

d_p=7 mm

The radial-dispersion coefficient determined from Black's data ranges from 6×10^{-5} to 1.3×10^{-4} m^2/s. Compared to coefficients determined from data from Clément et al, the coefficients are greater by 1 to 2 orders of magnitude. This is not unreasonable given the larger drum diameter and the faster rotational speed. The radial-dispersion coefficient appears to increase when any one of the 4 variables (speed, fill, drum diameter, or particle roughness) is increased.

A predicted axial-dispersion coefficient is calculated for each run from Equation (51) using the parameters from Table 3-3 for rolling/cascading bed behaviour. The results are given in Tables 3-6 through 3-8. According to the proposed relationship given

by Equation (25), the square root of the ratio of the radial-dispersion coefficient and the axial-dispersion coefficient should approximate the ratio of the thickness of the static region to the thickness of the active region. This ratio of the coefficients is calculated for each run and the results are given in Tables 3-6 through 3-8. The ratio varies from 1.1 to 2.6. The expected ratio of the thicknesses of the static and active regions for the conditions used in Black's experiments is about 3 to 4.5. Thus the radial-dispersion coefficients are smaller than predicted by about a factor 4.

3.2.3 Data from Inoue et al. (1970)

Inoue et al. (1970) performed 4 particle-tracking experiments similar to Clément et al. (1995) and Black (1988). A drum (0.623 m diameter by 0.020 m long) had one transparent end wall to view the bed of particles. The particles consisted of spherical glass beads 6 mm diameter. The drum was rotated at speeds ranging from 3.75 to 20 rpm giving rolling, cascading and cataracting bed behaviour. The fill level was approximately 40 volume per cent. A single particle differing only by colour from the other particles was observed.

For each of the experiments, the static region of the bed was divided into 9 imaginary concentric layers of equal thickness. The cycle time and the layer occupied by the particle was recorded every time the tracer particle crosses a reference line that connected the centre of the bed to the wall. Each test included 5000 to 7000 cycles. The distribution probability is reported for each layer as a standard deviation calculated by the following equation:

$$\sigma_i = \left[\sum_{j=1}^{w} p_{ij} \ (j-i)^2 \right]^{1/2} \tag{64}$$

where i is the layer occupied by the particle at the beginning of the cycle and j is the layer at the end of the cycle.

The average and standard deviation of the cycle time of a particle in each layer are reported. The thickness of the concentric layers in the static region, which is not reported, is assumed to be 25 mm.

To determine the radial-dispersion coefficient for experiments by Inoue et al. (1970), a guess for the coefficient is made. The distribution probabilities after the reported mean cycle time is determined by using the same finite difference simulation as in the 2 previous sections. Equation (64) is used to calculate the standard deviation of the radial distribution that is compared to the experimental value. By trial and error, the guess for radial-dispersion coefficient is adjusted until the reported standard deviation is obtained. This is done to determine a best-fit coefficient for each layer. Table 3-9 shows the results for Run 3. No relationship between the layer radius and the local coefficient is apparent. A similar result was found for the other three experiments at different rotational speeds.

Table 3-9 Radial-dispersion coefficients determined for Run 3 from Inoue et al. (1970)

Initial layer, *i*	Mean radius of initial layer (m)	Mean cycle time (s)	Radial-dispersion coefficient D_r (m^2/s)
1	0.112	1.282	5.00×10^{-5}
2	0.137	1.514	1.13×10^{-4}
3	0.162	1.691	9.00×10^{-5}
4	0.187	1.837	1.09×10^{-4}
5	0.212	2.000	1.40×10^{-4}
6	0.237	2.158	1.53×10^{-4}
7	0.262	2.265	1.55×10^{-5}
8	0.287	2.405	1.30×10^{-4}
9	0.312	2.640	1.70×10^{-4}
Average		1.977	1.23×10^{-4}
Std. Dev.			3.74×10^{-5}

R=0.3115 m, X= 0.4, n= 14 rpm, n/n_c = 0.262, d_p= 6 mm, N=9, Δr=25 mm

An overall radial-dispersion coefficient is determined for each test by averaging the results for all the layers. Results are given in Table 3-10. The radial-dispersion coefficients range from 1.0×10^{-4} to 1.3×10^{-3} m^2/s. This is about one order of magnitude larger than coefficients determined from Black's experiments. This is consistent with the

larger drum diameter and fill level. The coefficient decreases as speed is increased ($D_r \propto n^{-1.0}$). Note that this is the opposite of the axial-dispersion coefficient, which increases as the rotational speed is increased. It is possible for the radial-dispersion coefficient to decrease as the speed is increased due to increase in the thickness of the active layer.

Table 3-10 Mean radial-dispersion coefficients determined from experiments by Inoue et al. (1970)

Test #	Rotational speed n (rpm)	Relative speed n/n_c (-)	Radial diffusion coefficient D_r (m^2/s)	Predicted axial diffusion coefficient D_z (m^2/s)	$(D_r/D_z)^{0.5}$
1	3.75	0.07	1.26×10^{-3}	2.70×10^{-5}	6.83
2	7	0.13	2.16×10^{-4}	3.53×10^{-5}	2.47
3	14	0.26	1.23×10^{-4}	4.75×10^{-5}	1.61
4	20	0.37	1.00×10^{-4}	5.54×10^{-5}	1.34

$R = 0.3115$ m, $X = 0.4$, $d_p = 6$ mm, $N = 9$, $\Delta r = 25$ mm

The predicted axial-dispersion coefficient is determined using Equation (51) with parameters from Table 3-3 for all modes of bed behaviour. The square root of the ratio of the radial-dispersion coefficient and the axial-dispersion coefficient is also determined. Results are given in Table 3-10. The predicted ratio of the thicknesses of the static and the active regions are reasonable and decreases as the rotational speed is increased as expected. The actual thickness ratios were not reported but are expected to range from 6 at the slow speed to 3 at the highest speed.

3.3 Angular-Dispersion Coefficient

Dispersion in the angular direction is caused by diffusion in the active layer in the stream-wise direction. Boateng (1993) measured the velocity fluctuations parallel to the flow direction in a 1-m diameter drum. The magnitude of the fluctuations increased with rotational speed.

3.3.1 Data from Inoue et al. (1970)

During the experiments by Inoue et al. (1970) that are described in Section 3.2.3, the cycle time was also measured. The mean and standard deviation of the cycle time for each of the 9 concentric layers for each test are reported. The angular-dispersion coefficient for a layer is calculated from this data using an equation analogous to Equation (34), which was used to determine the axial-dispersion coefficients in a continuous drum.

$$D_\theta = \frac{(2L+\beta R)^2 \sigma^2}{2\langle \tau_1 + \tau_2 \rangle^3} \tag{65}$$

The results for Run 3 are given in Table 3-11. The coefficient is greatest for the core and wall layers and decreases for the middle layers. A similar pattern was seen for the other runs at different rotational speeds.

Table 3-11 Angular-dispersion coefficients determined for Run 3 from Inoue et al. (1970)

Initial layer, *i*	Mean radius of initial layer (m)	Mean cycle time (s)	Std. dev. Of cycle time (s)	Angular-dispersion coefficient D_θ (m^2/s)
1	0.112	1.282	0.200	3.42×10^{-3}
2	0.137	1.514	0.112	6.51×10^{-4}
3	0.162	1.691	0.093	3.22×10^{-4}
4	0.187	1.837	0.079	1.81×10^{-4}
5	0.212	2.000	0.080	1.44×10^{-4}
6	0.237	2.158	0.082	1.20×10^{-4}
7	0.262	2.265	0.077	9.19×10^{-5}
8	0.287	2.405	0.089	1.02×10^{-4}
9	0.312	2.640	0.132	1.70×10^{-4}
Average		1.977		5.78×10^{-4}
Std. Dev.				1.08×10^{-3}

D=0.3115 m, X= 0.4, n= 14 rpm, n/n_c = 0.262, d_p= 6 mm, N=9, Δr=25 mm

A mean angular-dispersion coefficient is determined for each test by averaging the results for all the layers. Results are given in Table 3-12. The angular-dispersion coefficients range from 1.1×10^{-4} to 1.0×10^{-3} m^2/s. The coefficient increases as the speed is increased ($D_r \propto n^{1.5}$). Note that this is the opposite of the radial-dispersion coefficient, which decreased as the rotational speed was increased.

Table 3-12 Mean angular-dispersion coefficients determined from experiments by Inoue et al. (1970)

Test #	Rotational speed n (rpm)	Relative speed n/n_c (-)	Angular-dispersion coefficient D_θ (m^2/s)	Predicted axial-dispersion coefficient D_z (m^2/s)	$(D_\theta/D_z)^{0.5}$
1	3.75	0.07	1.07×10^{-4}	2.70×10^{-5}	1.99
2	7	0.13	3.46×10^{-4}	3.53×10^{-5}	3.13
3	14	0.26	5.78×10^{-4}	4.75×10^{-5}	3.48
4	20	0.37	1.03×10^{-3}	5.54×10^{-5}	4.35

$R = 0.3115$ m, $X = 0.4$, $d_p = 6$ mm, $N = 9$, $\Delta r = 25$ mm

The predicted axial-dispersion coefficient is determined using Equation (51) with parameters from Table 3-3 for all modes of bed behaviour. The square root of the ratio of the angular-dispersion coefficient and the axial-dispersion coefficient is also determined. Results are given in Table 3-12. The ratio varies from 2 to 4.4 and increases as the rotational speed increases. From Equation (26) the expected ratio is equal to the ratio of the total length of bed periphery to the surface chord length which also varies between 1 and 2. The larger than predicted coefficient may be due to the anisotropic nature of particle diffusion in granular flow with larger diffusion in the same direction as the particle circulation.

3.4 Summary

Because particle dispersion in each direction of the rotating drum is primarily due to the same phenomenon i.e random collisions in the active region, one can expect that

the axial, radial and angular dispersion coefficients can be related. Simple relationships are proposed, allowing the radial and angular coefficients to be predicted from the more easily measured axial coefficient and an approximation of the relative thicknesses of the active and static regions.

From published data, the axial-dispersion coefficient in both batch and continuous flow rotary drums range from 1×10^{-7} to 1×10^{-4} m^2/s. The coefficient increases proportionally with increases in the drum diameter and the square root of the particle diameter. The effect of rotational speed varies with the bed behaviour mode. For rolling or cascading behaviour, the coefficient increases proportionally to the square root of the rotational speed.

A method was developed to determine the radial- and angular-dispersion coefficient from experiments that track a single particle in the transverse plane. From the limited published data available, the radial-dispersion coefficient was found to be about 2 to 5 times larger than the axial-dispersion coefficient at the same conditions. This is approximately equal to the square of the ratio of the thicknesses of the static and active regions. The radial-dispersion coefficient increases with speed, fill, drum diameter and particle diameter.

Only one source was found with published data to calculate the angular-dispersion coefficient. The calculated coefficients were 4 to 20 times larger than the predicted axial-dispersion coefficient at the same conditions. This is slightly larger than the square of the ratio of the total cycle length to the surface chord length. This may be due to the anisotropic nature of particle diffusion in granular flow with larger diffusion in the same direction as the particle circulation. The angular-dispersion coefficient increased with rotational speed.

CHAPTER 4
EXPERIMENTS

In the previous chapter, the axial-, radial- and angular-dispersion coefficients were determined from data available in the literature and the relationship between the coefficients was examined. Unfortunately, in none of the experiments were the coefficients in two different directions determined in the same drum for the same conditions. Also important variables such as cycle time, dimensions and residence times of the active and static regions, and particle properties were seldom reported and had to be approximated.

This chapter describes experiments that attempted a non-invasive technique to measure mixing of solids in a rotating drum. The objective of the experiments was to determine axial-, radial- and angular-dispersion coefficients for the same conditions in the same drum by tracking a single radioactive particle. Data were collected to determine the axial, radial and tangential mixing in the same experiment.

The experiments were similar to those performed by Parker et al. (1997) and the axial-dispersion coefficient could be determined by the same method. The radial- and angular-dispersion coefficients could be determined for the same experiments by using the method developed in the previous chapter. Other variables such as cycle time and the dimensions of the active and static regions could also be determined from the same experimental data.

4.1 Apparatus

A schematic of the apparatus is shown in Figure 4-1. The transparent plastic, horizontal drum used for the experiments was about 200-mm diameter and 900-mm long. The drum had two tires that sat on four support rollers. A common axle that was driven by a motor with a variable speed transducer connected two of the rollers. The inside surface of the drum had several thin ridges of plastic to prevent slipping between the bed of solids and the wall.

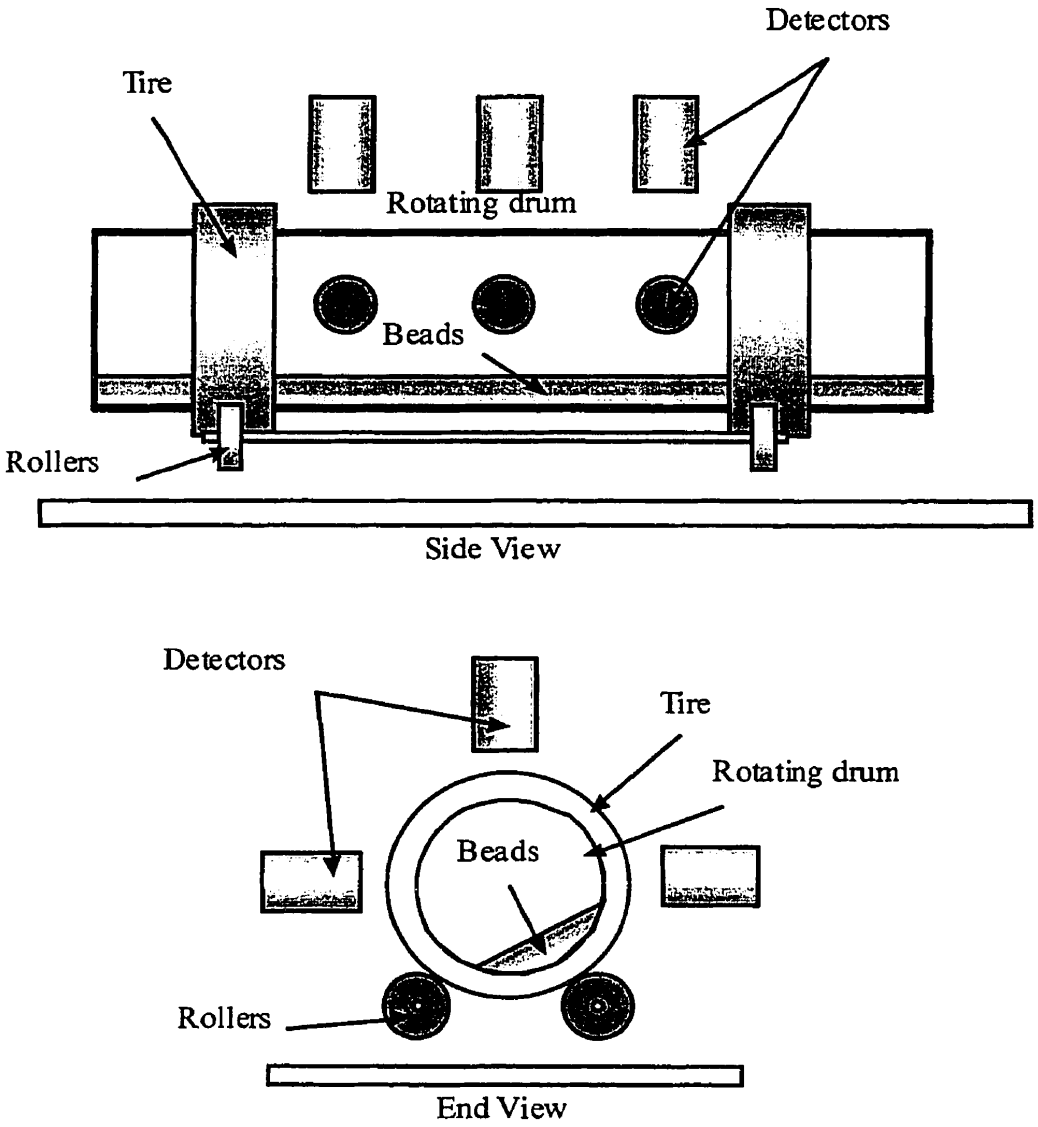

Figure 4-1 Schematic diagram of rotating drum and detectors used in radioactive particle tracking experiments

The drum contained a bed of uniform 3mm diameter, spherical glass beads (ρ_s = 2500 kg/m^3).

A facility for tracking a single radioactive particle in multiphase fluidized beds developed at the École Polytechnique de Montréal (Larachi et al., 1995, and Cassanello et al. 1995) was adapted to perform the same function for the rotary drum. Nine 76 mm by 76 mm NaI scintillation detectors were supported around the drum on sliding rails. The detectors were placed at 90-degree spacing on both sides and above the drum. The detectors were staggered at different axial locations along the drum. The distance between the front of the detector and the drum wall was between 72 and 184 mm in order to achieve the greatest sensitivity without exceeding the maximum count-rate of the detectors.

The tracer particle was a sphere formed by melting a mixture of soda lime powder and scandium oxide melted at high temperature. With 10-12% Sc, the density and size of the tracer particle was within 5% of that of a glass bead in the drum. The tracer particle was coated with a diamond-like carbon layer in order to prevent its rupture due to attrition in the drum. The particle was activated in the institution's SLOW-POKE nuclear reactor. ^{45}Sc captures a neutron to produce ^{46}Sc which has a half-life of 83.8 d.

Nuclear decay of the tracer particle emits gamma-rays that are detected by the scintillation detectors. The count-rate in each detector depends on the distance from the tracer particle to the detector. The count-rate is approximately inversely proportional to the square of the distance. However, the amount of absorbing and scattering material between the particle and the detector and the efficiency of the detector also has a significant effect on the count-rate.

4.2 Procedure

A Monte Carlo simulation of gamma-ray emmision and detection was used to generate a map that related the gamma-ray count rates from the nine detectors to each position on a three-dimensional grid inside the drum (Larachi et al., 1994). Before an actual experiment, the detection system was calibrated. A row of aluminum probe ports

along the drum wall allowed insertion of a Plexiglas rod used to place a tracer particle at a number of calibration location in the stationary drum. The drum was turned to locate the tracer particle at different angular locations. While the drum could not be rotated during the calibration, the drum was turned so that the stationary bed was in the approximate position that it would be during an experiment. The calibration was used to adjust the linear attenuation assumed for the contents of the drum.

For an actual experiment, a single tracer particle was placed in the bed in the rotating drum. Gamma rays were counted simultaneously from the 9 detectors for 30 ms. After 4096 counting intervals (128 s), the acquisition was momentarily interrupted and the data was transferred and stored in temporary computer memory. Data acquisition was triggered to resume after the data transfer. After a tracking experiment, which lasted about 1.5 to 3 hours, the acquired data were transferred to permanent computer memory and then converted to ASCII format. These files were transferred to a faster computer where the tracer co-ordinates were reconstructed from the gamma-ray counts. A least squares method was used to find the grid point that gives the best agreement with the nine detector count-rates. A second least squares search was used to find the position of the tracer in the neighbourhood of the grid point. The three dimensional position of the tracer particle was calculated for each 30 ms interval for the three hour period. Experiments using a three-phase fluidized bed indicated that this technique allowed the position of the tracer particle to be determined with a typical precision of 5 mm (Larachi et al., 1994).

Five tests were performed using various rotational speeds and fill levels. Table 4-1 gives the rotational speed and level of fill for each test. All the tests exhibited rolling or cascading bed behaviour. Calibration of the detection system was performed prior to the first, second and fifth tests.

Table 4-1 Operating parameters for radioactive particle tracking experiments

Test no.	1	2	3	4	5
Rotational speed, rpm	15	15	5	25	15
Fill, volume %	10	20	20	20	30

4.3 Results

4.3.1 Axial Dispersion

Figure 4-2 shows the axial position of the tracer particle in the drum during a test. The particle randomly migrated along the drum's length. When the tracer particle migrated within one drum diameter of the end wall, it was relocated to the center of the drum during an interruption in the data acquisition.

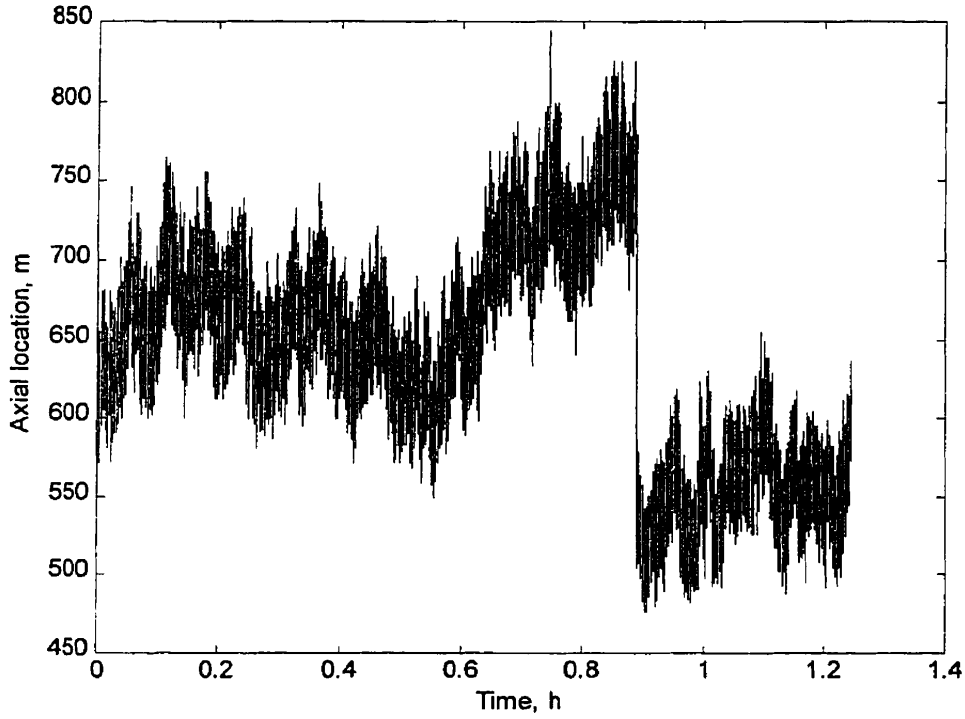

Figure 4-2 Random migration of tracer particle along the length of the rotating drum during Test 1

Assuming that the particle migration in the axial direction approximates diffusion in an infinite one-dimensional medium, then the distribution of the particle's displacements in the axial direction after time interval Δt is related to the axial-dispersion coefficient by the following equation.

$$C(z,t) = \frac{1}{\sqrt{4\pi\Delta t D_z}} \exp\left[-\frac{\Delta z^2}{4tD_z}\right] \tag{66}$$

Normal distribution is defined as:

$$C(z,t) = \frac{1}{\sqrt{2\pi}\sigma_z} \exp\left[-\frac{\Delta z^2}{2\sigma_z^2}\right] \tag{67}$$

Therefore, the axial-dispersion coefficient is related to the variance of the tracer displacement in the axial position after time interval Δt by the following equation.

$$D_z = \frac{\sigma_z^2}{2\Delta t} \tag{68}$$

where the variance of the tracer displacement is determined by the following equation.

$$\sigma_z^2 = \frac{\sum \Delta z^2 - \left(\sum \Delta z\right)^2}{N(N-1)} \tag{69}$$

The variance of the measured displacement is the sum of the variance due to the tracer particle dispersion and the variance due to measurement error.

$$\sigma_z^2 = \sigma_D^2 + \sigma_R^2 \tag{70}$$

The displacement variance due to dispersion increases as the time interval increases but the variance due to measurement error is constant. For short time intervals, the error in measuring the axial location increases the calculated dispersion coefficient. As the size of the time increment is increased the measurement error becomes less significant. By determining the dispersion coefficient for different time intervals the effect of the measurement error can be determined and eliminated.

Using the time and position data collected during a test, the variance of the displacement in the z-direction was determined for time intervals ranging from 2 to 128 s. An axial-dispersion coefficient was calculated for each pair of variance and time interval using Equation (68). The process was repeated for each of the five tests. Results are plotted in Figure 4-3.

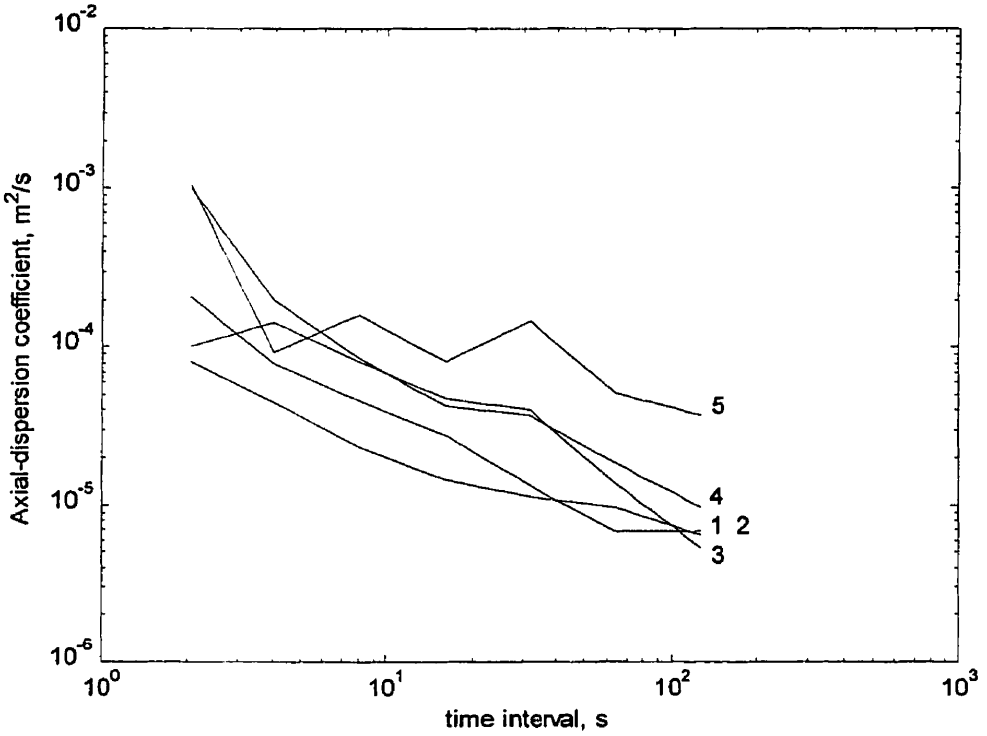

Figure 4-3 Axial-dispersion coefficient determined from tracer displacement distribution for various time intervals. As the size of the time interval increases, the measurement error becomes less significant and the true axial-dispersion coefficient is approached

As expected, the calculated axial-dispersion coefficient decreases as the time interval increases. For most of the tests, the axial-dispersion approached 10^{-5} m^2/s but was still decreasing for a maximum time interval of 128 s. Axial-dispersion coefficients predicted for the experiments using the correlation given by Equation (51) and parameters from Table 3.3 for rolling/cascading bed behaviour range from 6×10^{-6} to 1×10^{-5} m^2/s. The standard deviation of the measurement error was approximated by using Equations (68) and (70) to be at least 20 mm.

4.3.2 Mixing in the Transverse Plane

Due to the size of the measurement error it was not possible to determine the particle position over a short time interval (less than 1 s) with sufficient accuracy to determine radial- and angular-dispersion coefficients. Nor was it possible to determine the thickness of the active region from the data collected.

A number of changes to the experiment and the treatment of the data could be made to reduce the measurement error or allow the size of the error to be overcome.

i) The calibration is an important step in getting better results. One calibration was used for the 3 tests with 20% fill. The quality of the results deteriorated with each successive test.

ii) For the rotating drum, the calibration points and the mapped coordinates could have been concentrated in the bed at the bottom of the drum. The allowance for linear attenuation by the drum contents could take into account that the content is concentrated in a bed at the bottom of the drum.

iii) The position of the detectors could be improved. All the detectors were essentially mounted above the bed of particles. The detectors mounted directly above the drum were too far from the bed to get the best results. Some detectors could have been mounted below the drum.

iv) Using a larger drum with a deeper bed could reduce the precision required to determine dispersion coefficients. If the drum was large enough, some of the detectors could have been mounted inside the drum above the bed.

4.4 Summary

Experiments using a non-intrusive particle tracking technique were performed with the intention of determining the three-dimensional co-ordinates of a single tracer particle in a bed of particles in a rotating drum. The dispersion coefficients in each direction were to be calculated from the migration of the tracer in the drum. While it was possible to determine the axial-dispersion coefficient, a long time interval (128 s) was necessary to overcome the low precision of the determined tracer location. Due to the

low precision, the dispersion coefficients in the radial and angular directions could not be determined. The precision of the determined tracer location could be improved.

CHAPTER 5
TRANSVERSE MIXING MODEL

In this chapter, a mixing model for the transverse plane is developed. The model includes both convective and diffusive mixing. The particles are assumed to be non-cohesive and the effect of the interstitial fluid is neglected. Diffusion occurs in the radial direction only. The model assumes the previously described behaviour of a rolling or cascading bed. The bed consists of 2 regions; an active region above a static region. While in the static region, particles follow concentric paths parallel to the wall. Upon reaching the interface between the active and static regions, the particles flow through the active region before re-entering the static region. Due to random collisions occurring in the active region, the particles may re-enter the static region at a different radius than the previous cycle. The actual mixing occurs in the active region; however, the mixedness of the bed is tracked in terms of the condition of the static region. This is consistent with the methods used to determine the radial-dispersion coefficients in the previous chapters.

The aim of the model is to account for convective and diffusive mixing in the transverse plane and examine the effects of fill fraction, scale-up and different initial conditions on the mixing rate.

5.1 Static Region

Figure 5-1 shows a rolling or cascading bed divided into active and static regions. The static region is divided into N concentric layers of equal thickness Δr. Layer 1 is at the core of the bed and layer N is next to the wall. The layers are divided into elements of equal angular intervals $\Delta\theta$. The layer next to the wall contains the most elements. The number of elements in a layer decreases with the distance of the layer from the core. Numbering of the angular intervals begins at the first element in the outer layer next to the interface where particles pass from the active region to the static region. For the inner layers, all elements in the same angular interval have the same number.

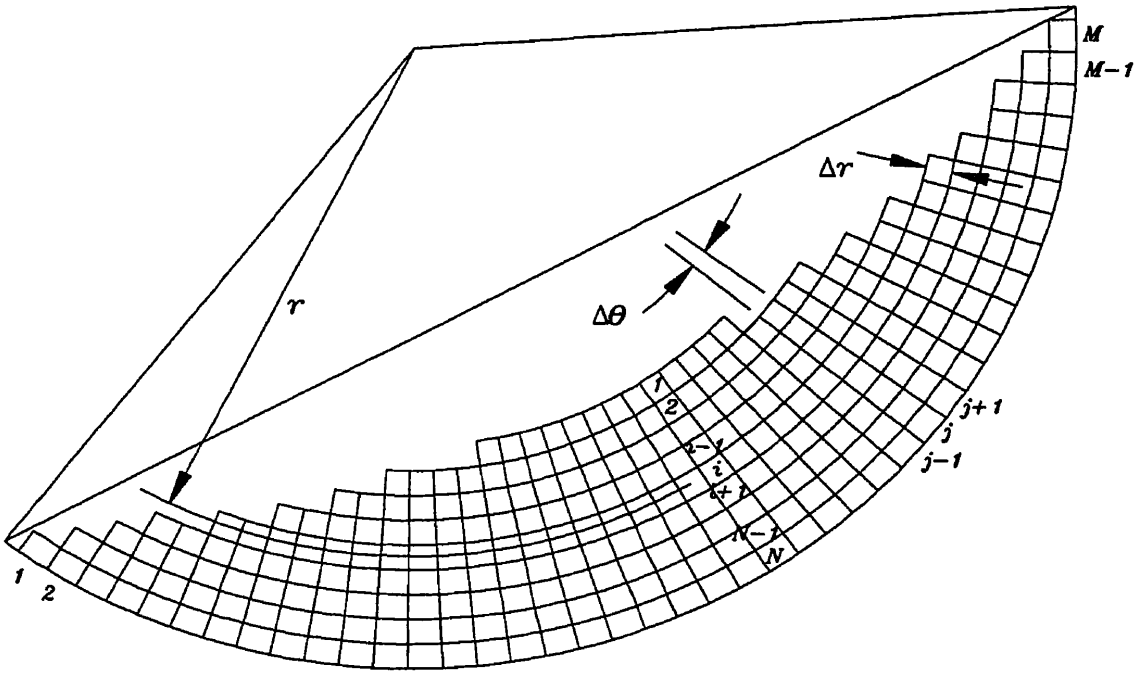

Figure 5-1 Discretization of static region for transverse mixing model

An element of the static region moves at the same angular velocity as the wall. The element velocities in the radial and axial direction are zero. No diffusion occurs between the elements in the static layer. Convective mixing is a result of the different number of elements in each layer of the static region.

For a time step equal to the angular length of the element divided by the angular velocity of the element, the contents of each element will advance to the next element in the direction of rotation.

$$C_{i,j}\big|_{t+\Delta t} = C_{i,j-1}\big|_{t} \quad \text{where} \qquad \Delta t = \frac{\Delta\theta}{2\pi\omega} \tag{71}$$

5.2 Active Region

Diffusive mixing occurs between the layers in the active region. To simplify the model, the time particles spend in the active region is neglected. The mass of the active

layer is also zero. The vector of the tracer concentration in the N elements entering the static layer is the product of the vector of concentrations in the N exiting elements and a $N \times N$ mixing matrix.

$$\mathbf{C}_1 = \mathbf{P} \times \mathbf{C}_2 \tag{72}$$

Elements of **P** are derived from the radial-dispersion coefficient and integration of the dispersion for one cycle. The radial-dispersion coefficient and the mixing matrix are independent of the concentration of tracer and therefore do not change with time. The finite differences equations for radial dispersion between layers were derived in §3.2.

$$-A_{i-1/2} D_r \frac{(C_i - C_{i-1})}{\Delta r} = -A_{i+1/2} D_r \frac{(C_{i+1} - C_i)}{\Delta r} + \Delta V_i \frac{(C_{i,t+\Delta t} - C_i)}{\Delta t} \quad \text{where} \quad 2 \le i \le N-1 \tag{73}$$

$$0 = -A_{3/2} D_r \frac{(C_2 - C_1)}{\Delta r} + \Delta V_1 \frac{(C_{1,t+\Delta t} - C_1)}{\Delta t} \tag{74}$$

$$-A_{N-1/2} D_r \frac{(C_N - C_{N-1})}{\Delta r} = \Delta V_N \frac{(C_{N,t+\Delta t} - C_N)}{\Delta t} \tag{75}$$

The areas for dispersion between the layers are:

$$A_{i+1/2} = \Delta\theta \left(r_i + \frac{\Delta r}{2} \right) \tag{76}$$

$$A_{i-1/2} = \Delta\theta \left(r_i - \frac{\Delta r}{2} \right) \tag{77}$$

The volume of a layer is:

$$\Delta V_i = \Delta\theta \Delta r (r_i) \tag{78}$$

The change in concentration in a layer with respect to time due to radial dispersion is approximated by the following differential equations

$$\frac{dC_i}{dt} = \frac{D_r}{(\Delta r)^2} \left[\left(1 + \frac{\Delta r}{2r_i} \right) C_{i+1} - 2C_i + \left(1 - \frac{\Delta r}{2r_i} \right) C_{i-1} \right] \quad \text{where} \quad 2 \le i \le N-1 \tag{79}$$

$$\frac{dC_1}{dt} = \frac{D_r}{(\Delta r)^2} \left(1 + \frac{\Delta r}{2r_1} \right) (C_2 - C_1) \tag{80}$$

$$\frac{dC_N}{dt} = \frac{D_r}{(\Delta r)^2}\left(1 - \frac{\Delta r}{2r_N}\right)(C_{N-1} - C_N) \tag{81}$$

For each layer, the set of N ordinary differential equations given by Equations (79) through (81) are integrated simultaneously beginning with a concentration vector with 100% tracer in the ith element and zero tracer in the other elements. The radial-dispersion coefficient is the same for each layer. The integration is terminated at the end of the cycle time.

$$t_i = \frac{60\beta}{2\pi n} \tag{82}$$

The vector of concentration at the end of the cycle time forms the ith row in the mixing matrix.

The radial-dispersion coefficient is approximated from the axial-dispersion coefficient and the relative thicknesses of the active and static regions using Equation (25) in §3.0.

$$D_r = D_z\left(\frac{h - \delta_0}{\delta_0}\right)^2 \tag{83}$$

The axial-dispersion coefficient is determined from the empirical Equation (51) with parameters for a rolling/cascading bed given in Table 3-3. The correlation was derived from experimental data from both batch and continuous flow drums. The drum rotational speeds were between 3 and 30 percent of the critical speed and the fill level was less than 50 percent. The drum diameter ranged from 0.05 to 0.60 m and the particle diameter ranged from 0.125 to 13 mm.

$$D_z = 5.82 \times 10^{-4}\,(n/n_c)^{0.44}\,(2R)^{1.29}\,d_p^{0.35}\,X^{-0.55} \tag{84}$$

The thickness of the active layer is approximated from the equation derived from data given by Van Puyvelde et al. (2000a). The ratio of the thickness of the active region to the bed depth is assumed to be equal to the ratio of the area of the active region to the area of the bed.

$$\frac{\delta_0}{h-\delta_0} = 0.277\left(n/n_c\right)^{0.36}(2R)^{-0.19}X^{-0.34} \tag{85}$$

$$\frac{h-\delta_0}{\delta_0} = \frac{1-\delta_0/h}{\delta_0/h} \tag{86}$$

5.3 Interface

The interface between the active and static region is obtained from the mass balance by Khakhar et al. (1997). The derivation assumes a constant density in the active and static regions and a flat upper surface for the active region. A point on the interface that is at a distance r_i from the drum centre is angle θ_i from the axis perpendicular to the bed surface as shown in Figure 5-2. The angle θ_i is determined for each layer of the static region from the following equations.

$$\delta = \frac{1}{2}\left(\frac{L^2}{\delta_0} - 2H\right) - \frac{1}{2}\left[\left(\frac{L^2}{\delta_0} - 2H\right)^2 - 4\left(L^2 + H^2 - r_i^2\right)\right]^{1/2} \tag{87}$$

$$\theta_i = \cos^{-1}\left(\frac{H+\delta}{r_i}\right) \tag{88}$$

The length of the bed surface chord is:

$$L = R\sin\left(\beta/2\right) \tag{89}$$

The distance from bed surface to centre of drum is:

$$H = R\cos\left(\beta/2\right) \tag{90}$$

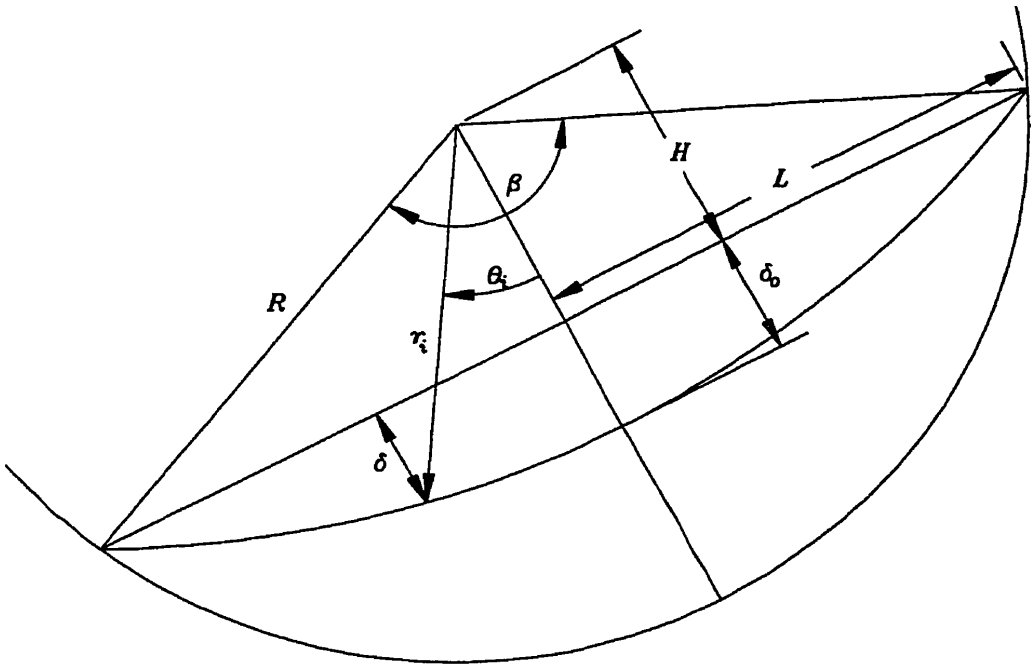

Figure 5-2 Tranverse plane of bed showing the parameters that define the interface between the active and static regions

5.4 Extent of Mixing

The extent of mixing of the bed at any time is the standard deviation from the mean of the concentration of tracer in all the elements.

$$I = \sqrt{\frac{\sum \left(C_{ij} V_{ij} - \overline{C}\right)^2}{\sum V_{ij}}} \tag{91}$$

where the mean concentration is a constant given by:

$$\overline{C} = \frac{\sum C_{ij} V_{ij}}{\sum V_{ij}} \tag{92}$$

5.5 Simulation

Inputs to the mixing model include drum diameter, drum rotational speed, particle diameter, and fill fraction. The number of layers in the static region and the number of angular intervals in outer layer are required. The concentration of tracer in each of the elements in the static region is initialized.

The algorithm for simulating the mixing in the transverse plane is as follows:

1. Calculate the thickness of the active region using Equation (87).
2. Calculate the contact angle between the bed and the wall.
3. Calculate the bed depth.
4. Calculate the thickness of the static region.
5. Determine the co-ordinates that define the grid in the static region.
6. Determine the static region elements at the interface between the static and active regions using Equation (88).
7. Initialise the concentration of tracer in each of the static region elements.
8. Calculate the axial-dispersion coefficient using Equation (84).
9. Calculate the radial-dispersion coefficient using Equation (83).
10. Calculate the cycle time using Equation (82).
11. Calculate the mixing matrix by integrating Equations (79), (80) and (81).
12. For each time step:
    a. Determine the vector of concentrations leaving static region.
    b. Advance the elements in the static region one interval using Equation (71).
    c. Determine the vector of concentrations entering the static region using Equation (72).
    d. Calculate mean and standard deviation of the tracer concentrations in the static region using Equations (92) and (91) respectively.

The mathematical software MATLAB 5.3 is use to solve the mixing simulation. The code is given in Appendix B.

5.6 Results

The model for transverse mixing in a rotating drum was used to simulate an experiment conducted by Carley-Macauly and Donald (1962). At the start of the experiment the bed was split in half perpendicular to the surface. The concentration of tracer on the right hand side of the bed was zero and the concentration in the other half of

the bed was one. Other conditions of the experiment that are inputs to the model are given in Table 5-1.

Table 5-1 Inputs to transverse mixing simulation for comparison to experiment by Carley-Macauly and Donald (1962)

Input variable	Value
Drum diameter	0.1016 m
Drum rotational speed	20 rpm
Particle diameter	0.46 mm
Fill fraction	0.33
Number of layers in static region	27
Number of angular intervals in outer layer	131

For the inputs given in Table 5-1, the simulation results in Table 5-2 were predicted. From the correlation derived in §3.1.3, the model predicted an axial-dispersion coefficient of 1.66×10^{-6} m^2/s. From the axial mixing experiment conducted by Carley-Macauly and Donald in the same drum, with the same fill level and rotational speed, but with slightly larger particles, a smaller axial-dispersion coefficient of 6.39×10^{-7} m^2/s was measured.

Table 5-2 Results of transverse mixing simulation for comparison with experiment by Carley-Macauly and Donald (1962)

Parameter	Value
Relative speed	15.1 % of critical speed
Thickness of active region	31.4% of bed depth
Axial-dispersion coefficient	1.66×10^{-6} m^2/s
Radial-dispersion coefficient	7.88×10^{-6} m^2/s
Number of static region elements	2559

The predicted rate of transverse mixing is compared to experimental measurements in Figure 5-3. For both the predicted and experimental results, the standard deviation of the tracer concentration decays approximately exponentially with time. However, the predicted mixing rate is about 45% faster. The model axial- and radial-dispersion coefficients need to be reduced by about one order of magnitude to get

the best match between the prediction and the experimental results. Using the axial-dispersion coefficient determined in the same drum to estimate radial-dispersion coefficient would give a good match between the predicted and measured mixing rate.

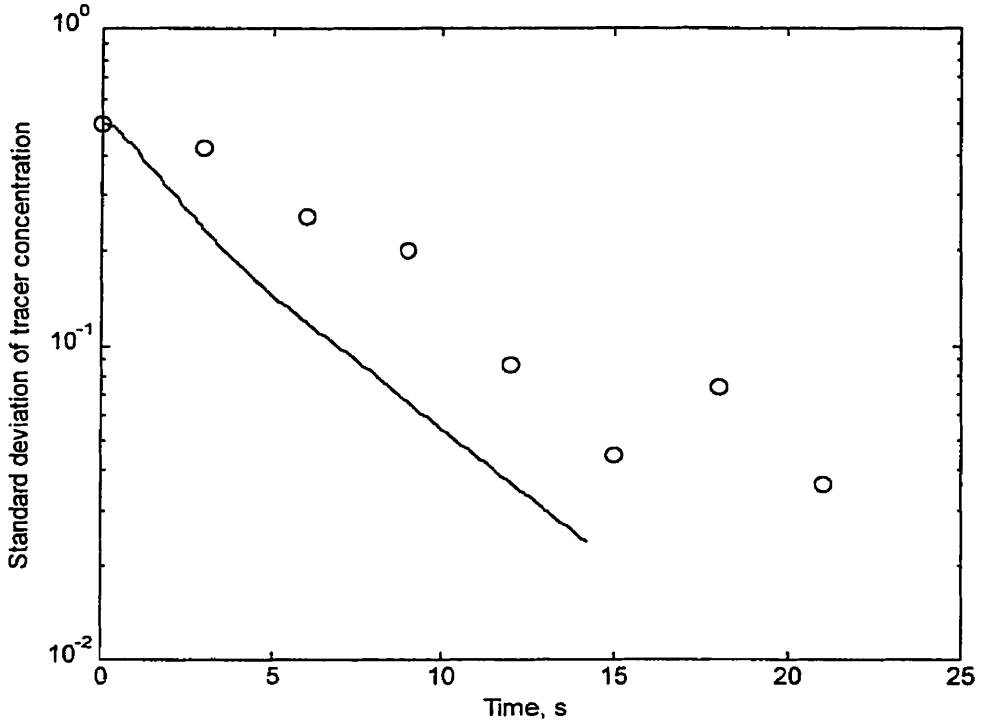

Figure 5-3 Comparison of mixing rate predicted by transverse mixing model (solid line) and experimental measurements (circles) by Carley-Macauly and Donald (1962)

To explore the effects of fill level, scale-up and the initial orientation of the tracer, the mixing simulation was run with the 'base case' inputs given in Table 5-3. Beside matching the conditions for one of the experiments by Black (1988), the inputs are arbitrary.

Table 5-3 Inputs to transverse mixing simulation inputs for base case

Input variable	Value
Drum diameter	0.45 m
Drum rotational speed	12.1 rpm
Particle diameter	0.007 m
Fill fraction	0.24
Number of layers in static region	27
Number of angular intervals in outer layer	131

At the start of the simulation the bed is split in half perpendicular to the surface. The concentration of tracer on the right hand side of the bed is zero and the concentration in the other half of the bed is one.

For the 'base case' inputs given in Table 5-3 the results in Table 5-4 are obtained.

Table 5-4 Results of transverse mixing simulation results for base case

Parameter	Value
Relative speed	19.2 % of critical speed
Thickness of active region	29% of bed depth
Axial-dispersion coefficient	3.88×10^{-5} m^2/s
Radial-dispersion coefficient	2.37×10^{-4} m^2/s
Number of static region elements	2519

Figure 5-4 shows a series of plots for the base case illustrating the tracer concentration pattern with time. As a check, a material balance on the amount of tracer was calculated at each time step. The sum of the tracer was confirmed to remain constant with time.

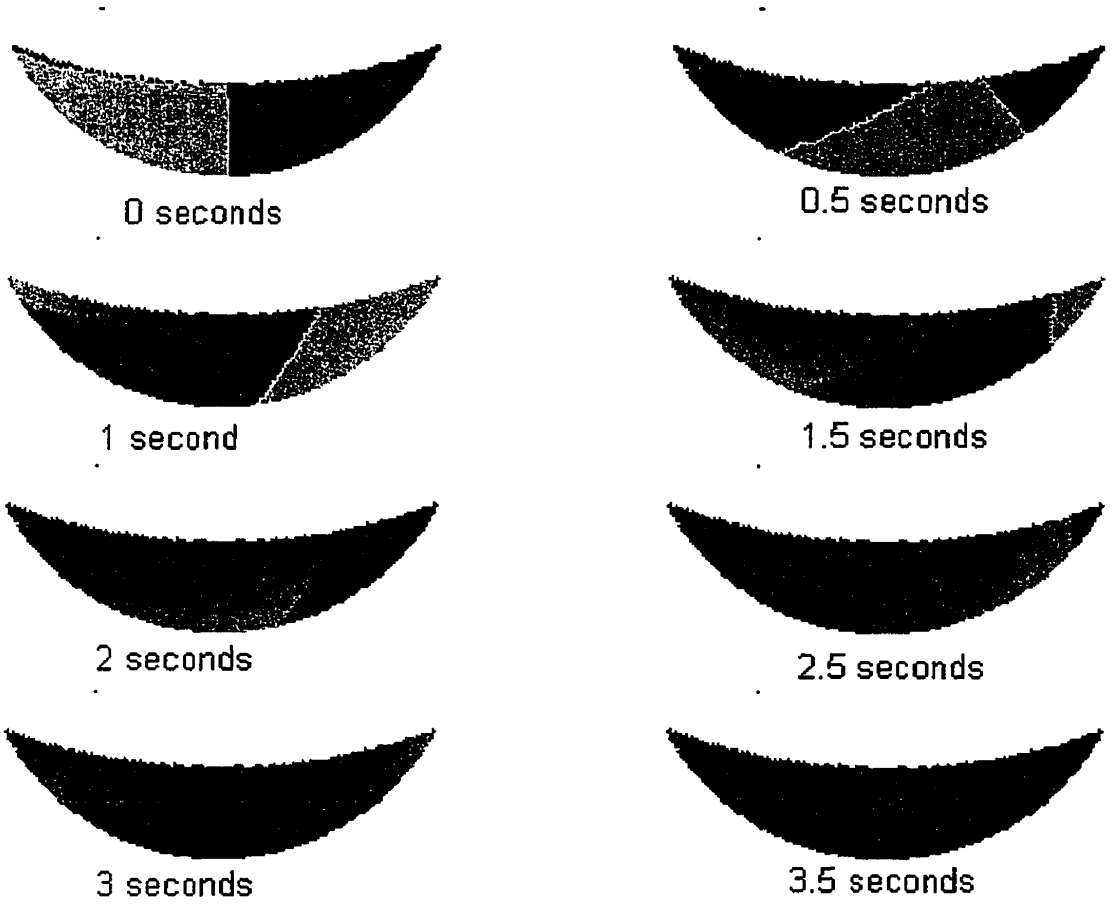

Figure 5-4 Time series of tracer pattern in the static region predicted by transverse mixing model for base case conditions

Base case inputs to the model were varied individually to determine the effect on the mixing rate. Figure 5-5 shows the predicted effect of the percentage of fill on the extent of mixing rate. The fill is varied from 10 to 50%. Increasing the fill by a factor of 5 requires about 6.5 times as long to achieve the same degree of mixing.

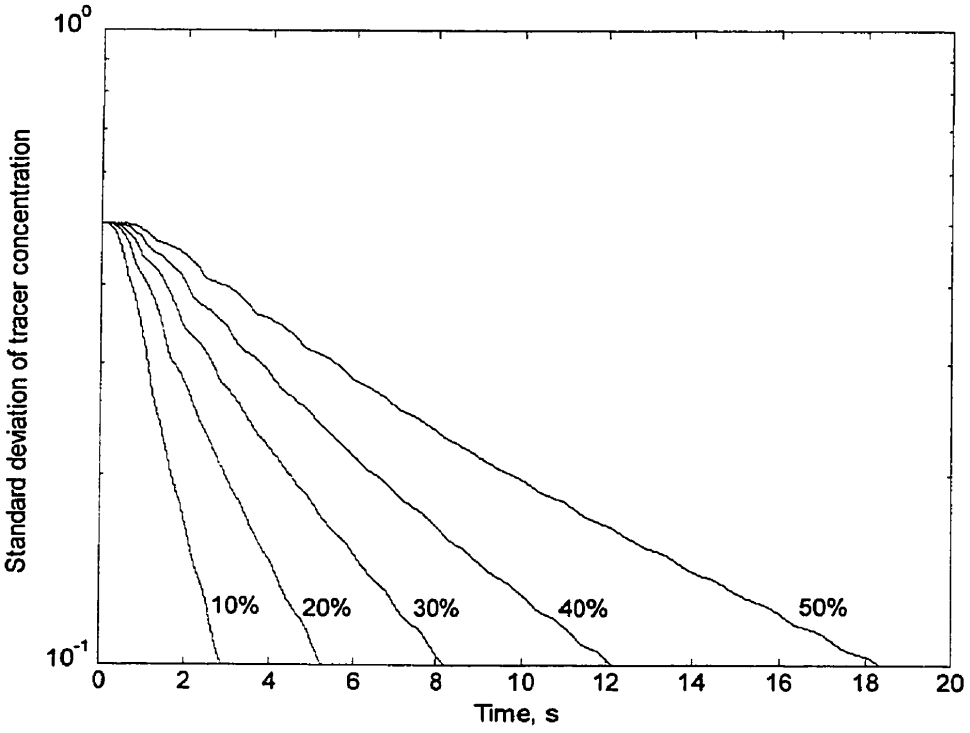

Figure 5-5 Effect of volumetric fill percentage on the mixing rate predicted by transverse mixing simulation

Figure 5-6 shows the effect of scale-up on the mixing rate. The diameter is increased and the speed is reduced to maintain the same fraction of the critical speed. Doubling the diameter results in a 30% increase in the mixing time. The model also indicated that even when the speed is not decreased there is an increase in the mixing time due to the larger diameter.

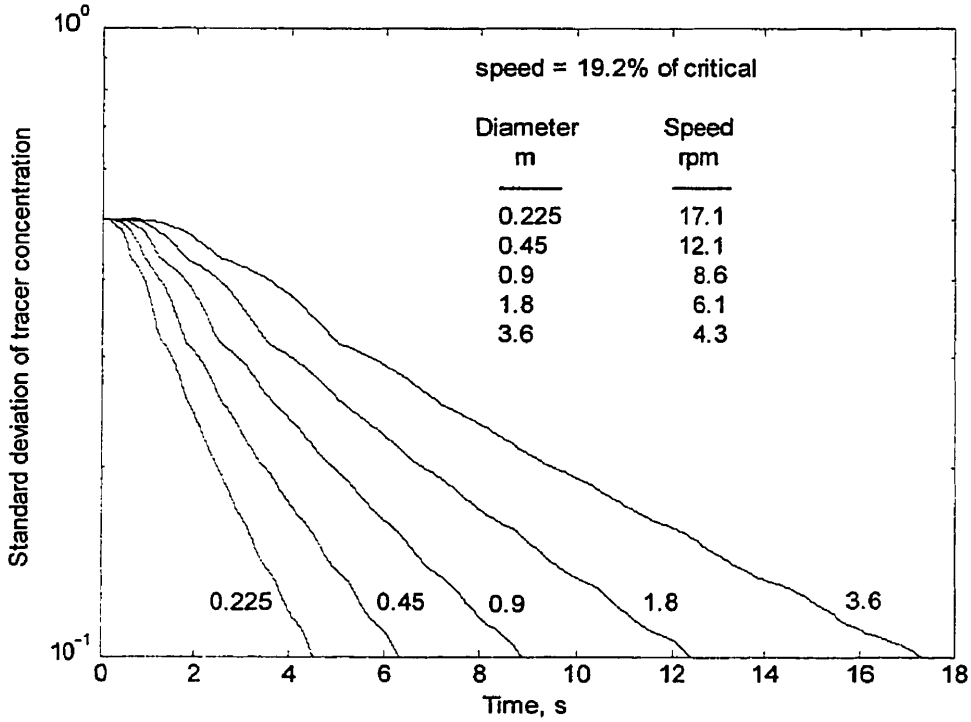

Figure 5-6 Effect of scale-up on the mixing rate predicted by transverse mixing simulation

Figure 5-7 shows two initial orientations of the tracer. For both cases, half the static bed initially contains all the tracer. For the 'smile' initial condition, the bed is divided into equal volumes by a circular arc parallel to the wall. Only radial dispersion is needed to mix the 'smile' pattern.

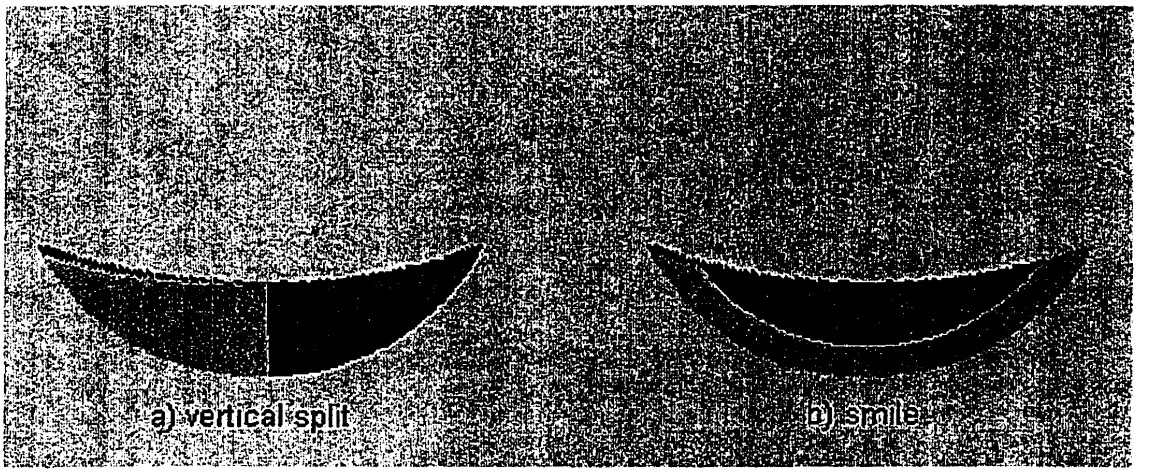

Figure 5-7 Initial tracer orientation used in transverse mixing simulation

Figure 5-8 plots the mixing rate for the two initial orientations of the tracer. The standard deviation of the tracer concentration decays exponentially with time for both initial orientations. However, the 'smile' condition takes about half the time to achieve the same extent of mixing as the bed with the vertical split. The simulation illustrates that because the mixing rate is not the same in all directions, the initial orientation of the tracer affects the speed that it mixes with the rest of the bed.

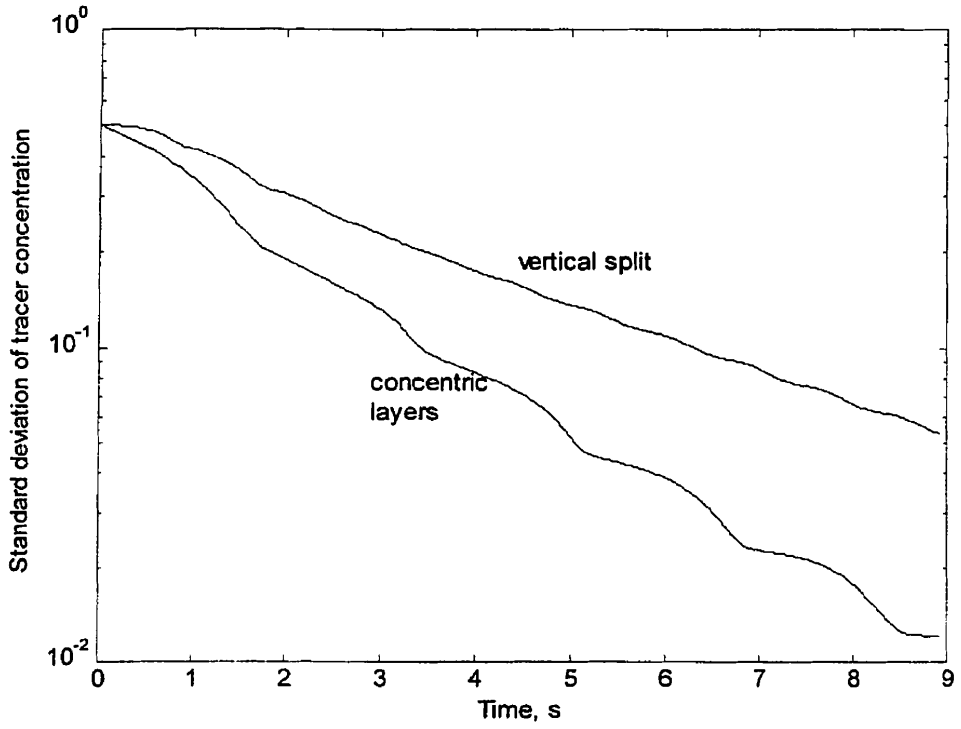

Figure 5-8 Effect of initial tracer orientation on the mixing rate predicted by transverse mixing simulation

5.7 Summary

Using the relationships developed in the previous chapters a simulation model for the mixing in the transverse plane of a rotating drum was developed. The model represents both convective and diffusive mixing. The model displayed the exponential decay of the standard deviation of the tracer concentration with time as observed in experiments. Comparison to an actual experiment showed that the model overstated the mixing rate. The prediction was improved when the axial-dispersion coefficient measured for the same conditions was used rather than the correlation derived in §3.1.3.

The model was used to examine the effect of fill fraction, scale-up and initial tracer position on the mixing rate. For the base conditions chosen, increasing the fill

fraction increased the mixing time. Scale-up (increasing drum diameter while keeping the speed relative to critical speed constant) increases the mixing time. Finally changing the initial orientation of the tracer also has a significant effect on the mixing time.

CHAPTER 6
WALL-TO-BED HEAT TRANSFER

The transverse mixing model developed in the previous chapter is extended to simulate wall-to-bed heat transfer by adding heat conduction in the radial direction. Particles in the static region adjacent to the wall are heated by conduction from the wall into the bed. When the heated particles enter the active region, they are mixed with the bulk of the bed material. Thus, conduction and dispersion toward the core both contribute to the rate that heat is transferred to the bulk of the bed. The temperature of the wall is assumed to be low enough to neglect radiative heat transfer from the wall to the upper surface of the bed.

6.1 Static Region

The distance that heat is conducted into the bed is very small (several millimetres) relative to the depth of the bed and thinner layers are needed to get an accurate result for the penetration of heat into the bed. To keep the total number of layers to a reasonable number, a finer spacing is used near the wall. Figure 6-1 shows the revised discretization pattern used to simulate wall-to-bed heat transfer. The static region is divided into N thick layer of thickness Δr and N' fine layers of thickness $\Delta r'$ next to the drum wall.

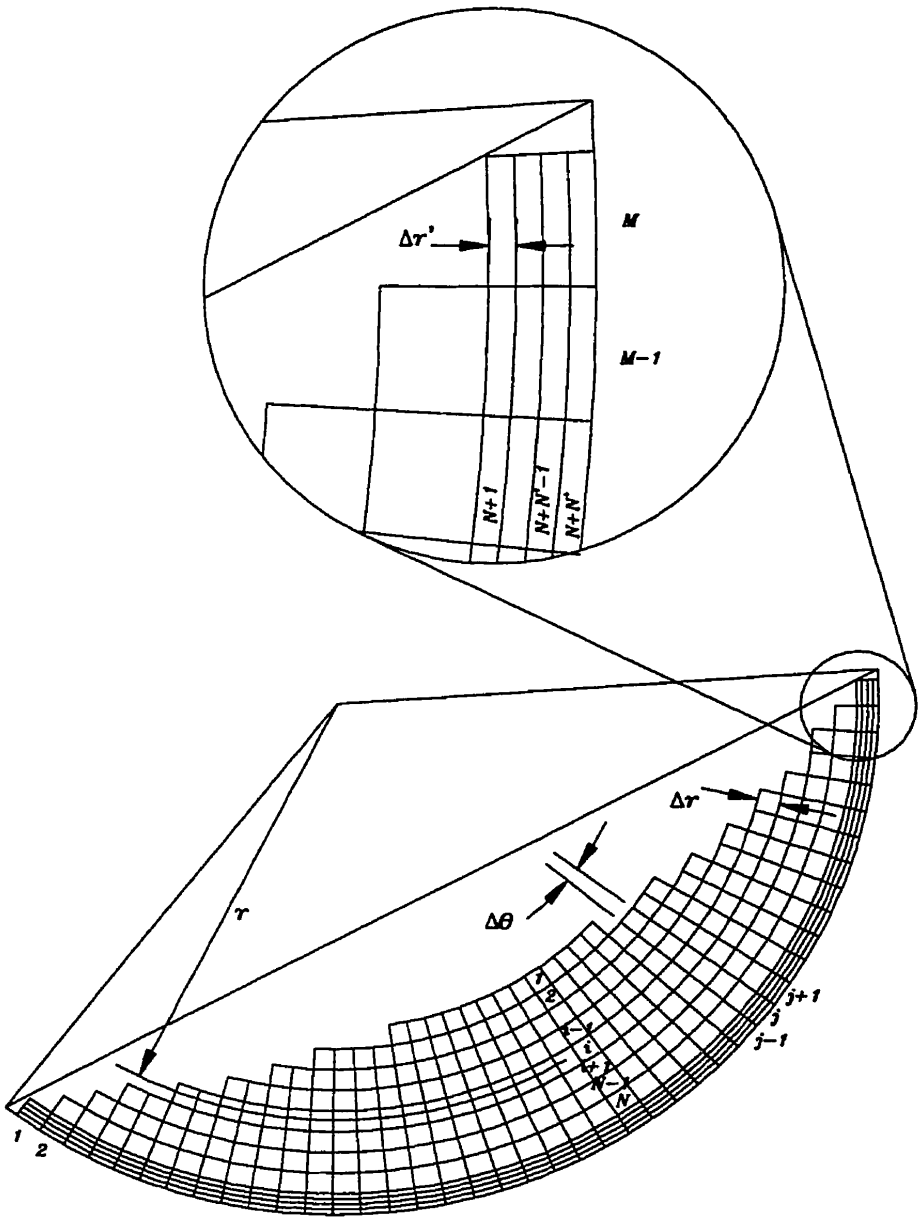

Figure 6-1 Discretization of static region in transverse plane for wall-to-bed heat transfer model

For a time step equal to the interval angle divided by the angular velocity of the drum, the contents of each element in the static region advances to the next element in the direction of rotation. The temperature of the latter element is equal the temperature of the previous element adjusted for the heat transfer with the adjacent element during the time step.

For elements in the thick layers, $2 \le i \le N - 1$

$$T_{i,j}\big|_{t+\Delta t} = T_{i,j-1} + \frac{\alpha \Delta t}{(\Delta r)^2}\left[\left(1+\frac{\Delta r}{2r_i}\right)T_{i+1,j-1} - 2T_{i,j-1} + \left(1-\frac{\Delta r}{2r_i}\right)T_{i-1,j-1}\right] \tag{93}$$

For elements in the fine layers, $N + 1 \le i \le N + N' - 1$

$$T_{i,j}\big|_{t+\Delta t} = T_{i,j-1} + \frac{\alpha \Delta t}{(\Delta r')^2}\left[\left(1+\frac{\Delta r'}{2r_i}\right)T_{i+1,j-1} - 2T_{i,j-1} + \left(1-\frac{\Delta r'}{2r_i}\right)T_{i-1,j-1}\right] \tag{94}$$

where

$$\Delta t = \frac{\Delta \theta}{2\pi\omega} \tag{95}$$

The thermal diffusivity is determined from the bulk properties of the bed material.

$$\alpha = \frac{k}{C_p \rho} \tag{96}$$

For a thick element near the interface, the temperature after one time step is:

$$T_{i,j}\big|_{t+\Delta t} = T_{i,j-1} + \frac{\alpha \Delta t}{(\Delta r)^2}\left[\left(1+\frac{\Delta r}{2r_i}\right)\left(T_{i+1,j-1} - T_{i,j-1}\right)\right] \tag{97}$$

For a fine element near the interface, the temperature after one time step is:

$$T_{i,j}\big|_{t+\Delta t} = T_{i,j-1} + \frac{\alpha \Delta t}{(\Delta r)^2}\left[\left(1+\frac{\Delta r'}{2r_i}\right)\left(T_{i+1,j-1} - T_{i,j-1}\right)\right] \tag{98}$$

For a thick element next to a fine layer, the temperature after one time step is:

$$T_{N,j}\big|_{t+\Delta t} = T_{N,j-1} + \frac{\alpha \Delta t}{(\Delta r)^2}\left[\frac{2\Delta r}{\Delta r + \Delta r'}\left(1+\frac{\Delta r}{2r_i}\right)\left(T_{N+1,j-1} - T_{N,j-1}\right) - \left(1-\frac{\Delta r}{2r_i}\right)\left(T_{N,j-1} - T_{N-1,j-1}\right)\right] \tag{99}$$

For a fine element next to a thick layer, the temperature after one time step is:

$$T_{N+1,j}\big|_{t+\Delta t} = T_{N+1,j-1} + \frac{\alpha\Delta t}{(\Delta r')^2}\left[\left(1+\frac{\Delta r'}{2r_i}\right)\left(T_{N+2,j-1} - T_{N+1,j-1}\right) - \frac{2\Delta r'}{\Delta r + \Delta r'}\left(1-\frac{\Delta r'}{2r_i}\right)\left(T_{N+1,j-1} - T_{N,j-1}\right)\right] \tag{100}$$

For an element next to the wall, the temperature after one time step is:

$$T_{N+N',j}\big|_{t+\Delta t} = T_{N+N',j-1} + \frac{\alpha\Delta t}{(\Delta r')^2}\left[2\left(1+\frac{\Delta r'}{2r_i}\right)T_w - \left(3+\frac{\Delta r'}{2r_i}\right)T_{N+N',j-1} + \left(1-\frac{\Delta r'}{2r_i}\right)T_{N+N'-1,j-1}\right] \tag{101}$$

6.2 Active Region

Hot particles in the fine outer layers mix with the thick inner layers in the active region. The vector of the temperatures in the $N+N'$ elements entering the static region is the product of the vector of the temperatures of the $N+N'$ exiting elements and a $(N+N')$ $\times$ $(N+N')$ mixing matrix.

$$\mathbf{T}_1 = \mathbf{P} \times \mathbf{T}_2 \tag{102}$$

Elements of **P** are derived from the radial-dispersion coefficient and integration of the dispersion for one cycle as in the transverse mixing model. The change in temperature in a layer with respect to time due to radial dispersion is approximated by the following equations. For the first thick layer, $i = 1$,

$$\frac{dT_1}{dt} = \frac{D_r}{(\Delta r)^2}\left(1+\frac{\Delta r}{2r_i}\right)\left(T_2 - T_1\right) \tag{103}$$

For thick layers, $2 \le i \le N\text{-}1$,

$$\frac{dT_i}{dt} = \frac{D_r}{(\Delta r)^2}\left[\left(1+\frac{\Delta r}{2r_i}\right)T_{i+1} - 2T_i + \left(1-\frac{\Delta r}{2r_i}\right)T_{i-1}\right] \tag{104}$$

For the thick layer next to a fine layer, $i = N$,

$$\frac{dT_N}{dt} = \frac{D_r}{(\Delta r)^2}\left[\frac{2\Delta r}{\Delta r + \Delta r'}\left(1+\frac{\Delta r}{2r_i}\right)\left(T_{N+1} - T_N\right) - \left(1-\frac{\Delta r}{2r_i}\right)\left(T_N - T_{N-1}\right)\right] \tag{105}$$

For the fine layer next to a thick layer, $i = N+1$,

$$\frac{dT_{N+1}}{dt} = \frac{D_r}{(\Delta r')^2}\left[\left(1+\frac{\Delta r'}{2r_i}\right)(T_{N+2}-T_{N+1}) - \frac{2\Delta r'}{\Delta r+\Delta r'}\left(1-\frac{\Delta r'}{2r_i}\right)(T_{N+1}-T_N)\right] \quad (106)$$

For fine layers, $N+2 \le i \le N+N'-1$,

$$\frac{dT_i}{dt} = \frac{D_r}{(\Delta r')^2}\left[\left(1+\frac{\Delta r'}{2r_i}\right)T_{i+1} - 2T_i + \left(1-\frac{\Delta r'}{2r_i}\right)T_{i-1}\right] \quad (107)$$

For the fine layer next to the wall, $i = N+N'$,

$$\frac{dT_{N+N'}}{dt} = \frac{D_r}{(\Delta r')^2}\left[-\left(1-\frac{\Delta r'}{2r_i}\right)(T_{N+N'}-T_{N+N'-1})\right] \quad (108)$$

For each layer, the set of $N+N'$ ordinary differential equations given by Equations (103) through (108) are integrated simultaneously beginning with a vector with the temperature of the ith element equal to one and zero for the other elements. Like the mixing model in the previous chapter, the integration is terminated at the end of the one cycle time. The vector at the end of one cycle time forms the ith row in the mixing matrix.

6.3 Heat Transfer Rate and Coefficient

The wall-to-bed heat transfer rate is approximated from the rate of increase in the mean bed temperature.

$$Q = C_p \rho \frac{\overline{T_{t+\Delta t}} - \overline{T}_t}{\Delta t} \sum V_{ij} \quad (109)$$

where the mean temperature of the bed is given by:

$$\overline{T} = \frac{\sum T_{ij}\Delta V_{ij}}{\sum \Delta V_{ij}} \quad (110)$$

The overall heat transfer coefficient from the wall to the bed is calculated by the following equation. The coefficient is based on the total wall surface area. The wall temperature remains constant.

$$h = \frac{Q}{2\pi R\left(T_w - \overline{T}\right)} \quad (111)$$

Table 6-1 gives the inputs to the heat transfer simulation. Thermal properties for oil shale from the Stuart deposit near Gladstone, Queensland are used.

Table 6-1 Inputs to wall-to-bed heat transfer simulation for base case

Input variable		Value
Drum diameter	$2R$	0.45 m
Drum rotational speed	n	12.1 rpm
Particle diameter	d_p	0.007 m
Fill fraction	X	0.24
Effective thermal conductivity	k	0.2 W/m·°C
Bulk density	ρ	880 kg/m^3
Heat capacity	C_p	1000 J/kg·°C
Wall temperature	T_w	400 °C
Initial bed temperature	T_o	100 °C
Number of thick layers in static region	N	20
Thickness of thick layers	Δr	4.5 mm
Number of fine layers near wall	N'	5
Thickness of fine layers	$\Delta r'$	0.56 mm
Number of angular intervals in outer layer	M	65

6.4 Results

Using the inputs given in Table 6-1, the heat transfer model predicts the results given in Table 6-2.

Table 6-2 Results of wall-to-bed heat transfer simulation for base case

Parameter		Value
Relative speed	n/n_c	19.2 % of critical speed
Thickness of active region	δ_o/h	29% of bed depth
Axial-dispersion coefficient	D_z	3.88×10^{-5} m^2/s
Radial-dispersion coefficient	D_r	2.37×10^{-4} m^2/s
Thermal diffusivity	α	2.27×10^{-7} m^2/s
Number of thick elements		910
Number of fine elements		325
Wall-to-bed heat transfer coefficient	h	121 W/m^2-K

The predicted wall-to-bed heat transfer coefficient based on the total inside wall area is 121 W/m^2·K. This is only slightly smaller than the wall-to-bed heat transfer coefficient predicted using penetration theory and the perfect mixing assumption from Wachters and Kramers (1964).

$$h = \frac{k}{\pi}\sqrt{\frac{2n\beta}{60\alpha}} = 128 \text{ W/m}^2\cdot\text{K} \tag{112}$$

For this set of conditions, the conduction next to the wall controls the heat transfer rate. This is expected when the radial-dispersion coefficient is about 1000 times larger than the thermal diffusivity. For this case, the effect of speed and fill level on the heat transfer coefficient can be predicted directly from Equation (112).

6.5 Summary

The transverse mixing model derived in the previous chapter was extended to simulate the transfer of heat from the drum wall to the bed material. The wall-to-bed heat transfer coefficient was determined from the simulation results.

CHAPTER 7
CONCLUSIONS

Mixing of non-cohesive granular solids in a partially-filled, horizontal, rotating drum occurs in the axial, radial and angular directions. Mixing in the axial direction is purely diffusive and can be represented accurately by a one-dimensional diffusion equation. The primary mixing mechanism and the dispersion coefficient are the same in continuous-feed and batch drums.

From the published experimental data, an empirical design correlation was derived to relate the particle dispersion coefficients in the axial direction to rotational speed, degree of fill, drum diameter and particle size. A separate correlation was also derived for each of the possible types of bed behaviour. The axial-dispersion coefficient ranges from 1×10^{-7} to 1×10^{-4} m^2/s for drum diameters ranging from 0.08 m to 0.90 m. For all types of bed behaviour, the coefficient is approximately proportional to the drum diameter and the square root of the particle diameter. The effect of the rotational speed and fill level depends on the type of bed behaviour. For rolling and cascading bed behaviour, the coefficient is proportional to the square root of the rotational speed.

Unlike mixing in the axial direction, particle mixing in the transverse plane is a combination of convection and diffusion. Also, little published data exists to quantify the dispersion coefficients let alone the effects of rotational speed, degree of fill, drum diameter and particle size. However, dispersion in each direction is primarily due to the same phenomenon i.e random collisions in the active region. Relationships between the axial, radial and angular dispersion coefficients are proposed, allowing the radial and angular coefficients to be predicted from the more easily measured axial coefficient with an approximation of the relative thicknesses of the active and static regions.

A method of deriving the radial- and angular-dispersion coefficients from a single-particle tracking experiment was developed. The method was used to determine the radial- and angular-dispersion coefficients from published data from 3 sources. The

coefficients were compared to the axial-dispersion coefficient predicted using the correlation derived from the published data for axial mixing in rotary drums.

The proposed relationships are consistent with the radial and angular coefficients that can be determined from the published experimental data. The radial-dispersion coefficient is usually about 2 to 4 times larger than the axial-dispersion coefficient. This is approximately equal to the square of the ratio of the thicknesses of the active and static regions. The radial-dispersion coefficient increases with speed, fill, drum diameter and particle diameter.

Experiments using a non-intrusive particle tracking technique were performed with the intention of determining dispersion coefficients in each of the three dimensions in the same drum with the same conditions. While it was possible to determine the axial-dispersion coefficient, the precision of determining the location of the tracer particle was not enough to determine the radial- or angular-dispersion coefficients. A number of changes could be made in future experiments to obtain coefficients in the transverse plane using this technique.

A granular-solids mixing model for the transverse plane in a partially filled horizontal rotating drum was developed. The model included convective mixing and particle diffusion perpendicular to the circulation streamlines. Using the proposed relationship between the axial- and radial-dispersion coefficients, the model simulates the state of mixing in the static region.

The model predicts the exponential decay of the standard deviation of the tracer concentration as observed in experiments by others. While the correlation derived to predict the axial-dispersion coefficient can be used to predict the radial dispersion coefficient, the transverse mixing rate can be predicted more accurately if the axial-dispersion coefficient in the same drum with the same conditions is known.

The model was used to examine the effects of fill fraction, scale-up and initial tracer orientation on the mixing rate. For the base conditions chosen, increasing the fill fraction increased the mixing time. Scale-up (increasing the drum diameter while

keeping the speed relative to critical speed constant) increases the mixing time. Finally changing the initial orientation of the tracer can change the mixing time by a factor of 2.

A number of improvements could be made to the mixing model. For simplicity the current model neglects the time the particles spend in active region. To accurately model the particle time in the active region, the velocity profile in the active region is required. The current model also relies on empirical correlation to estimate the relative thickness of the active layer from the drum speed and fill. Ideally the thickness of the active region should be derived from both the particle properties and the geometry and operating condition of the drum.

By adding heat conduction in the radial direction, the mixing model was extended to simulate wall-to-bed heat transfer. The model was used to predict the significance of mixing on the wall-to-bed heat transfer rate. For the conditions chosen, the heat transfer rate was essentially independent of the mixing. The conduction near the wall in the static region determined the heat transfer rate.

The heat transfer model illustrates how the mixing model can be extended to simulate processes in the granular bed in a rotating kiln which depend on mixing. Future modifications to the mixing model could include the addition of particle segregation or chemical reactions.

Bibliography

Abouzeid, A.S.M.A., Mika, T.S., Sastry, K.V., and Fuerstenau, D.W., "The influence of operating variables on the residence time distribution for material transport in a continuous rotary drum", Powder Tech., **10**, 273 (1974).

Alonso, M., Satoh, M., and Miyanami, K., "Optimum combination of size ratio, density ratio and concentration to minimize free surface segregation", Powder Tech., **68**, 145-152 (1991).

Ang, H.M., Tade, M.D., and Sze, M.W., "Residence time distribution for a cold model rotary kiln", The AusIMM Proceedings, **1**, 11-16 (1998).

Augenstein, D., "A study of the flow of dry particulate solids", PhD thesis, Pennsylvania State University (1974).

Augenstein, D. and Hogg, D., "An experimental study of the flow of dry powders over inclined surfaces", Powder Technology **19**, 205-215 (1978).

Baumann, G., Jánosi, I. M., and Wolf, D. E., "Surface properties and flow of granular material in a two-dimensional rotating-drum model", Physical Review E **51**(3), 1879-88 (1995).

Black, J.M., "Particle motion and heat transfer in rotary drums", PhD thesis, Edinburgh University (1988).

Boateng, A. A., "Rotary kiln transport phenomena: Study of the bed motion and heat transfer", PhD thesis, University of British Columbia (1993).

Boateng, A. A. and Barr, P.V., "Modelling of particle mixing and segregation in the transverse plane of the rotary kiln", Chem. Eng. Sci., **51**(1), 4167-4181 (1996).

Boateng, A. A. and Barr, P.V., "Granular flow behavior in the transverse plane of a partially filled rotating cylinder", J. Fluid. Mech., **330**, 233-249 (1997).

Boateng, A. A., "On flow-induced kinetic diffusion and rotary kiln bed burden heat transport", Chem. Eng. Comm., **170**, 51-66 (1998).

Buchholtz, V., Pöschel, T., and Tillemans, H., "Simulation of rotating drum experiments using non-circular particles", Physica A **216**(3), 199-212 (1995).

Cahn, D.S. and Fuerstenau, D.W., "Simulation of diffusional mixing of particulate solids by Monte Carlo techniques", Powder Technology, **1**, 174-182 (1967).

Campbell, C.S., "Self-diffusion in granular shear flows", J. Fluid Mech., **348**, 85-101 (1997).

Cantelaube, F., Bideau, D. And Roux, S., "Kinetics of segregation of granular media in a two-dimensional rotating drum', Powder Technology, **93**, 1-11 (1997).

Carley-Macauly, K. and Donald, M., "The mixing of solids in tumbling mixers - I", Chem. Eng. Sci. **17**, 493-506 (1962).

Carley-Macauly, K. and Donald, M., "The mixing of solids in tumbling mixers - II", Chem. Eng. Sci. **19**, 191-199 (1964).

Cassanello, M., Larachi, F., Marie, M-N., Guy, C., Chaouki, J., "Experimental characterization of the solid phase chaotic dynamics in three-phase fluidization", Ind. Eng. Chem. Res., **34**(9), 2971-2980 (1995).

Chapman, S. and Cowling, T.G., *The Mathematical Theory on Non-uniform Gases*, 3rd ed., Cambridge University Press, Cambridge, UK (1970).

Clément, E., Rajchenbach, J., and Duran, J., "Mixing of granular material in a bidirectional rotating drum", Europhysics Letters **30**(1), 7-12 (1995).

Das Gupta, S., Khakhar, D., and Bhatia, S., "Axial transport of granular solids in horizontal rotating cylinders. Part 1: Theory", Powder Technology, **67**, 145-151 (1991).

Ferron, J. and Singh, D., "Rotary kiln transport processes", AIChE J. **37**(5), 747-58 (1991).

Goodman, M. and Cowin, S., "Two problems in the gravity flow of granular materials", J. Fluid Mech. **45**(2), 321-329 (1971).

Gorog, J., Adam, T., and Brimacombe, J., "Regenerative heat transfer in rotary kilns", Metallurgical Transactions B, **13B**, 153-163 (1982).

Hatzilyberis, K.S. and Androutsophoulos, G.P., "An RTD study for the flow of lignite particles through a pilot rotary dryer", Drying Technology, **17**(4&5), 745-757 (1999).

Hehl, M., Kroger, H., Helmrich, H., and Schugerl, K., "Longitudinal mixing in horizontal rotary drum reactors", Powder Technology, **20**, 29-37 (1978).

Henein, H., Brimacombe, J., and Watkinson, A.P., "The modeling of transverse solids motion in rotary kilns", Metallurgical Transactions B **14B**, 207-220 (1983a).

Henein, H., Brimacombe, J., and Watkinson, A.P., "Experimental study of transverse bed motion in rotary kilns", Metallurgical Transactions B **14B**, 191-205 (1983b).

Hogg, R., Cahn, D., Healy, T., and Fuerstenau, D., "Diffusional mixing in an ideal system", Chemical Engineering Science, **21**, 1025-1038 (1966).

Hogg, R., "The mixing of particulate solid materials", PhD Thesis, University of California, (1969).

Hogg, R., Mempel, G. and Fuerstenau, D.W., "The mixing of trace quantities into particulate solids", Powder Technol., **2**, 223-228 (1969).

Hogg, R., Shoji, K. and Austin, L.G., "Axial transport of dry powders in horizontal rotating cylinders", Powder Technol., **9**, 99-106 (1974).

Hogg, R. and Fuerstenau, D., "Transverse mixing in rotating cylinders", Powder Technology **6**, 139-148 (1972).

Hsiau, S.-S. and Hunt, M., "Shear-induced particle diffusion and longitudinal velocity fluctuations in a granular-flow mixing layer", J. Fluid Mech. **251**, 299-313 (1993a).

Hsiau, S.-S. and Hunt, M., "Kinetic theory analysis of flow-induced particle diffusion and thermal conduction in granular material flows", J. Heat Transfer. **115**, 541-8 (1993b).

Hsiau, S.-S. and Jang, H.-W., "Measurement of velocity fluctuations of granular matrials in a shear cell", Experimental Thermal and Fluid Science **17**, 202-209 (1998).

Hsiau, S.-S. and Shieh, Y.-M., "Fluctuations and self-diffusion of sheared granular material flows", J. Reol. **43**(5), 1049-1065 (1999).

Hsiau, S.-S. and Shieh, Y.-M., "Effect of solids fraction on fluctuations and self-diffusion of shear granular flows", Chemical Engineering Science **55**, 1969-1979 (2000).

Inoue, I., Yamaguchi, K. and Sato, K., "Motion of particle and mixing process in a horizontal drum mixer" Kagaku K_gaku **35** (12), 1323-29 (1970).

Karra, V.K., and Fuerstenau, D.W., "Material transport in a continuous rotating drum. Effect of discharge plate geometry", Powder Tech., **16**, 23-28 (1977).

Kelbert, F. and Royere, C., "Lateral mixing and heat transfer in a rolling bed", Int. Chem. Eng. **31**(3), 441-449 (1991).

Khakhar, D.V., McCarthy, J.J., Shinbrot, T. and Ottino, J.M., "Transverse flow and mixing of granular material in a rotating cylinder", Phys. Fluids **9**(1), 31-43 (1997).

Kohav, T., Richardson, J. and Luss, D. "Axial dispersion of solid particles in a continuous rotary kiln", AIChE J., **41**(11), 2465-76 (1995).

Kohring, G.A., "Studies of diffusional mixing in rotating drums via computer simulations", J. Phys. I France, **5**, 1551-1561 (1995).

Kramers, H. and Croockewit, P., "The passage of granular solids through inclined rotary kilns", Chem. Eng. Sci., **1**(6), 259-265 (1952).

Larachi, F., Chaouki, J., and Kennedy, G., "3-D mapping of solids flow fields in multiphase reactors with RPT", AIChE Journal, **41**(2), 439-443 (1995).

Larachi, F., Kennedy, G. and Chaouki, J., "A γ-ray detection system for 3-D particle tracking in multiphase reactors", Nuclear Instruments and Methods in Physics Research, A **338**, 568-576 (1994).

Lebas, E., Hanrot, F., Ablitzer, D., and Houzelot, J.-L., "Experimental study of residence time, particle movement and bed depth profile in rotary kilns", The Canadian Journal of Chemical Engineering, **73**(2), 173-180 (1995).

Leger, C., Cook, C., Cundy, V., Sterling, A., Deng, X., and Lighty, J., "Bed mixing and heat transfer in a batch loaded rotary kiln", Environmental Progress **12**(2), 101-9 (1993).

Lehmberg, J., Hehl, M., and Schügerl, K., "Transverse mixing and heat transfer in horizontal rotary drum reactors", Powder Technology **18**, 149-163 (1977).

Lun, C., Savage, S., Jeffrey, D. and Chepurniy, N., "Kinetic theories for granular flow: inelastic particles in Couette flow and slightly inelastic particles in a general flowfield", J. Fluid Mech. **140**, 223-56 (1984).

McCarthy, J.J. and Ottino, J.M., "Particle dynamics simulation: a hybrid technique applied to granular mixing", Powder Technology **97**, 91-99 (1998).

McTait, G., Scott, D. and Davidson, J. "Residence time distribution of particles in rotary kilns", Fluidization IX, Proc. of 9th Eng. Foundation Conf. On Fluidization, Durango, CO, May 17-22 (1998).

Mellmann, J. "The transverse motion of solids in rotating cylinders – forms of motion and transition behavior", Powder Technology **118**, 251-270 (2001).

Moriyama, A. and Suga, T., "Axial dispersion and residence time distribution of spherical particles in rotary kiln", Tetsu-to-Hague, **60**(9), 1283-1288 (1974).

Mu, J. and Perlmutter, D., "The mixing of granular solids in a rotary cylinder", Amer. Inst. Chem. Eng., **26**(6), 928-934 (1980).

Nakagawa, M., Altobelli, S.A., Caprihan, A., Fukushima, E., and Jeong, E.-K. "Non-invasive measurement of granular flows by magnetic resonance imaging", Experiments in Fluids, **16**, 54-60 (1993).

Nityanand, N., Manley, B., and Henein, H., "An analysis of radial segregation for different sized spherical solids in rotary cylinders", Metallurgical Transactions B **17B**, 247-57 (1986).

Ottino, J.M. and Khakhar, D.V., "Mixing and segregation of granular materials", Annu. Rev. Fluid Mech., **32**, 55-91 (2000).

Parker, D.J., Dijkstra, A.E., Martin, T.W., and Seville, J.P.K., "Positron emission particle tracking studies of spherical particle motion in rotating drums", Chemical Engineering Science, **52**(13), 2011-2022 (1997).

Perron, J. and Bui, R., "Rotary cylinders: solid transport prediction by dimensional and rheological analysis", Can. J. Chem. Eng. **68**, 61-8 (1990).

Perron, J. and Bui, R., "Rotary cylinders: transverse bed motion prediction by rheological analysis", Can. J. Chem. Eng. **70**, 223-31 (1992).

Pershin, V., "Modeling of loose material mixing process in the cross section of a rotary drum", Theoretical Foundations of Chemical Engineering **20**(4), 324-9 (1987).

Pershin, V., "Modelling the mixing of granular material in a cross section of a smooth rotating drum", Theoretical Foundations of Chemical Engineering **23**(3), 249-55 (1990).

Pollard, B. and Henein, H., "Kinetics of radial segregation of different sized irregular particles in rotary cylinders", Canadian Metallurgical Quarterly **28**(1), 29-40 (1989).

Rao, S., Bhatia, S., and Khakhar, D., "Axial transport of granular solids in rotating cylinders. Part 2: Experiments in a non-flow system", Powder Technology, **67**, 153-162 (1991).

Ray, A.K., Prasad, H.S., Ray, H.S., and Sen, P.K., "Residence time in a rotary kiln for sponge iron making – Prediction from kinetic data", Steel India, **17**(1), 16-20 (1994).

Ristow, G., "Particle mass segregation in a two-dimensional rotating drum", Europhysics Letters **28**(2), 97-101 (1994).

Rogers, R.S.C. and Gardner, R.P., "A Monte Carlo method for simulating dispersion and transport through horizontal rotating cylinders", Powder Technology, **23**, 159-167 (1979).

Rutgers, R., "Longitudinal mixing of granular material flowing through a rotating cylinder Part II. Experimental", Chem. Eng. Sci., 20, 1089-1100 (1965).

Saeman, W.C., "Passage of solids through rotary kilns. Factors affecting time passage", Chem. Eng. Prog. **47**(10), 508-514 (1951).

Sai, P.S.T., Surender, G.D., Damodaram, A.D., Suresh, V., Philip, Z.G., and Sankaran, K., "Residence time distribution and material flow studies in a rotary kiln", Met. Trans. B, **21B**, 1005, (1990).

Savage, S., "Gravity flow of cohesionless granular materials in chutes and channels", J. Fluid Mech. **92**(1), 53-96 (1979).

Savage, S. and Dai, R., "Studies of granular shear flows - Wall slip velocities, 'layering' and self-diffusion", Mechanics of Materials **16**(½), 225-38 (1993).

Sherritt, R.G., Behie, L.A. and Mehrotra, A.K., "The movement of solids in flighted rotating drums" Chap. 18, p. 421-441, Mixed-Flow Hydrodynamics, Advances in Engineering Fluid Mechanics Series ed. Cheremisinoff, N.P., Gulf Publishing Co., Texas, (1996).

Shoji, K., Hogg, R., and Austin, L.G., "Axial mixing of particles in batch ball mills", Powder Technol.., 7, 331-336 (1973).

Singh, D., "A fundamental study of the mixing of solid particles", PhD Thesis, University of Rochester (1979).

Sugimoto, M., "An estimation of the residence time distribution of particles flowing through a rotary cylinder", Kagaka Kogaku, **32**(3), 291 (1968a).

Sze, M.W., Ang, H.M., and Tade, M.O., "Particle dynamics in a cold rotary kiln", Chemeca '95 Proceedings, **4**, 27-32 (1995).

Tscheng, S., "Convective heat transfer in a rotary kiln", PhD Thesis, University of British Columbia (1978).

Turner, R., Wright, B.C., and Taciuk, W., "Oil shale processing with the AOSTRA Taciuk Processor", 4th UNITAR/UNDP Conf. Proc., **5**(237), (1089).

Vahl, L. and Kingma, H., "Transport of solids through horizontal rotary cylinders", Chem. Eng. Sci., **1**(6), 253-258 (1952).

Van Puyvelde, D.R., Young, B.R., Wilson, M.A. and Schmidt, S.J., "Modelling transverse mixing in a rolling drum", Can. J. Chem. Eng., **78**, 635-642 (2000a).

Van Puyvelde, D.R., Young, B.R., Wilson, M.A. and Schmidt, S.J., "Modelling transverse segregation of particulate solids in a rolling drum", Trans. I. Chem. Eng., **78A**, 643-650 (2000b).

Wachters, L. and Kramers, H., "The calcining of sodium bicarbonate in a rotary kiln", Proc. 3rd European Symposium Chemical Reaction Engineering, 77-87 (1964).

Wes, G., Drinkenburg, A., and Stemerding, S., "Solids mixing and residence time distribution in a horizontal rotary drum reactor", Powder Technology **13**, 177-184 (1976).

Woodle, G. and Monro, J., "Particle motion and mixing in a rotary kiln", Powder Technology **76**, 241-5 (1993).

Wrightman, C. and Muzzio, J.F., "Mixing of granular material in a drum mixer undergoing rotational and rocking motions I. Uniform particles", Powder Technology **98**, 113-124 (1998).

Yamane, K., Nakagawa, M., Altobelli, S.A., Tanaka, T. and Tsuji, Y., "Steady particulate flows in a horizontal rotating cylinder", Physics of Fluids **10**(6), 1419-1427 (1998).

Yang, L. and Farouk, B., "Modeling of solid particle flow and heat transfer in rotary kiln calciners", J. Air & Waste Manage. Assoc. 47, 1189-96 (1997).

Zhang, Y. and Campbell, C., "The interface between fluid-like and solid-like behavior in two-dimensional granular flows", J. Fluid Mech. **237**, 541-68 (1992).

Zik, O., Levine, D., Lipson, S., Shtrikman, S., and Stavans, J., "Rotationally induced segregation of granular materials", Physical Review Letters **73**(5), 644-7 (1994).

APPENDIX A

Axial-Dispersion Coefficients from Published Literature

Table A-1 Particle dispersion coefficients in the axial direction from residence time distribution experiments in continuous feed rotating drums

Reference	Drum diameter, m	Fill, vol. %	Relative speed, % critical	Granular material	Mean particle diameter, mm	Angle of repose, deg	Axial-dispersion coefficient, m^2/s
Karra and Fuerstenau (1977)	0.08	33.7	6.7	dolomite	0.357	N/A	1.40×10^{-6}
		20.9					1.90×10^{-6}
		14.2					$1.10\times e^{-6}$
		8.3					7.30×10^{-6}
		4.9					1.91×10^{-5}
		8.0					6.60×10^{-6}
Abouzeid et al. (1974)	0.08	34.6	7.4	dolomite	0.359	N/A	7.40×10^{-7}
		28.8	13.4				9.60×10^{-7}
		32.1	28.1				1.47×10^{-6}
		32.1	56.2				2.85×10^{-6}
		43.6	84.3				3.81×10^{-6}
		27.8	28.1				1.10×10^{-6}
		27.3	28.1				1.20×10^{-6}
		22.5	28.1				1.60×10^{-6}
		17.7	28.1				2.40×10^{-6}
		27.2	28.1				7.20×10^{-7}
		30.7	28.1				9.80×10^{-7}
		36.5	28.1				1.82×10^{-6}
Rogers and Gardner (1979)	0.095	23.5	65.6	dry powder	0.335	38	1.49×10^{-6}
		40.5					6.46×10^{-7}
McTait et al. (1998)	0.105	14.5	0.8	ballitini	0.2	28	1.55×10^{-6}
Mu and Perlmutter (1980)	0.102	12.2	15.1	rice	2x5	35	1.10×10^{-5}
Hatzily-beris and Androut-sopoulos (1999)	0.12	42.5	1.2	lignite	9.6		2.74×10^{-6}
		18.4	1.6				5.10×10^{-6}
		9.7	2.5				1.77×10^{-6}
		6.7	4.1				4.94×10^{-6}
		6.3	4.9				1.16×10^{-5}
		3.5	6.6				1.77×10^{-5}
Ang et al. (1998)	0.14	14.9	1.8	zircon + coal	2.7		7.28×10^{-7}
		22.7	1.8		1.7		4.73×10^{-7}
		23.1	1.8		2.7		2.85×10^{-7}
		27.6	1.8		2.7		6.21×10^{-7}
		37.2	1.3		2.7		4.28×10^{-7}

Reference	Drum diameter, m	Fill, vol. %	Relative speed, % critical	Granular material	Mean particle diameter, mm	Angle of repose, deg	Axial-dispersion coefficient, m^2/s
		18.9	1.8		2.7		6.75×10^{-7}
		18.3	1.8		1.7		9.08×10^{-7}
		27.2	1.8		1.7		7.64×10^{-7}
		29.7	1.3		1.7		5.18×10^{-7}
		35.8	1.3		1.7		6.77×10^{-7}
		30.2	1.3		2.7		2.75×10^{-7}
		25.5	1.3		2.7		5.39×10^{-7}
		20.2	1.3		1.7		5.16×10^{-7}
		16.9	1.8		1.7		6.40×10^{-7}
		23.6	1.3		1.7		7.86×10^{-7}
		18.3	1.3		2.7		5.23×10^{-7}
		11.5	1.8		2.7		8.83×10^{-7}
		20.5	1.8		2.7		5.33×10^{-7}
		15.3	1.8		2.7		8.17×10^{-7}
		35.5	1.3		2.7		7.17×10^{-7}
Sai et al. (1990)	0.147	18.7	2.7	Ilmenite	0.2	27.4	1.75×10^{-6}
		12.3	2.7				1.47×10^{-6}
		6.6	2.7				1.67×10^{-6}
		19.3	0.9				2.02×10^{-6}
		10.5	0.9				2.02×10^{-6}
		10.6	1.8				1.43×10^{-6}
		12.8	2.7				1.25×10^{-6}
		10.1	2.7				1.95×10^{-6}
		16.5	2.7				1.46×10^{-6}
		13.2	1.8				1.36×10^{-6}
		7.7	1.8				1.42×10^{-6}
		18.7	2.7				2.22×10^{-6}
		12.3	2.7				2.52×10^{-6}
		6.6	2.7				1.98×10^{-6}
		19.3	0.9				2.61×10^{-6}
		10.5	0.9				2.42×10^{-6}
		10.6	1.8				2.00×10^{-6}
		12.8	2.7				1.66×10^{-6}
		10.1	2.7				1.75×10^{-6}
		7.7	1.8				1.47×10^{-6}

Reference	Drum diameter, m	Fill, vol. %	Relative speed, % critical	Granular material	Mean particle diameter, mm	Angle of repose, deg	Axial-dispersion coefficient, m^2/s
Rutgers (1965)	0.16	63.7	28.4	rice, oats	2	N/A	6.40×10^{-6}
		41.6	28.4				7.40×10^{-6}
		43.7	28.4				8.30×10^{-6}
		22.1	28.4				9.10×10^{-6}
		27.9	28.4				9.50×10^{-6}
		25.0	28.4				9.20×10^{-6}
		25.7	7.5				4.40×10^{-6}
		26.0	56.7				9.30×10^{-6}
		29.4	56.7				1.29×10^{-5}
		39.5	91.9				2.70×10^{-5}
		32.2	28.4				1.27×10^{-5}
		21.3	28.4				1.10×10^{-5}
		20.7	28.4				1.04×10^{-5}
		24.4	28.4				9.30×10^{-6}
		23.2	28.4				8.50×10^{-6}
		41.2	28.4				4.10×10^{-6}
		41.0	28.4				4.50×10^{-6}
		40.0	28.4				5.30×10^{-6}
		40.5	28.4				7.00×10^{-6}
		25.4	28.4				7.10×10^{-6}
		22.9	28.4				7.50×10^{-6}
		21.0	28.4				5.80×10^{-6}
		20.6	28.4				5.00×10^{-6}
		39.8	28.4				7.90×10^{-6}
		41.9	28.4				6.30×10^{-6}
		34.1	28.4				1.40×10^{-5}
		36.0	28.4				7.10×10^{-6}
		22.6	28.4				2.20×10^{-5}
		22.0	28.4				1.74×10^{-5}
Tscheng (1978)	0.1905	19.3	7.08	polystyrene	1.9x3.1x3.6	29	1.28×10^{-5}
		20.8	16.1				2.91×10^{-5}
		18.6	5.7				6.90×10^{-6}
		20.6	4.9				9.00×10^{-6}
Hehl et al. (1978)	0.250	9.9	1.2	soda	0.137	N/A	1.30×10^{-6}
		8.1	2.4				1.70×10^{-6}
		5.3	5.9				3.40×10^{-6}
		4.4	11.8				5.60×10^{-6}
		4.9	5.9				2.10×10^{-6}
		7.1	5.9				3.90×10^{-6}
		8.4	5.9				4.00×10^{-6}

Reference	Drum diameter, m	Fill, vol. %	Relative speed, % critical	Granular material	Mean particle diameter, mm	Angle of repose, deg	Axial-dispersion coefficient, m^2/s
Sugimoto (1968)	0.255	19.1	10.1	sand	1.5	N/A	3.75×10^{-6}
		19.6	30.4				7.50×10^{-6}
		21.6	50.1				1.75×10^{-5}
Lebas et al. (1995)	0.6	8.0	3.7	coal	0.5-20	37	3.85×10^{-5}
		8.0					3.50×10^{-5}
		13.0					3.08×10^{-5}
		13.0					2.67×10^{-5}
		18.0					3.02×10^{-5}
		18.0					2.37×10^{-5}
		23.0					2.66×10^{-5}
		23.0					2.61×10^{-5}
Wes et al. (1976)	0.6	19.8	11.0	potato	0.015-0.10	30	4.30×10^{-5}
		31.4	3.7	starch			3.90×10^{-5}
Rutgers (1965)	0.765	44	31	oat	2	N/A	7.00×10^{-5}
		0.84	39	groats			1.00×10^{-4}
Ray et al. (1994)	0.90	22.6	1.3	coal +ore	6-15	N/A	3.22×10^{-6}

Table A-2 Particle dispersion coefficients in the axial direction from experiments in batch rotating drums

Reference	Drum diameter m	Fill vol. %	Relative speed, % critical	Granular material	Particle diameter mm	Angle of repose deg	Axial-dispersion coefficient, m^2/s
Rao et al. (1991)	0.076	16.2	18.2	Sodium (bi)carbonate	0.214	42.5	5.92×10^{-7}
		27.0	18.2		0.214	40	5.88×10^{-7}
		37.8	18.2		0.214	38	5.24×10^{-7}
		27.0	18.2		0.125		8.10×10^{-7}
		27.0	18.2		0.388		5.15×10^{-7}
		27.0	7.2		0.214		1.50×10^{-7}
		27.0	15.6		0.214		4.70×10^{-7}
		27.0	33.2		0.214		1.35×10^{-6}
Singh (1979)	0.10	40	2.6	glass beads	0.78	27.4	4.77×10^{-7}
		40	7.8		0.78		5.30×10^{-7}
		40	7.4		0.60		2.67×10^{-6}
		40	2.8		0.60		5.70×10^{-7}
		30	2.8		0.78		5.30×10^{-7}
		40	1.3		0.60		4.77×10^{-7}
		40	2.2		0.60		5.25×10^{-7}
Shoji et al. (1973)	0.095	25	67	Silicon carbide	0.335	N/A	1.50×10^{-6}
		40					6.50×10^{-7}
Hogg et al. (1969)	0.102	60	20	glass beads	0.100	N/A	4.94×10^{-7}
	0.051	40	20	quartz	0.253	N/A	3.72×10^{-7}
Hogg (1969)	0.10	60	20	glass beads	0.090	N/A	3.55×10^{-7}

Reference	Drum diameter m	Fill vol. %	Relative speed, % critical	Granular material	Particle diameter mm	Angle of repose deg	Axial-dispersion coefficient, m^2/s
Cahn and Fuerstenau (1967)	0.102	30	20.4	Lucite beads	6.35	N/A	5.90×10^{-6}
		40	20.4				9.10×10^{-6}
		50	20.4				9.70×10^{-6}
		60	20.4				8.10×10^{-6}
		30	30.2				8.60×10^{-6}
		40	30.2				1.18×10^{-5}
		50	30.2				1.29×10^{-5}
		60	30.2				1.02×10^{-5}
		30	40.0				1.02×10^{-5}
		40	40.0				1.45×10^{-5}
		50	40.0				1.61×10^{-5}
		60	40.0				1.29×10^{-5}
		30	49.8				1.61×10^{-5}
		40	49.8				1.99×10^{-5}
		50	49.8				2.20×10^{-5}
		60	49.8				1.45×10^{-5}
		30	60.4				2.31×10^{-5}
		40	60.4				3.12×10^{-5}
		50	60.4				3.76×10^{-5}
		60	60.4				1.45×10^{-5}
Carley-Macauly and Donald (1962)	0.102	33	15.1	Sand	0.6-0.85	N/A	6.39×10^{-7}
Wrightman and Muzzio (1998)	0.106	30	3.8		0.066		3.1×10^{-7}
Parker et al. (1997)	0.136	32	11.3	glass beads	1.5		9.90×10^{-7}
			28.8				1.44×10^{-6}
			36.6				1.84×10^{-6}
			47.1				2.10×10^{-6}
	0.144	33	16.1	glass beads	3		4.70×10^{-6}
			33.2				7.80×10^{-6}
			43.1				7.10×10^{-6}
			56.5				9.80×10^{-6}

Reference	Drum diameter m	Fill vol. %	Relative speed, % critical	Granular material	Particle diameter mm	Angle of repose deg	Axial-dispersion coefficient, m^2/s
	0.100	36	7.5	glass beads	3		3.50×10^{-6}
			15.0				6.90×10^{-6}
			31.4				1.04×10^{-5}
			39.6				9.20×10^{-6}
			48.6				8.30×10^{-6}

APPENDIX B

MATLAB 5.3 Code for Simulating Transverse Mixing in a Rotating Drum

```
% Radial mixing model
% Makes movie of radial mixing if movie = TRUE
TRUE=1; FALSE=0;
RHS=0; SMILE=1; LAYER=2;
movie = FALSE;
init = RHS;
nFrames=1500;

%Black(1988)
%dia = 0.45; %drum diameter, m
%drum.fill = 0.24; %drum fill, vol frac
%drum.speed = 12.1; %drum speed, rpm
%particle.diameter = 0.007; %particle diameter, m

%Carley-Macauly and Donald (1962)
dia = 0.1016; %drum diameter, m
drum.fill = 0.33; %drum fill, vol frac
drum.speed = 20; %drum speed, rpm
particle.diameter = 0.00046; %particle diameter, m
n=27;    %number of layers in static region
m=131;   %number of angular segments in static region

crit_speed=60/(2*3.14)*(2*9.81/dia)^0.5;%rpm
active = 0.276*(drum.speed/crit_speed)^0.36*dia^-0.19*drum.fill^-0.34;
%fraction of depth that is active layer
beta = drumbeta(drum.fill);
depth = dia/2*(1-cos(beta/2)); %metres

dtheta=beta/m;
static = depth*(1-active);
drho=static/n;

[THETA, RHO]=meshgrid(-beta/2-pi/2:dtheta:beta/2-pi/2, dia/2-
static:drho:dia/2);
[X,Y]=pol2cart(THETA,RHO);

%Define interface
L=dia/2*sin(beta/2);
d=depth*active;
h=dia/2*cos(beta/2);
for i=1:n
   r=h+d+(i-0.5)*drho;
   del=0.5*(L^2/d-2*h)-0.5*((L^2/d-2*h)^2-4*(L^2+h^2-r^2))^(1/2);
   phi=acos((h+del)/(r));
   k1(i)=round(m/2*(beta-2*phi)/beta)+1;
   k2(i)=round(m/2*(1+2*phi/beta));
end

%give color to each element of S
S=ones(n+1,m+1)*1;
for i=1:n-1 %elements outside static layer
   S(i,1:k1(i)-1)=1;
   S(i,k2(i)+1:m)=1;
```

```
end
S(1,1)=0;%black
if init == RHS
      for i=1:n
      S(i,round(m/2):k2(i))=0;%RHS of static layer
   end
end
if init == SMILE
      for i=1:round(n/2)+4
        S(i,k1(i):k2(i))=0;%smile
      end
end
if init == LAYER
   del1=round(n*0.65)*drho;
   for i=1:n
      r=h+d+(i-0.5)*drho;
      if r <= (h+del1)
         S(i,k1(i):k2(i))=0;%layer
      else
         phi=acos((h+del1)/(r));
            t1=round(m/2*(beta-2*phi)/beta)+1;
         t2=round(m/2*(1+2*phi/beta));
            S(i,k1(i):t1)=0;%layer
         S(i,t2:k2(i))=0;%layer
      end
   end
end

iFrames=1;
if movie
      % initialize movie
      iFrames=20;
      MOV = moviein(iFrames+nFrames);
      set(gca,'NextPlot','replacechildren')
   %plot initial condition
   figure(1)
      pcolor(X, Y, S);
      axis equal tight
      colormap(gray(100))
      shading flat
      for j=1:iFrames
         MOV(:,j) = getframe;
      end
end
%Create mixing matrix M[nxn]
%   Calculate axial dispersion coefficient, m2/s
Dz=5.82e-
4*(drum.speed/crit_speed)^0.44*dia^1.29*particle.diameter^0.35*drum.fil
l^-0.55;

% Calculate radial dispersion coefficient, m2/s
Dr=Dz*((1-active)/active)^2;
% Integrate over cycle time (contact time)
```

```
M=eye(n);
tend=beta/drum.speed*60/(2*3.14);
for i=1:n
   C0=M(i,:);
   [t,C]=ode45('mixode',[0,tend],C0,odeset('RelTol', 1e-
3),n,Dr,drho,dia,k1,k2);
      M(i,:)=C(end,:);
end


tstep=dtheta*60/(drum.speed*2*3.14);
for j = iFrames:nFrames+iFrames
      % for each time step
      %   set slice leaving static region A2=S(k2)
      for i=1:n
         A2(i)=S(i,k2(i));
      end
      %   advance elements in static region 1 angular segment
      for i=m:-1:2
      S(:,i)=S(:,i-1);
   end
   S(1,2)=1;
      for i=1:n
      S(i,k2(i)+1)=1;
      end
      %   use mixing matrix to calculate slice entering static region
A1=M*A2
   A1=A2*M;
   %for i=1:n
    %  r(i)=h+d+(i-1/2)*drho;
   %end

   %for i=1:n
   %   A1(i)=0;
   %      for k=1:n
   %     A1(i)=M(i,k)*A2(k)*r(k)/(h+d+(n/2-1/2)*drho);
   %   end
   %end


      %   set elements of S(k1)=A1
      for i=1:n
      S(i,k1(i))=A1(i);
   end
   %  calculate mean and standard deviation concentraion
   sumA=0;
   sumS=0;
   count=0;
   for i=1:n
      r1=d+h+(i-1)*drho;
      A=dtheta*drho*(r1+drho/2);
      for k=k1(i):k2(i)
         sumA=sumA+A;
```

```
            sumS=sumS+S(i,k)*A;
            count=count+1;
         end
      end
      sumAS2=0;
      mean(j)=sumS/sumA;
      for i=1:n
         r1=d+h+(i-1)*drho;
         A=dtheta*drho*(r1+drho/2);
         for k=k1(i):k2(i)
            sumAS2=sumAS2+A*(S(i,k)-mean(j))^2;
         end
      end
      time(j)=j*tstep;
      stdev(j)=(sumAS2/sumA)^0.5;
      if movie
         %   record a frame of the movie
         pcolor(X, Y, S);
         shading flat
         MOV(:,j) = getframe;
      end

% next step
end
if movie
   mpgwrite(MOV,gray(100),'drummix3');
end

figure(2)
semilogy(time, stdev, 'k-')
xlabel('Time, s')
ylabel('Standard deviation of tracer concentration')


%figure(3)
%subplot(4,2,8)
      %pcolor(X, Y, S);
      %axis equal tight
      %colormap(gray(100))
      %shading flat
      %axis off

figure(3)
subplot(2,1,2)
      pcolor(X, Y, S);
      axis equal tight
      colormap(gray(100))
      shading flat
      axis off
```

```
% Wall-to-bed heat transfer model with fine layers next to wall
% Makes movie of bed temperatures if movie = TRUE
TRUE=1; FALSE=0;
movie = FALSE;
nFrames=500;
dia = 0.45; %drum diameter, m
drum.fill = 0.24; %drum fill, vol frac
drum.speed = 12.1; %drum speed, rpm
particle.diameter = 0.007; %particle diameter, m
conductivity = 0.2; % W/m C
density = 880; % kg/m3
heatcapacity =1000; % J/kg C
wallT = 400; % deg C (white)
bedT = 100; % deg C (black)
n=20;    %number of thick layers in core of static region
np=5; %number of fine layers next to wall in static region
e=8;        %ratio of thickness of thick layer to thickness of fine
layer
m=65;   %number of angular segments in static region

crit_speed=60/(2*3.14)*(2*9.81/dia)^0.5;%rpm
active = 0.276*(drum.speed/crit_speed)^0.36*dia^-0.19*drum.fill^-0.34;
%fraction of depth that is active layer
beta = drumbeta(drum.fill);
depth = dia/2*(1-cos(beta/2)); %metres

dtheta=beta/m;
static = depth*(1-active);
drhop=static/(n*e+np);
drho=e*drhop;

[THETA1, RHO1]=meshgrid(-beta/2-pi/2:dtheta:beta/2-pi/2, dia/2-
static:drho:dia/2-np*drhop);
[THETA2, RHO2]=meshgrid(-beta/2-pi/2:dtheta:beta/2-pi/2, dia/2-(np-
1)*drhop:drhop:dia/2);
THETA=cat(1,THETA1,THETA2);
RHO=cat(1,RHO1,RHO2);
[X,Y]=pol2cart(THETA,RHO);

%Define interface
L=dia/2*sin(beta/2);
d=depth*active;
h=dia/2*cos(beta/2);
for i=1:n
   r=h+d+(i-0.5)*drho;
   del=0.5*(L^2/d-2*h)-0.5*((L^2/d-2*h)^2-4*(L^2+h^2-r^2))^(1/2);
   phi=acos((h+del)/(r));
   k1(i)=round(m/2*(beta-2*phi)/beta)+1;
   k2(i)=round(m/2*(1+2*phi/beta));
end
for i=1:np
   r=h+d+n*drho+(i-0.5)*drhop;
   del=0.5*(L^2/d-2*h)-0.5*((L^2/d-2*h)^2-4*(L^2+h^2-r^2))^(1/2);
```

```
   phi=acos((h+del)/(r));
   k1(n+i)=round(m/2*(beta-2*phi)/beta)+1;
   k2(n+i)=round(m/2*(1+2*phi/beta));
end

%give temperature to each element of S
S=ones(n+np+1,m+1)*bedT; %(black)
for i=1:n+np-1 %elements outside static layer
   S(i,1:k1(i)-1)=wallT; %(white)
   S(i,k2(i)+1:m)=wallT;
end
S(1,1)=bedT; % (black)

iFrames=1;
if movie
      % initialize movie
      iFrames=20;
      %MOV = moviein(iFrames+nFrames);
      set(gca,'NextPlot','replacechildren')
   %plot initial condition
   figure(1)
      pcolor(X, Y, S);
      axis equal tight
      colormap(gray(100))
      shading flat
      for j=1:iFrames
         %MOV(:,j) = getframe;
      end
end
%Create mixing matrix M[nxn]
%   Calculate axial dispersion coefficient, m2/s
Dz=5.82e-
4*(drum.speed/crit_speed)^0.44*dia^1.29*particle.diameter^0.35*drum.fil
l^-0.55;
% Calculate radial dispersion coefficient, m2/s
Dr=Dz*((1-active)/active)^2;
% Integrate over cycle time (contact time)
tend=beta/drum.speed*60/(2*3.14);
M=eye(n+np);
for i=1:n+np
   C0=M(i,:);
   [t,C]=ode45('mix2ode',[0,tend],C0,...
      odeset('RelTol', 1e-3,'AbsTol', 1e-
3),n,np,Dr,drho,drhop,dia,k1,k2);
      M(i,:)=C(end,:);
end
%M=M'
alpha=conductivity/(heatcapacity*density); %m2/s
tstep=dtheta*60/(drum.speed*2*3.14); %seconds
for k = iFrames:nFrames+iFrames
      % for each time step
      %   set slice leaving static region A2=S(k2)
      for i=1:n+np
```

```
         A2(i)=S(i,k2(i));
      end
      %   advance elements in static region 1 angular segment
   for j=m:-1:2
         if k2(1)>=j
            if k1(1)<j
               r=h+d+drho/2;
                  S(1,j)=S(1,j-1)+alpha*tstep/drho^2*...
                     ((1+drho/(2*r))*(S(2,j-1)-S(1,j-1)));
            end
         end

         for i=2:n-1
            r=h+d+(i-1/2)*drho;
         if k2(i)>=j
            if k1(i)<j
                  if k2(i-1)<j-1
                        S(i,j)=S(i,j-1)+alpha*tstep/drho^2*...
                     ((1+drho/(2*r))*(S(i+1,j-1)-S(i,j-1)));
               elseif k1(i-1)>j-1
                  S(i,j)=S(i,j-1)+alpha*tstep/drho^2*...
                     ((1+drho/(2*r))*(S(i+1,j-1)-S(i,j-1)));
                              else
                     S(i,j)=S(i,j-1)+alpha*tstep/drho^2*...
                     ((1+drho/(2*r))*S(i+1,j-1)...
                        -2*S(i,j-1)...
                                          +(1-drho/(2*r))*S(i-1,j-1));
               end
            end
         end
      end
      r=h+d+(n-1/2)*drho;
      if k2(n-1)<j-1
         S(n,j)=S(n,j-1)+alpha*tstep/drho^2*...
            (2*drho/(drho+drhop))*(1+drho/(2*r))*(S(n+1,j-1)-S(n,j-1));
      elseif k1(n-1)>j-1
         S(n,j)=S(n,j-1)+alpha*tstep/drho^2*...
            (2*drho/(drho+drhop))*(1+drho/(2*r))*(S(n+1,j-1)-S(n,j-1));
      else
         S(n,j)=S(n,j-1)+alpha*tstep/drho^2*...
            ((2*drho/(drho+drhop))*(1+drho/(2*r))*(S(n+1,j-1)-S(n,j-
1))...
           -(1-drho/(2*r))*(S(n,j-1)-S(n-1,j-1)));
      end
      r=h+d+n*drho+0.5*drhop;
      if k2(n-1)<j-1
         S(n+1,j)=S(n+1,j-1)+alpha*tstep/drhop^2*...
            (-(2*drhop/(drho+drhop))*(1-drhop/(2*r))*(S(n+1,j-1)-S(n,j-
1)));
      elseif k1(n-1)>j-1
         S(n+1,j)=S(n+1,j-1)+alpha*tstep/drhop^2*...
            (-(2*drhop/(drho+drhop))*(1-drhop/(2*r))*(S(n+1,j-1)-S(n,j-
1)));
```

```
      else
         S(n+1,j)=S(n+1,j-1)+alpha*tstep/drhop^2*...
            ((1+drhop/(2*r))*(S(n+2,j-1)-S(n+1,j-1))...
            -(2*drhop/(drho+drhop))*(1-drhop/(2*r))*(S(n+1,j-1)-S(n,j-
1)));
      end

      for i=2:np-1
         r=h+d+n*drho+(i-1/2)*drhop;
         if k2(n+i)>=j
            if k1(n+i)<j
                  if k2(n+i-1)<j-1
                        S(n+i,j)=S(n+i,j-1)+alpha*tstep/drhop^2*...
                     ((1+drhop/(2*r))*(S(n+i+1,j-1)-S(n+i,j-1)));
               elseif k1(n+i-1)>j-1
                  S(n+i,j)=S(n+i,j-1)+alpha*tstep/drhop^2*...
                     ((1+drhop/(2*r))*(S(n+i+1,j-1)-S(n+i,j-1)));
                           else
                     S(n+i,j)=S(n+i,j-1)+alpha*tstep/drhop^2*...
                     ((1+drhop/(2*r))*S(n+i+1,j-1)...
                        -2*S(n+i,j-1)...
                        +(1-drhop/(2*r))*S(n+i-1,j-1));
               end
            end
         end
      end
      r=h+d+n*drho+(np-0.5)*drhop;
      if k2(n+np-1)<j-1
         S(n+np,j)=S(n+np,j-1)+alpha*tstep/drhop^2*...
            2*(1+drhop/(2*r))*(wallT-S(n+np,j-1));
      elseif k1(n-1)>j-1
         S(n+np,j)=S(n+np,j-1)+alpha*tstep/drhop^2*...
            2*(1+drhop/(2*r))*(wallT-S(n+np,j-1));
      else
         S(n+np,j)=S(n+np,j-1)+alpha*tstep/drhop^2*...
            (2*(1+drhop/(2*r))*wallT...
            -(3+drhop/(2*r))*S(n+np,j-1)...
            +(1-drhop/(2*r))*S(n+np-1,j-1));
      end
   end
      %   use mixing matrix to calculate slice entering static region
A1=M*A2
      A1=A2*M;
      %   set elements of S(k1)=A1
      for i=1:n+np
      S(i,k1(i))=A1(i);
   end
   %  calculate mean and standard deviation concentraion
   sumS=0;
   sumA=0;
   count1=0;
   count2=0;
   for i=1:n
```

```
        r=d+h+(i-1)*drho;
        A=dtheta*drho*(r+drho/2);
        for j=k1(i):k2(i)
            sumA=sumA+A;
            sumS=sumS+S(i,j)*A;
            count1=count1+1;
        end
    end
    for i=1:np
        r=d+h+n*drho+(i-1)*drhop;
        A=dtheta*drhop*(r+drhop/2);
        for j=k1(n+i):k2(n+i)
            sumA=sumA+A;
            sumS=sumS+S(n+i,j)*A;
            count2=count2+1;
        end
    end
        time(k)=k*tstep;
    mean(k)=sumS/sumA;
    if k>1
            Q(k)=heatcapacity*density*sumA*(mean(k)-mean(k-1))/tstep;%W/m
        U(k)=Q(k)/(pi*dia*(wallT-mean(k)));

    end
    if movie
        %   record a frame of the movie
        pcolor(X, Y, S);
        shading flat
        %MOV(:,k) = getframe;
    end

% next step
end
if movie
    %mpgwrite(MOV,gray(100),'drumheat');
end

figure(2)
plot(time, U)
grid on
```

```
function angle = beta(X)
% BETA Contact angle between bed and wall in horizontal drum.
%    ANGLE = BETA(X)returns contact angle in radians for fill X
%    in volume fraction.
      OPTIONS=[];
      f=inline('drumfill(ANGLE)-X');
      angle = fzero(f,[0 pi],OPTIONS,X);
return


function volfrac=drumfill(beta)
%DRUMFILL Volumetric fraction of bed in horizontal drum.
%   DRUMFILL(BETA) returns volumetic fill fraction given contact
%   angle between bed and wall of horizontal drum.
      volfrac = (beta-sin(beta))/(2*pi);
return
```

```
function dC = mixode(t,C,flag,n,Dr,drho,D,k1,k2)
%for i=1:n
%   phi(i)=k2(i)-k1(i)+1;
%end

r=D/2-(n-1/2)*drho;
dC=zeros(n,1);
%dC(1)=2*Dr/drho^2*((r+drho)/(2*r+drho)*C(2)-(r+drho)/(2*r+drho)*C(1));
%dC(1)=2*Dr/drho^2*(1/2*C(2)-1/2*C(1));
dC(1)=Dr/(2*drho^2)*((2*r+drho)/r*C(2)-(2*r+drho)/r*C(1));
for i=2:n-1
   r=r+drho;
%   dC(i)=2*Dr/drho^2*((r+drho)/(2*r+drho)*C(i+1)...
%      -(phi(i)*(r+drho)+phi(i-1)*r)/(phi(i)*(2*r+drho))*C(i)...
%      +(r)/(2*r+drho)*phi(i-1)/phi(i)*C(i-1));
%   dC(i)=2*Dr/drho^2*(1/2*C(i+1)-C(i)+1/2*C(i-1));
   dC(i)=Dr/(2*drho^2)*((2*r+drho)/r*C(i+1)-4*C(i)+(2*r-drho)/r*C(i-
1));
end
r=r+drho;
%dC(n)=2*Dr/drho^2*(-r/(2*r+drho)*phi(n-
1)/phi(n)*C(n)+(r)/(2*r+drho)*phi(n-1)/phi(n)*C(n-1));
%dC(n)=2*Dr/drho^2*(-1/2*C(n)+1/2*C(n-1));
dC(n)=Dr/(2*drho^2)*(-(2*r-drho)/r*C(n)+(2*r-drho)/r*C(n-1));
```

```
function dC = mix2ode(t,C,flag,n,np,Dr,drho,drhop,D,k1,k2)

r=D/2-(n-1/2)*drho-np*drhop;
dC=zeros(n+np,1);
dC(1)=Dr/drho^2*(1+drho/(2*r))*(C(2)-C(1));

for i=2:n-1
   r=r+drho;
   dC(i)=Dr/drho^2*((1+drho/(2*r))*C(i+1)...
      -2*C(i)...
      +(1-drho/(2*r))*C(i-1));
end

r=r+drho;
dC(n)=Dr/drho^2*(2*drho/(drho+drhop)*(1+drho/(2*r))*(C(n+1)-C(n))...
   -(1-drho/(2*r))*(C(n)-C(n-1)));

r=r+(drho+drhop)/2;
dC(n+1)=Dr/drhop^2*((1+drhop/(2*r))*(C(n+2)-C(n+1))-...
   (2*drhop/(drho+drhop))*(1-drhop/(2*r))*(C(n+1)-C(n)));

for i=n+2:n+np-1
   r=r+drhop;
   dC(i)=Dr/drhop^2*((1+drhop/(2*r))*C(i+1)...
      -2*C(i)...
      +(1-drhop/(2*r))*C(i-1));
end
r=r+drhop;
dC(n+np)=Dr/drhop^2*(-(1-drhop/(2*r))*(C(n+np)-C(n+np-1)));
```